Imaging neuropeptide release and localization with genetically engineered reporters

Thesis by

Ke Ding

In Partial Fulfillment of the Requirements for

the degree of

Doctor of Philosophy

CALIFORNIA INSTITUTE OF TECHNOLOGY

Pasadena, California

2022

(Defended May 25th, 2022)

Ke Ding
ORCID: 0000-0002-5261-4843

ACKNOWLEDGEMENTS

My strongest, heartfelt appreciation goes to my great advisor Dr. David Anderson. David has incredible passion and dedication to science, which result in his insurmountable yet ever-growing pool of knowledge. Case in point, my project is quite different from other projects in the lab, which requires deep understanding of cell biology and optical imaging. The former contains much of David's "bread and butter" in the 1980s, and the latter is filled with cutting-edge technical advances. It is surprising that David often easily recalled some 40-year-old paper for reference, and in a few minutes, pointed me to some 2-month-old imaging techniques that I should consider trying. These jaw-dropping moments percolated through my 1-on-1 meetings over these years. A trained neuroscientist myself, I cannot resist proposing a series of non-invasive recordings to unlock the mystery behind David's brain. The brain slice histology may have to wait until the next century though.

David is more than a wonderful scientist. He is a supportive mentor, an excellent speaker, a top-notch writer, and an amazing philosopher. In the wake of the COVID-19 outburst, I started to think about my career choice beyond academia, and David supported my decision of leaving campus for a stint in management consulting. I enjoyed the internship, but suffered the collateral damage, as geopolitical conflicts ignited by an unusual US president blocked my way back. It took me several months to resolve the issue, and David was standing by me all the way through. We had biweekly meetings despite knowing that I cannot generate any data. David fed me with many new ideas and results from the lab, and he tried hard to make sure I was doing well in the involuntary social isolation, a topic that David knows scientifically better than anybody on earth. Life did not turn easier after my reunion with the

lab, and David helped me again, with his emotional support and concrete, executable life advice. Things could have been much more difficult if David were not around. I thank him from the bottom of my heart for all he has done for me.

David's love for science and his good heart are shared by the lab members as well. I thank Dr. Eric Hoopfer for his instructions on note taking, Dr. Brian Duistermars for his deep comments in the lab meetings, Dr. Kiichi Watanabe for his technical help and support, Dr. Joe Ouadah for his incredible book list, Dr. Lingyun Li for her generous advice on project planning, Dr. Ann Kennedy for the help on data storage, the stats guru Dr. Moriel Zelikowsky for including my ideas in her review, Dr. Tomomi Karigo for her participation in the early phase of my project, Dr. George Mountoufaris for his unreserved help in the later phase and spicy global news, Dr. Brandon Weissbourd for his instruction on using camera and his interest in testing reporters in his lovely jellyfish, Dr. Ryan Remedios for taking me to a club (my first and very likely my last time. Thanks, but sorry, Ryan), Dr. Amit Vinograd for his sharing of Jewish culture, Dr. Stefanos Stagkourakis for his "How's life" greetings, and I am very jealous of his nice T-shirt collection.

I would love to thank my good friend and rotation mentor Dr. Yon-il Jung for his rigorous training and his introduction of many novel things outside the lab. We have many memorable good laughs and I genuinely appreciate his unorthodox personal style and unique sense of humor. He kept reminding me that earlier years of grad school transpire in a "sink-or-swim" fashion. To substantiate the metaphor, I taught Yon-il how to swim and Yon-il took me to

sink (scuba diving) from time to time. My late confession to him: I still very much prefer swimming.

Graduate students in the lab are the best peers. I thank Dr. Vivian Chiu for her insightful suggestions for my project and her share of colorful stories. We spent so much time trading anecdotes about movies, cats, and life in the fly pushing room. Dr. Dongwook Kim taught me so much about single cell sequencing and tolerated my countless lame jokes. Shuo Cao was kind enough to give ways to my heavy use of confocal and he never complained. Bin Yang cares very much about my career and life. He took me out for dinner during the recruitment and motivated me to join the lab. Kathy Cheung is warm-hearted and cheers me up all the time. The K-Pop star-looking couple Mengyu Liu and Zikun Zhu are the sweetest people I met. Thanks to them, I am now paying attention to my haircut, or at least to have one. I also thank the admins and technicians in our lab, Celine, Xiaolin, Xiao, Helen, Jung-sook, Gina, and Arnold. Many of them helped with experiments in my projects; talking to them also slowed down the degeneration of my Mandarin speaking skills.

The progress of my projects relied heavily on the students, volunteers, and technicians who worked directly with me. Taylor Seid was a high school student, but she learnt so fast that I got intimidated that I could not catch up. Dr. Shishuo Zhang has the best skills in molecular cloning and RT-PCR. I still believe that her pipetting skill is no second to any automated robot hands. Ling Zhao worked with me only for a few months, but he picked up an astonishing number of new techniques. Many a time he started experiments from *de novo*

designing. His intellectual input and clinical insight were extremely valuable to the project. I enjoyed working with every one of them.

The properties of my projects necessitate extensive collaboration. I would like to thank Drs. Yifu Han, Dion Dickman, Chris Buser, James Tan, Han Wang, Paul Sternberg, Yi Shen, David Prober, and later-to-be Dr. Altyn Rymbek for their kindness and interest in all these projects.

Many other Caltech members helped me in various way. My committee member Dr. David Chan provided invaluable advice at the beginning of my projects. I thank Yicheng Luo for his supply of multiple fly strains and cDNA, Dr. Brian He for his algorithms, Xiaozhe Ding for a trustworthy pAAV backbone, Dr. Andres Collazo for choosing me as his TA many times, and Dr. Henry Lester for providing tips and equipment to aid my research. I often met Henry in the locker room of Caltech gym, and most scientific discussion was done there. It is hard to justify that I earned any “naked truth”, but I did take away quite a bit of “naked facts” from him. Dr. Olivia Wan has been extremely helpful in and out of the lab. The worm pickers she made helped me win the battle with the annoyingly tiny nematodes. She was also my designated cat-sitter last year while I was out-of-town. Dr. Yan Jin too took care of my cats for months while I was trapped overseas. I am lucky to cross paths with these people.

My college friends/alumni play a significant role in my life. I thank Chuanyun Xu and Bowen Tan for supporting me through the ups and downs of my life. They never cease to help me by all means. I am not who I am now without them. Dr. Kai Chen, Danni Ma, and Dr. Jiaming

Li are ZJU-Caltech dual alumni. Our weekly groceries trips were the most relaxing times between experiments. Cindy Qin, though from a rival college, buried the hatchet and brought fun, joy, and vigor to my life. Dr. Ke Yu (aka Ke No.1), a great guy with whom I shared an apartment for a few years and a name for life, never failed to make me chuckle with his humor and wittiness.

I would like to thank my three adorable cats, Green, Red, and Orange, for their company at home. These furry fellas are surprisingly well-behaved: never break a thing, never fight over food, and stay quiet during my numerous zoom meetings. I named them randomly by the color of their collar (Green and Red) or body hair (Orange), but the names coincide with the colors of the fluorescent reporters I constructed afterwards. Sometimes life does work wonders.

Finally, I am grateful to my parents Mr. Jingjian Lin and Mrs. Yifei Ding. They named me after the Chinese character (Ke, 可) that comes with humble connotations. It interestingly matches the word “fine” in English, used either as “acceptable” or as a grudging “yes.” I hope that I have lived up to their expectations.

ABSTRACT

Neuropeptides are a class of neural signaling molecules that play a pivotal role in brain function and human health through neuromodulatory influences. There are over 100 types of neuropeptides identified and characterized, yet genomic analysis suggests that it is only the tip of the iceberg, with extra hundreds of putative neuropeptides awaiting further investigation. Neuropeptides collectively regulate a variety of developmental, physiological, and behavioral functions. While each neuropeptide is idiosyncratic in regard to its molecular structure, chemical properties, and anatomical distribution, they impinge on the nervous system in a similar fashion.

Surprisingly, despite their fundamental importance, techniques for measuring the localization, expression and release of neuropeptides, at large scale and with high spatio-temporal resolution, have lagged far behind. Microdialysis and fast-scanning cyclic voltammetry are useful primarily for measuring "volume transmission," but are invasive, and have poor spatial resolution and limited general applicability. FP-tagged vesicle reporters are mainly tested and used in limited cell types. Little is characterized about their functional universality and specificity. GPCR-based sensors are designed to visualize the binding, instead of expression and release, of a neuropeptide.

Therefore, I aim to develop new methods for visualizing, detecting, and inhibiting NP expression and release *in vivo*. The long-term goal is to apply these methods to understanding the dynamics of neuromodulation of specific, behaviorally relevant neural circuits, and to providing a dynamic, high-resolution view of chemical modulation of circuit function.

In Chapter 2, I will describe the design, screening, and proof-of-concept validation of novel genetically engineered neuropeptide release reporters (NPRR) in *Drosophila*. I further demonstrated the idiosyncrasy of neuropeptide release dynamics, as well as cell-type specific release properties of a neuropeptide. In Chapter 3, I conceived and constructed a neuropeptide imaging platform that exploits the discoveries and strategies from *Drosophila* NPRRs. Besides a series of redesign of mammalian NPRRs, a collection of sister reporters to visualize localization and expression (Neuropeptide Localization and Expression Reporter, NPLER) were built in parallel. I also established a prototypical pipeline to systematically screen for appropriate cell lines for the purpose of NPRR/NPLER applications.

Malfunctioning of neuropeptide pathways can potentially result in a variety of mental illnesses triggered by stress, and metabolic disorders including obesity. Drugs targeting neuropeptide signaling have received heavy investment, but most have failed in the clinical trials. We therefore propose alternative strategies to target the processing/release of the neuropeptide from neurons, rather than blocking its receptor. In Chapter 4, I describe the ongoing process of adapting modern biotechnologies to the imaging platform to explore novel therapeutic strategies for neuropeptide-relevant disorders and abnormalities.

The Appendix includes a serendipitous finding from our attempt to generalize NPRR to *Caenorhabditis elegans*.

PUBLISHED CONTENT AND CONTRIBUTIONS

Ding, K., Han, Y., Seid, T. W., Buser, C., Karigo, T., Zhang, S., ... & Anderson, D. J. (2019). Imaging neuropeptide release at synapses with a genetically engineered reporter. *Elife*, *8*, e46421. https://doi.org/10.7554/elife.46421

K. D. contributed to: Conceptualization, Data curation, Formal analysis, Investigation, Methodology, Writing—original draft, Writing—review and editing.

Han, Y., & Ding, K. (2022). Imaging Neuropeptide Release at *Drosophila* Neuromuscular Junction with a Genetically Engineered Neuropeptide Release Reporter. *Methods in Molecular Biology*, 2417, 193–203. https://doi.org/10.1007/978-1-0716-1916-2_15

K. D. contributed to: Conceptualization, Data curation, Formal analysis, Investigation, Methodology, Writing—review and editing.

Zelikowsky, M., Ding, K., & Anderson, D. J. (2018). Neuropeptidergic Control of an Internal Brain State Produced by Prolonged Social Isolation Stress. *Cold Spring Harbor Symposia on Quantitative Biology*, 83, 97–103. https://doi.org/10.1101/SQB.2018.83.038109

K. D. contributed to: Data curation, Formal analysis, Methodology.

TABLE OF CONTENTS

Chapter 1

INTRODUCTION

Neuropeptides and the "Chemical Connectome"

A common metaphor to describe the brain is that it is like a supercomputer. Consequently, current efforts at improving technologies for large-scale recording of brain function are primarily focused on measuring its electrical activity. However, unlike a supercomputer, the brain is an electrochemical machine: its function is dependent on both electrical and chemical (neuromodulatory) signaling. Superimposed upon the brain's physical connectome is a "chemical connectome," a largely invisible network of neuromodulators, including biogenic amines and neuropeptides, that exert a profound influence on brain function (Bargmann & Marder, 2013). These neuromodulators influence brain states in a manner that changes the computations performed by neural circuits (Marder et al., 2014). For example, the ~25 neurons comprising the crustacean stomatogastric ganglion can produce close to half a dozen different motor outputs, depending on their pattern of neuromodulation (Marder & Bucher, 2007). Neuromodulators influence brain states that alter the computations performed by neural circuits, and are central to emotion, mood, and affect (Pert et al., 1985; Wang & Pereira, 2016). An understanding of neuromodulatory influences is particularly important because of their relevance to psychiatric disorders in humans (Kramer et al., 1998; Rotzinger et al., 2010). Without the ability to measure and perturb the release of specific neuromodulators with high spatio-temporal resolution. our understanding of neuronal circuit function will be fundamentally incomplete.

Surprisingly, despite the fundamental importance of neuromodulation, techniques for measuring the release of specific neuromodulators especially neuropeptides (NPs), at large scale and with high spatio-temporal resolution, have lagged far behind those for recording or imaging electrical activity. Available methods, such as microdialysis (Benveniste & Hüttemeier, 1990; Ernberg & Alstergren, 2004; Frost et al., 2008; Lee & Kwon, 2022) or fast-scanning cyclic voltammetry (Makos, Kim, et al., 2009; Makos, Kuklinski, et al., 2009) are useful primarily for measuring "volume transmission," but are invasive, have poor spatial resolution and limited general applicability. There is no generally applicable method for measuring, with millisecond time resolution, the release of specific neuropeptides from individual neurons or nerve terminals.

Our long-term goal is to develop new methods for visualizing, detecting, and inhibiting neuropeptide release *in vivo*, and to apply these methods to understanding the dynamics of neuromodulation of specific, behaviorally relevant neural circuits. The rationale for this research is that the development of new tools for imaging neuropeptide release *in vivo* could have a transformative impact on our ability to characterize and analyze neural circuit function, as well as facilitate the development of technologies for selectively perturbing release.

Over 100 neuropeptides have been identified, which collectively regulate a variety of developmental, physiological, and behavioral functions (Russo, 2017). While each neuropeptide is idiosyncratic in regard to its molecular structure, chemical properties, and anatomical distribution, they impinge on the nervous system in a similar fashion (Agrawal

et al., 2019)): peptidergic (i.e., neuropeptide-producing) neurons and the neuroendocrine cells synthesize and package a massive amount of neuropeptide molecules within a subcellular compartment called the Dense Core Vesicle (DCV), where they are stored and released to the extracellular space upon strong stimulation (electrical or hormonal) of the cells. The released neuropeptides undergo diffusion to bind a group of proteins named "receptors," which are membrane-embedded proteins, typically in the G protein-coupled receptor (GPCR) family on other cells (van den Pol, 2012). These receptors, once peptide-bound, activate downstream biochemical signaling cascades, to regulate many other genes (Zhang et al., 2010) and proteins that control neuronal excitability. These neuropeptide-induced changes in cell physiology can last for a long time, in contrast to the effects of "classical" neurotransmitters like glutamate or GABA, which typically last only milliseconds. In summary, a neuropeptide signaling pathway defines a "neuropeptide information flow" that enables cell-cell communications (Nusbaum et al., 2017) .

Imaging Neuropeptide Release and Localization with a Genetically Engineered Reporter

The central objective is to tag components of large dense core vesicles (LDCVs) and/or specific neuropeptides and to determine whether these reporters can be used to image neurosecretory granule release. In invertebrate systems, there is genetic evidence in *C. elegans* that mutating a neuropeptide precursor processing enzyme (UNC-31) can inhibit the release of some neuropeptides *in vivo* (X. G. Lin et al., 2010; Speese et al., 2007). The composition of neuropeptide processing machinery is well characterized in mammalian

chromaffin cells (Hook et al., 2010; Podvin et al., 2015; Wegrzyn et al., 2010). In bovine adrenal chromaffin cells for instance, 23 different proteases are found in DCVs. However, the catalytic specificity of each protease remains unknown—we have no idea which protease(s) processes which neuropeptide(s). In comparison to chromaffin cells, the understanding of mammalian neurons is even thinner, as neither the composition or specificity in DCVs is known. Therefore, tagging a neuropeptide per se to a fluorescent protein is a more practical way of constructing peptide-specific reporters. Neuropeptide precursor proteins, also called prepropeptides, are cleaved and matured into multiple neuropeptide isoforms. The cleavage sites are di-/tribasic amino acid sequences, whose variety is buttressed by distinct permutations of arginine, lysine, glycine and phenylalanine residues.

We reasoned that an optimal *in vivo* real-time NP release reporter should include (1) a reporter domain that reflects the physico-chemical contrast between the intravesicular milieu and the extracellular space and (2) a sorting domain that ensures its selective trafficking into DCVs. The NP precursor may function as the sorting domain. The sorting domain candidates will be various truncates of neuropeptide prepropeptides, and the reporter domain candidates will include a collection of previously reported fluorescent proteins whose biophysical properties provide contrast to reflect differences between intravesicular and extracellular microenvironments, such as pH, free calcium, and potentially others. The configurations of reporter domains in relation to the sorting domain, as well as the presence or absence of cleavage sites, are also considered in the design of these reporters.

Neuropeptides and their processing enzymes are evolutionarily conserved (Hoyle, 1998). It is highly likely that the development and engineering of NP reporters can be done in multiple model organisms in a similar fashion. Our lab has a long term interest in investigating neuropeptides and their behavioral relevance in fruit flies (Asahina et al., 2014; Hergarden et al., 2012; Tayler et al., 2012) and mice (Zelikowsky et al., 2018). Therefore, we selected our neuropeptides of interest based on the current understanding of biological process and the research relevance to our lab for prototypical studies. In Chapter 2, I will introduce a neuropeptide release reporter for *Drosophila* tachykinin (dTK) in flies. In Chapters 3-4, I included clinical significance as another dimension for the selection of neuropeptide in mammalian cell lines, which are heavily used and hold huge potential for large-scale drug screening that targets neuropeptide signaling (Figure 1A) (Hökfelt et al., 2003).

Exploring Novel Therapeutics with Genetically Engineered Reporters

A variety of psychiatric and metabolic disorders are associated with the dysfunction of neuropeptide signaling pathways (Griebel & Holsboer, 2012). For example, it is widely believed that disrupted cholecystokinin (CCK), neurokinin (NK), and corticotropin-release factor (CRF) pathways cause depression and anxiety (Bowers et al., 2012; Schank et al., 2012); abnormal neuropeptide Y (NPY) and Agouti-Related Peptide (AGRP) signaling results in feeding disorders which can potentially lead to obesity (Arora & Anubhuti, 2006; Dhillo & Bloom, 2001), Calcitonin gene-related peptide (CGRP) and substance P are thought to be related to the transmission of pain (Hökfelt et al., 2001; Russell et al., 2014). The list goes on. A huge battery of drugs has been developed in the hopes that targeting neuropeptide pathways will lead to novel therapies for neuropsychiatric, neurodegenerative, or

neurometabolic disorders. These drugs primarily function by competitively binding to a specific neuropeptide receptor to antagonize the binding of the endogenous peptide. Drugs that survived clinical trials can prove to be a big success. For example, Aimovig (erenumab), a potent CGRP receptor blocker (to CGRP-R1, specifically) generated by Amgen, is a highly acclaimed, novel therapy for the prevention of migraine (King et al., 2019) .

Many potential neuropeptide receptor antagonists, however, fail in the clinical trials. For example, one of the pharma industry's most notable failures was MK-869, a Substance P receptor (NK1) antagonist, which was developed by Merck as a novel therapy for depression (Argyropoulos & Nutt, 2000; Kramer et al., 1998). One potential reason that receptor antagonists may fail in the clinical phase is that each neuropeptide often exerts its function via multiple, functionally redundant receptors, instead of through one-to-one ligand/receptor correspondence. Therefore, inhibiting just one receptor may not suffice to have any effect. While combining multiple receptor antagonists for a given neuropeptide is possible, in theory, the potential for unwanted side- and off-target effects increases with each additional drug.

The complementary approach to blocking neuropeptide receptors is to block the synthesis, release, or function of the neuropeptide itself. Indeed, eptinezumab, a blocking monoclonal antibody to CGRP, has also been FDA-approved for migraine treatment (Edvinsson et al., 2018). An advantage of blocking the neuropeptide, rather than its receptor, is that receptor-binding antibodies, by inducing conformational changes in their targets, could cause unwanted signaling events in the receptor-expressing neurons, whereas neuropeptide-

binding antibodies would not. A problem with using monoclonal antibodies to treat neuropsychiatric or neurodegenerative disorders, however, is that they are macromolecules that do not cross the blood-brain barrier (BBB). While small molecule compounds that cross the BBB can be effective neuropeptide receptor antagonists, there is no rational pathway to design small-molecule inhibitors that bind to the neuropeptide itself.

The advent and iteration of cutting-edge technologies, such as CRISPR-Cas9 (Hsu et al., 2014), recombinant antibody (Holliger & Hudson, 2005; Hoogenboom, 2005), genetically-encoded biosensors (Lin & Schnitzer, 2016), and viral delivery (Berns & Muzyczka, 2017; Hudry & Vandenberghe, 2019), enabled us to explore the uncharted path to targeting neuropeptide signaling for treating human diseases. In the long term, we aim to establish and streamline an imaging platform that combines optimal neuropeptide reporters, cell lines, and imaging techniques. The platform potentially enables us to integrate modern biotechnologies, and collectively constitute a therapeutic ecosystem (Figure 1B).

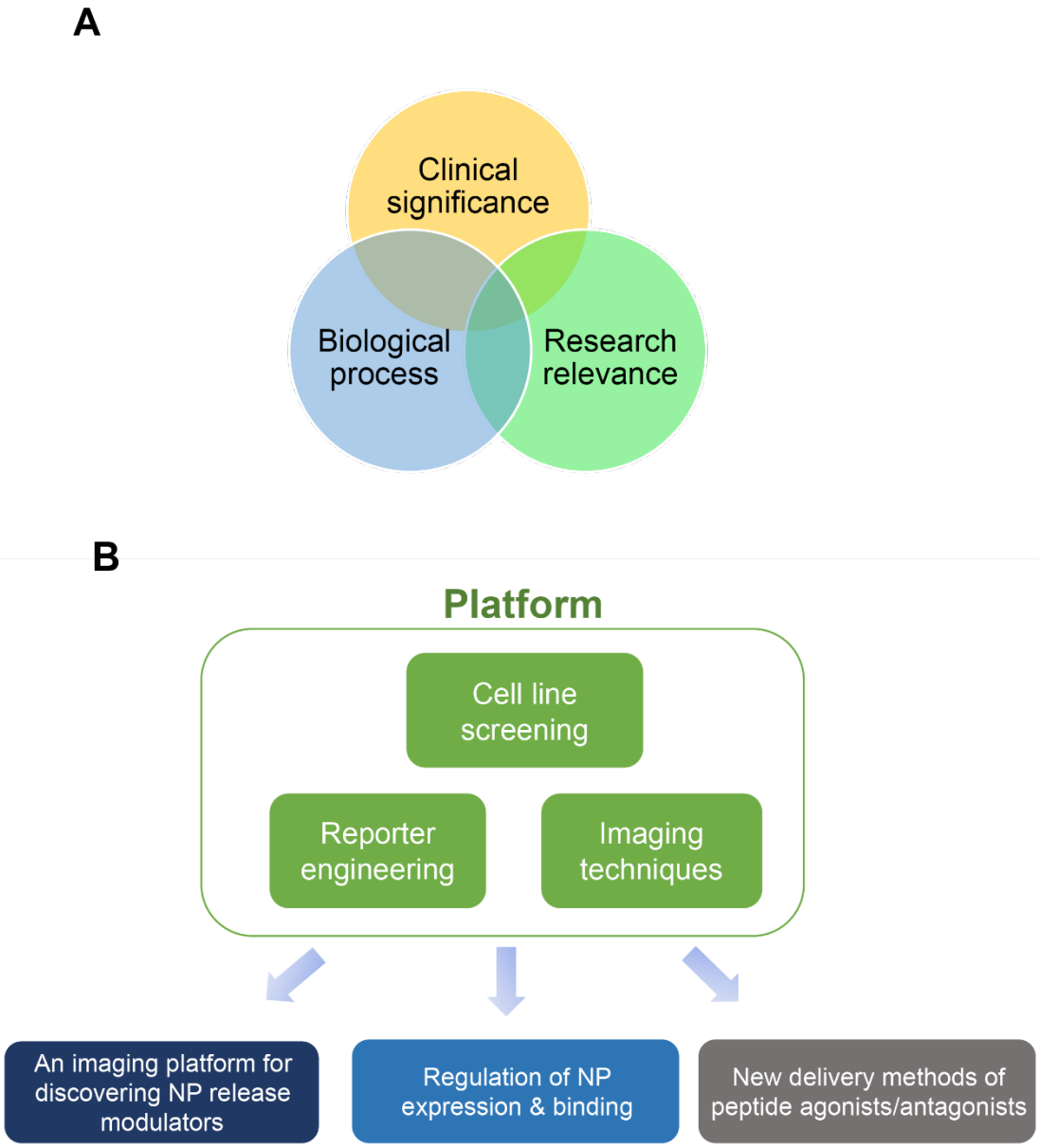

Figure 1: Rationales and visions of imaging neuropeptides

(A) Over 100 neuropeptides are identified. To shortlist our neuropeptide of interest, we consider three dimensions: understanding of biological process, relevance to current research, and clinical significance. (B) The neuropeptide imaging ecosystem. The long-term plan is to establish a platform that contains optimal reporters, cell lines and proper imaging techniques. With it we will further branch out to three arms: the discovery of neuropeptide release modulators, means to regulate neuropeptide expression and binding, and new delivery methods of peptide agonists and antagonists.

References

Agrawal, P., Kumar, S., Singh, A., Raghava, G. P. S., & Singh, I. K. (2019). NeuroPIpred: a tool to predict, design and scan insect neuropeptides. *Scientific Reports*. https://doi.org/10.1038/s41598-019-41538-x

Argyropoulos, S. V, & Nutt, D. J. (2000). Substance P antagonists: Novel agents in the treatment of depression. *Expert Opinion on Investigational Drugs*. https://doi.org/10.1517/13543784.9.8.1871

Arora, S., & Anubhuti. (2006). Role of neuropeptides in appetite regulation and obesity - A review. *Neuropeptides*. https://doi.org/10.1016/j.npep.2006.07.001

Asahina, K., Watanabe, K., Duistermars, B. J., Hoopfer, E., González, C. R., Eyjólfsdóttir, E. A., Perona, P., & Anderson, D. J. (2014). Tachykinin-expressing neurons control male-specific aggressive arousal in drosophila. *Cell*, *156*(1–2), 221–235. https://doi.org/10.1016/j.cell.2013.11.045

Bargmann, C. I., & Marder, E. (2013). From the connectome to brain function. *Nature Methods*. https://doi.org/10.1038/nmeth.2451

Benveniste, H., & Hüttemeier, P. C. (1990). Microdialysis-Theory and application. *Progress in Neurobiology*. Prog Neurobiol. https://doi.org/10.1016/0301-0082(90)90027-E

Berns, K. I., & Muzyczka, N. (2017). AAV: An Overview of Unanswered Questions. *Human Gene Therapy*. https://doi.org/10.1089/hum.2017.048

Bowers, M. E., Choi, D. C., & Ressler, K. J. (2012). Neuropeptide regulation of fear and anxiety: Implications of cholecystokinin, endogenous opioids, and neuropeptide Y. *Physiology and Behavior*. https://doi.org/10.1016/j.physbeh.2012.03.004

Dhillo, W. S., & Bloom, S. R. (2001). Hypothalamic peptides as drug targets for obesity. *Current Opinion in Pharmacology*. https://doi.org/10.1016/S1471-4892(01)00110-2

Edvinsson, L., Haanes, K. A., Warfvinge, K., & Krause, Di. N. (2018). CGRP as the target of new migraine therapies - Successful translation from bench to clinic. *Nature Reviews Neurology*. https://doi.org/10.1038/s41582-018-0003-1

Ernberg, M. M., & Alstergren, P. J. (2004). Microdialysis of neuropeptide Y in human muscle tissue. *Journal of Neuroscience Methods*, *132*(2), 185–190. https://doi.org/10.1016/j.jneumeth.2003.09.009

Frost, S. I., Keen, K. L., Levine, J. E., & Terasawa, E. (2008). Microdialysis methods for in vivo neuropeptide measurement in the Stalk-median eminence in the Rhesus monkey. *Journal of Neuroscience Methods*, *168*(1), 26–34. https://doi.org/10.1016/j.jneumeth.2007.09.001

Griebel, G., & Holsboer, F. (2012). Neuropeptide receptor ligands as drugs for psychiatric diseases: The end of the beginning? *Nature Reviews Drug Discovery*. https://doi.org/10.1038/nrd3702

Hergarden, A. C., Tayler, T. D., & Anderson, D. J. (2012). Allatostatin-A neurons inhibit feeding behavior in adult Drosophila. *Proceedings of the National Academy of Sciences of the United States of America*, *109*(10), 3967–3972. https://doi.org/10.1073/pnas.1200778109

Hökfelt, T., Bartfai, T., & Bloom, F. (2003). Neuropeptides: Opportunities for drug discovery. *Lancet Neurology*. https://doi.org/10.1016/S1474-4422(03)00482-4

Hökfelt, T., Pernow, B., & Wahren, J. (2001). Substance P: A pioneer amongst neuropeptides. *Journal of Internal Medicine*. https://doi.org/10.1046/j.0954-6820.2000.00773.x

Holliger, P., & Hudson, P. J. (2005). Engineered antibody fragments and the rise of single domains. *Nature Biotechnology*. https://doi.org/10.1038/nbt1142

Hoogenboom, H. R. (2005). Selecting and screening recombinant antibody libraries. *Nature Biotechnology*. https://doi.org/10.1038/nbt1126

Hook, V., Bark, S., Gupta, N., Lortie, M., Lu, W. D., Bandeira, N., Funkelstein, L., Wegrzyn, J., O'Connor, D. T., & Pevzner, P. (2010). Neuropeptidomic components generated by proteomic functions in secretory vesicles for cell-cell communication. *AAPS Journal*. https://doi.org/10.1208/s12248-010-9223-z

Hoyle, C. H. V. (1998). Neuropeptide families: Evolutionary perspectives. *Regulatory Peptides*. https://doi.org/10.1016/S0167-0115(97)01073-2

Hsu, P. D., Lander, E. S., & Zhang, F. (2014). Development and applications of CRISPR-Cas9 for genome engineering. *Cell*. https://doi.org/10.1016/j.cell.2014.05.010

Hudry, E., & Vandenberghe, L. H. (2019). Therapeutic AAV Gene Transfer to the Nervous System: A Clinical Reality. *Neuron*. https://doi.org/10.1016/j.neuron.2019.02.017

King, C. T., Gegg, C. V, Hu, S. N.-Y., Sen Lu, H., Chan, B. M., Berry, K. A., Brankow, D. W., Boone, T. J., Kezunovic, N., Kelley, M. R., Shi, L., & Xu, C. (2019). Discovery of the Migraine Prevention Therapeutic Aimovig (Erenumab), the First FDA-Approved Antibody against a G-Protein-Coupled Receptor. *ACS Pharmacology & Translational Science*, *2*(6), 485–490. https://doi.org/10.1021/acsptsci.9b00061

Kramer, M. S., Cutler, N., Feighner, J., Shrivastava, R., Carman, J., Sramek, J. J., Reines, S. A., Liu, G., Snavely, D., Wyatt-Knowles, E., Hale, J. J., Mills, S. G., MacCoss, M., Swain, C. J., Harrison, T., Hill, R. G., Hefti, F., Scolnick, E. M., Cascieri, M. A., … Rupniak, N. M. J. (1998). Distinct mechanism for antidepressant activity by blockade of central substance P receptors. *Science*. https://doi.org/10.1126/science.281.5383.1640

Lee, D., & Kwon, H. B. (2022). Current and future techniques for detecting oxytocin: Focusing on genetically-encoded GPCR sensors. *Journal of Neuroscience Methods*, *366*, 109407. https://doi.org/10.1016/j.jneumeth.2021.109407

Lin, M. Z., & Schnitzer, M. J. (2016). Genetically encoded indicators of neuronal activity. *Nature Neuroscience*. https://doi.org/10.1038/nn.4359

Lin, X. G., Ming, M., Chen, M. R., Niu, W. P., Zhang, Y. D., Liu, B., Jiu, Y. M., Yu, J. W., Xu, T., & Wu, Z. X. (2010). UNC-31/CAPS docks and primes dense core vesicles in C. elegans neurons. *Biochemical and Biophysical Research Communications*. https://doi.org/10.1016/j.bbrc.2010.05.148

Makos, M. A., Kim, Y. C., Han, K. A., Heien, M. L., & Ewing, A. G. (2009). In vivo electrochemical measurements of exogenously applied dopamine in Drosophila melanogaster. *Analytical Chemistry*, *81*(5), 1848–1854. https://doi.org/10.1021/ac802297b

Makos, M. A., Kuklinski, N. J., Berglund, E. C., Heien, M. L., & Ewing, A. G. (2009). Chemical measurements in Drosophila. *Trends in Analytical Chemistry : TRAC*, *28*(11), 1223–1234. https://doi.org/10.1016/j.trac.2009.08.005

Marder, E., & Bucher, D. (2007). Understanding circuit dynamics using the stomatogastric

nervous system of lobsters and crabs. *Annual Review of Physiology*. https://doi.org/10.1146/annurev.physiol.69.031905.161516

Marder, E., O'Leary, T., & Shruti, S. (2014). Neuromodulation of Circuits with Variable Parameters: Single Neurons and Small Circuits Reveal Principles of State-Dependent and Robust Neuromodulation. *Annual Review of Neuroscience*, *37*(1), 329–346. https://doi.org/10.1146/annurev-neuro-071013-013958

Nusbaum, M. P., Blitz, D. M., & Marder, E. (2017). Functional consequences of neuropeptide and small-molecule co-transmission. *Nature Reviews Neuroscience*. https://doi.org/10.1038/nrn.2017.56

Pert, C., Ruff, M., Weber, R., & Herkenham, M. (1985). Neuropeptides and their receptors: a psychosomatic network. *The Journal of Immunology*, *135*(2).

Podvin, S., Bundey, R., Toneff, T., Ziegler, M., & Hook, V. (2015). Profiles of secreted neuropeptides and catecholamines illustrate similarities and differences in response to stimulation by distinct secretagogues. *Molecular and Cellular Neuroscience*, *68*, 177–185. https://doi.org/10.1016/j.mcn.2015.06.008

Rotzinger, S., Lovejoy, D. A., & Tan, L. A. (2010). Behavioral effects of neuropeptides in rodent models of depression and anxiety. *Peptides*. https://doi.org/10.1016/j.peptides.2009.12.015

Russell, F. A., King, R., Smillie, S. J., Kodji, X., & Brain, S. D. (2014). Calcitonin gene-related peptide: physiology and pathophysiology. *Physiological reviews*. https://doi.org/10.1152/physrev.00034.2013

Russo, A. F. (2017). Overview of Neuropeptides: Awakening the Senses? *Headache*, *57*(Suppl 2), 37–46. https://doi.org/10.1111/head.13084

Schank, J. R., Ryabinin, A. E., Giardino, W. J., Ciccocioppo, R., & Heilig, M. (2012). Stress-Related Neuropeptides and Addictive Behaviors: Beyond the Usual Suspects. *Neuron*. https://doi.org/10.1016/j.neuron.2012.09.026

Speese, S., Petrie, M., Schuske, K., Ailion, M., Ann, K., Iwasaki, K., Jorgensen, E. M., & Martin, T. F. J. (2007). UNC-31 (CAPS) is required for dense-core vesicle but not synaptic vesicle exocytosis in Caenorhabditis elegans. *Journal of Neuroscience*. https://doi.org/10.1523/JNEUROSCI.1466-07.2007

Tayler, T. D., Pacheco, D. A., Hergarden, A. C., Murthy, M., & Anderson, D. J. (2012). A neuropeptide circuit that coordinates sperm transfer and copulation duration in Drosophila. *Proceedings of the National Academy of Sciences of the United States of America*, *109*(50), 20697–20702. https://doi.org/10.1073/pnas.1218246109

van den Pol, A. N. (2012). Neuropeptide Transmission in Brain Circuits. *Neuron*. https://doi.org/10.1016/j.neuron.2012.09.014

Wang, F., & Pereira, A. (2016). Neuromodulation, Emotional Feelings and Affective Disorders. *Mens Sana Monographs*. https://doi.org/10.4103/0973-1229.154533

Wegrzyn, J. L., Bark, S. J., Funkelstein, L., Mosier, C., Yap, A., Kazemi-Esfarjani, P., La Spada, A. R., Sigurdson, C., Oconnor, D. T., & Hook, V. (2010). Proteomics of dense core secretory vesicles reveal distinct protein categories for secretion of neuroeffectors for cell-cell communication. *Journal of Proteome Research*. https://doi.org/10.1021/pr1003104

Zelikowsky, M., Ding, K., & Anderson, D. J. (2018). Neuropeptidergic Control of an Internal Brain State Produced by Prolonged Social Isolation Stress. *Cold Spring*

Harbor Symposia on Quantitative Biology, *83*, 97–103. https://doi.org/10.1101/SQB.2018.83.038109

Zhang, X., Bao, L., & Ma, G.-Q. (2010). Sorting of neuropeptides and neuropeptide receptors into secretory pathways. *Progress in Neurobiology*, *90*(2), 276–283. https://doi.org/10.1016/J.PNEUROBIO.2009.10.011

Chapter 2

IMAGING NEUROPEPTIDE RELEASE AT *DROSOPHILA* SYNAPSES WITH A GENETICALLY ENGINEERED REPORTER

Ding, K., Han, Y., Seid, T. W., Buser, C., Karigo, T., Zhang, S., Dickman, D. K., & Anderson, D. J. (2019). Imaging neuropeptide release at synapses with a genetically engineered reporter. *ELife*, *8*. https://doi.org/10.7554/elife.46421

Han, Y., & Ding, K. (2022). Imaging Neuropeptide Release at *Drosophila* Neuromuscular Junction with a Genetically Engineered Neuropeptide Release Reporter. *Methods in Molecular Biology*, 2417, 193–203. https://doi.org/10.1007/978-1-0716-1916-2_15

Summary

Research on neuropeptide function has advanced rapidly, yet there is still no spatio-temporally resolved method to measure the release of neuropeptides *in vivo*. Here we introduce Neuropeptide Release Reporters (NPRRs): novel genetically-encoded sensors with high temporal resolution and genetic specificity. Using the *Drosophila* larval neuromuscular junction (NMJ) as a model, we provide evidence that NPRRs recapitulate the trafficking and packaging of native neuropeptides, and report stimulation-evoked neuropeptide release events as real-time changes in fluorescence intensity, with sub-second temporal resolution.

Introduction

Neuropeptides (NPs) exert an important but complex influence on neural function and behavior (Bargmann & Marder, 2013; Hokfelt et al., 2000; Insel & Young, 2000; Nassel & Winther, 2010). A major lacuna in the study of NPs is the lack of a method for imaging NP release *in vivo*, with subcellular spatial resolution and subsecond temporal resolution. Available techniques for measuring NP release include microdialysis (Kendrick, 1990), antibody-coated microprobes (Schaible, Jarrott, Hope, & Duggan, 1990), and GFP-tagged propeptides visualized either by standard fluorescence microscopy (van den Pol, 2012), or by TIRF imaging of cultured neurons (Xia, Lessmann, & Martin, 2009). In *Drosophila*, a fusion between rat Atrial Natriuretic Peptide/Factor (ANP/F) and GFP was used to investigate neuropeptide trafficking at the fly neuromuscular junction (NMJ) (Rao, Lang, Levitan, & Deitcher, 2001). Release was measured indirectly, as a decrease in ANP-GFP fluorescence intensity at nerve terminals reporting residual unreleased peptide, on a time-scale of seconds (Wong, Cavolo, & Levitan, 2015). None of these methods combined NP specificity, genetically addressable cell type-specificity, high temporal resolution and applicability to *in vivo* preparations (Supplementary Table 1). A major challenge is to develop a tool that encompasses all these features for direct, robust measurement of NP release *in vivo*.

Results

Neuropeptides are synthesized as precursors, sorted into dense core vesicles (DCVs), post-translationally modified and cleaved into active forms prior to release (Taghert & Veenstra, 2003). We reasoned that an optimal *in vivo* real-time NP release reporter should include (1) a reporter domain that reflects the physico-chemical contrast between the intravesicular milieu and the extracellular space (Figure 1—figure supplement 1A); and (2) a sorting domain that ensures its

selective trafficking into DCVs (Figure 1—figure supplement 1b). The NP precursor may function as the sorting domain, suggested by studies of DCV fusion using pIAPP-EGFP (Barg et al., 2002) and NPY-pHluorin (Zhu et al., 2007) in cultured neurons, or ANP-GFP in *Drosophila* (Rao et al., 2001). We therefore developed a pipeline to screen various transgenes comprising NP precursors fused at different sites to fluorescent reporters, in adult flies (Figure 1—figure supplement 1B-C). A total of 54 constructs were tested. We found that optimal trafficking was achieved by substituting the reporter for the NP precursor C-terminal domain that follows the final peptide (Figure 1—figure supplement 1B). In order to maintain covalent linkage with the reporter domain, we removed the dibasic cleavage site C-terminal to the final peptide.

The DCV lumen has lower pH and free calcium (pH = 5.5-6.75, $[Ca^{2+}]$ ~30 μM) compared to the extracellular space (pH =7.3, $[Ca^{2+}]$ ~2 mM) (Mitchell et al., 2001; Sturman, Shakiryanova, Hewes, Deitcher, & Levitan, 2006). These differences prompted us to test validated sorting domains in a functional *ex vivo* screen using either pH-sensitive fluorescent proteins (Miesenbock, De Angelis, & Rothman, 1998) or genetically-encoded calcium indicators (GECIs) (Lin & Schnitzer, 2016; Tian, Hires, & Looger, 2012) (Figure 1—figure supplement 1A-D). Reporters based on pHluorins (Miesenbock et al., 1998) did not perform well in our hands, therefore we focused on GCaMP6s (Chen et al., 2013). The calcium sensitivity threshold of GCaMP6s is below the calcium concentration in both DCVs and the extracellular space. However, GCaMP6s fluorescence is quenched in the acidic DCV lumen (Barykina et al., 2016), enabling it to function as a dual calcium/pH indicator (Figure 1A). These key properties should boost the contrast between GCaMP6s fluorescence in unreleased vs. released DCVs, potentially allowing us to trace NP release at the cellular level *in vivo*.

We sought to test several NP precursor-GCaMP6s fusion proteins, called NPRRs (NeuroPeptide Release Reporters; unless otherwise indicated all NPRRs refer to fusions with GCaMP6s), in an intact preparation using electrical stimulation to evoke release. Initially for proof-of-principle experiments, we used the Dro*sophila* larval NMJ to test $NPRR^{ANP}$, a GCaMP6s fusion with rat ANP (Burke et al., 1997). NMJ terminals are large, individually identifiable, and easy to image and record. In particular, boutons on muscle 12/13 are diverse—Type Ib and Type Is boutons contain mostly synaptic vesicles and few DCVs, while Type III boutons contain an abundance of DCVs but no synaptic vesicles (Menon, Carrillo, & Zinn, 2013); moreover, Type III-specific GAL4 drivers are available (Koon & Budnik, 2012) (Figure 1B).

Expression of $NPRR^{ANP}$ pan-neuronally (under the control of nsyb-GAL4) followed by double immuno-staining for ANP and GCaMP (anti-GFP) indicated that the sorting domain and the reporter domains showed a similar localization in Type III neurons (Figure 1—figure supplement 2). Moreover, the distribution of $NPRR^{ANP}$ overlapped that of Bursicon (Figure 1—figure supplement 3D), an NP that is endogenously expressed in Type III neurons (Loveall & Deitcher, 2010). Both GCaMP and Bursicon immunoreactivity were strongest within boutons, consistent with the known subcellular localization of DCVs (Gorczyca & Budnik, 2006).

Glutamate is the only known canonical neurotransmitter used at the larval NMJ (Menon et al., 2013). This allowed visualization of the subcellular localization of small synaptic vesicles (SV) by immuno-staining for vGluT, a vesicular glutamate transporter (Fremeau et al., 2001; Kempf et al., 2013). In Type Ib neurons (which contain relatively few DCVs relative to SVs (Menon et al., 2013)), vGluT

staining was observed as patches with dim center, which may reflect clustered SVs, while $NPRR^{ANP}$ immunoreactivity was seen in dispersed, non-overlapping punctae (Figure 1C, α-GFP, inset). In Type III neurons, NPRRs were strongly expressed but no vGluT immunoreactivity was detected (Figure 1C). The subcellular distribution of this NPRR in larval NMJ neurons, therefore, is similar to that of other DCV-targeted markers previously used in this system (Rao et al., 2001; Shakiryanova, Tully, & Levitan, 2006), and appears to reflect exclusion from SVs.

The diffraction limit of light microscopy precluded definitive co-localization of NPRRs in DCVs. Therefore, we employed Immuno-Electron microscopy (Immuno-EM) to investigate the subcellular localization of NPRRs at the nanometer scale. To maximize antigenicity for Immuno-EM, we generated constructs that replaced GCaMP6s with GFP ($NPRR^{ANP\text{-}GFP}$;). $NPRR^{ANP\text{-}GFP}$ showed dense labeling in association with DCVs (Figure 1D, arrows), where the average number of gold particles/μm^2 was substantially and significantly higher than in neighboring bouton cytoplasm (DCV/Bouton ~14.26) (Figure 1E, Supplementary Table 2). Taken together, these data indicate that $NPRR^{ANP\text{-}GFP}$ is localized to DCVs. By extension, they suggest that $NPRR^{ANP\text{-}GCaMP6s}$ (which has an identical structure to $NPRR^{ANP\text{-}GFP}$ except for the modifications that confer calcium sensitivity) is similarly packaged in DCVs. While these two reporters show indistinguishable distributions by immunofluorescence, we cannot formally exclude that the substitution of GCaMP for GFP may subtly alter subcellular localization of the NPRR in a manner undetectable by light microscopy.

To measure the release of NPRRs from DCVs, we next expressed $NPRR^{ANP}$ in Type III neurons using a specific GAL4 driver for these cells (Koon & Budnik, 2012) (Figure 2E and Figure 1—figure supplement 3D). We delivered 4 trials of 70 Hz electrical stimulation to the nerve bundle, a

frequency reported to trigger NP release as measured by ANF-GFP fluorescence decrease (Rao et al., 2001; Shakiryanova et al., 2006), and used an extracellular calcium concentration that promotes full fusion mode (Ales et al., 1999). This stimulation paradigm produced a relative increase in $NPRR^{ANP}$ fluorescence intensity (ΔF/F), whose peak magnitude increased across successive trials (Figure 2A, red bars and 2D; Video 1; Figure 2—figure supplement 1, A_1 vs. A_7). Responses in each trial showed a tri-phasic temporal pattern: (1) In the "rising" phase, $NPRR^{ANP}$ ΔF/F peaked 0.5-5 secs after stimulation onset, in contrast to the virtually instantaneous peak seen in positive control specimens expressing conventional GCaMP6s in Type III neurons (Figure 2A-B). The $NPRR^{ANP}$ latency to peak was similar to the reported DCV fusion latency following depolarization in hippocampal neurons (Xia et al., 2009). This delay is thought to reflect the kinetic difference between calcium influx and DCV exocytosis due to the loose association between DCVs and calcium channels (Xia et al., 2009). (2) In the "falling" phase, $NPRR^{ANP}$ ΔF/F began to decline 1-5 seconds before the termination of each stimulation trial, presumably reflecting depletion of the available pool of releasable vesicles. In contrast, GCaMP6s fluorescence did not return to baseline until after stimulation offset (Figure 2A-B). (3) Finally, unlike GCaMP6s, $NPRR^{ANP}$ exhibited an "undershoot" (ΔF/F below baseline) during the post-stimulation intervals, followed by a "recovery" phase (Figure 2A; Figure 2C, I1-4). This undershoot may reflect dilution of released fluorescent NPRR molecules by diffusion into the synaptic cleft (van den Pol, 2012), while recovery may reflect DCV replenishment in the boutons from vesicles proximal to the imaged release site.

Because $NPRR^{ANP}$ fluorescence was preferentially accumulated within boutons, we asked whether these regions contributed to ΔF/F peaks more significantly than the inter-bouton intervals (IBIs). To do this, we partitioned the processes into boutons and IBI fields (Figure 2—figure supplement 2A), and compared the ΔF/F in these regions during stimulation trials. The time-averaged ratio of

bouton/IBI ΔF/F (see Materials and Methods) was significantly higher for $NPRR^{ANP}$ than for GCaMP6s, particularly during later stimulation trials (Figure 2—figure supplement 2B, green bars, S2-4). This contrast indicates that $NPRR^{ANP}$ signals are preferentially observed in boutons, where DCVs are located, and do not reflect differences in cytoplasmic free Ca^{2+} levels between these regions as detected by GCaMP6s.

To test definitively if $NPRR^{ANP}$ ΔF/F signals are dependent upon NP release, we blocked vesicle fusion at terminals of Type III neurons using expression of tetanus toxin light chain (TNT) (Sweeney, Broadie, Keane, Niemann, & O'Kane, 1995), a protease that cleaves n-synaptobrevin, a v-snare required for DCV fusion (Figure 2—figure supplement 3) (T. Xu, Binz, Niemann, & Neher, 1998). As a control, we used impotent TNT (TNT^{imp}), a reduced activity variant (Sweeney et al., 1995). TNT expression completely abolished stimulation-induced ΔF/F increases from $NPRR^{ANP}$, while TNT^{imp} did not (Figure 2F). Further analysis revealed that both the ΔF/F peaks and inter-stimulation undershoots were diminished by TNT (Figure 2G-H). In contrast, neither TNT nor TNT^{imp} affected the kinetics of GCaMP6s signals in Type III neurons (Figure 2—figure supplement 2C), which report cytosolic Ca^{2+} influx. Taken together, these data support the idea that $NPRR^{ANP}$ signals specifically reflect DCV release.

ANP is a rat NP that lacks a *Drosophila* homolog (Rao et al., 2001). To determine whether our method could be applied to detect the release of a specific, endogenous fly NP, we tested $NPRR^{dTK}$, one of 6 different reporter variants we initially generated from the *Drosophila* neuropeptide precursor, DTK (Figure 1—figure supplement 1B). In contrast to ANP which encodes a single peptide, DTK yields multiple NP derivatives (Winther, Siviter, Isaac, Predel, & Nassel, 2003). Light

microscopy (Figure 3A) and Immuno-EM (Figure 3B, arrows) confirmed that NPRR^{dTK}, like NPRR^{ANP}, was localized to DCVs (DCV/bouton ~22.19, Figure 3C). Using the Type III-specific GAL4 driver to express NPRR^{dTK} and the same stimulation protocol as used for NPRR^{ANP}, the basic tri-phasic response profile was also observed (Figure 3D). However, peak heights and baseline fluorescence fell progressively with successive stimulation trials (Figure 3E), in contrast to NPRR^{ANP} where the first peak and undershoot were lower (Figure 2C-D). The reason for this difference is currently unclear.

We next investigated the relationship between NPRR signal and stimulation intensity, by delivering to the Type III neurons a series of low to high frequency electrical stimuli (1-70 Hz; (Levitan, Lanni, & Shakiryanova, 2007)) while imaging the nerve terminals. For direct comparison of NPRR responses across different preparations, we applied *a posteriori normalization of fluorescent peaks in each trial to the highest response obtained among all trials.* For both NPRR^{ANP} and NPRR^{dTK} (Figure 4A-B), the peak responses showed a positive correlation with stimulation frequency, analogous to that observed using cytosolic GCaMP6s (Figure 4C). In Type III neurons, the responses of both NPRRs to stimulation frequencies<30 Hz (1,5,10,20 Hz) were not statistically significant from zero. NPRR^{ANP} showed a higher sensitivity to high stimulation frequencies (30 Hz: 18.14%, 50 Hz: 82.40% Normalized peak $\Delta F/F$), while NPRR^{dTK} showed a higher stimulation threshold and lower sensitivity (30Hz: 3.57%, 50Hz: 24.67% Normalized peak $\Delta F/F$).

We next investigated whether the relatively high stimulation frequency required to observe significant responses with NPRRs was a function of the reporters, or rather of the cell class in which they were tested. To do this, we expressed both NPRRs in Type Ib neurons, a class of motor neurons

that contains both SVs and DCVs (Figure 1B, Figure 4D-F), and performed stimulation frequency titration experiments. Strikingly, in Type Ib neurons, significant increases in ΔF/F could be observed at frequencies as low as 10 Hz (Figure 4D, E; $NPRR^{ANP}$ @ 20 Hz: 12.50%, $NPRR^{dTK}$ @ 20 Hz: 17.67% normalized peak ΔF/F). The reason for the difference in NPRR threshold between Type III and Type Ib neurons is unknown, but parallels their difference in GCaMP6s response to electrical stimulation (Figure. 4C vs. 4F).

Notably, although $NPRR^{ANP}$ and $NPRR^{dTK}$ presented distinct response profiles in Type III neurons, their performance in Type Ib neurons was more similar (Fig. 4A vs. 4B; cf. 4D vs. 4E). In summary, the differences in performance we observed between the two NPRRs appeared to be specific to Type III neurons, and were minor in comparison to the differences in performance of both reporters between the two cell classes in. The reason for the differences between $NPRR^{ANP}$ and $NPRR^{dTK}$ sensitivity and kinetics in Type III neurons is unknown but may reflect differences in how well these reporters compete with the high levels of endogenous neuropeptide (Bursicon) for packaging, transport or release.

Discussion

Here we present proof-of-principle for a method to detect the release of different neuropeptides in intact neural tissue, with subcellular spatial and sub-second temporal resolution. By exploiting the fluorescent change of GCaMP in response to a shift in pH and $[Ca^{2+}]$, we visualized the release of neuropeptides by capturing the difference between the intravesicular and extracellular microenvironment. NPRR responses exhibited triphasic kinetics, including rising, falling and recovery phases. In the falling phase, a post-stimulus "undershoot," was observed in which the

fluorescent intensity fell below pre-stimulation baseline. This undershoot presumably reflects the slow kinetics of DCV replenishment relative to release.

The molecular mechanisms of NP release are incompletely understood (Tao Xu & Xu, 2008). It is possible that individual DCVs only unload part of their cargo during stimulation, in which case many DCVs that underwent fusion may still contain unreleased NPRR molecules following a stimulus pulse. Although we are convinced that NPRR signals do indeed reflect NP release, due to the presence of the recovery phase, we cannot formally exclude that unreleased NPRRs may contribute to the signal change due to their experience of intravesicular $[Ca^{2+}]$/pH changes that occur during stimulation. To resolve this issue in the future, an ideal experiment would be to co-express an NPRR together with a $[Ca^{2+}]$/pH-invariant NP-reporter fusion. Multiple attempts to generate such fusions with RFP were unsuccessful, due to cryptic proteolytic cleavage sites in the protein which presumably result in degradation by DCV proteases during packaging.

To test if $NPRR^{ANP}$ $\Delta F/F$ signals are dependent on NP release, we expressed the light chain of tetanus toxin (TNT), a reagent shown to effectively block NP release in many (Hentze, Carlsson, Kondo, Nassel, & Rewitz, 2015; McNabb & Truman, 2008; Zandawala et al., 2018), if not all (Umezaki, Yasuyama, Nakagoshi, & Tomioka, 2011), systems. We observed a striking difference in NPRR kinetics in flies co-expressing TNT vs. its proteolytically inactive "impotent" control form TNT^{imp} (Figure 2F). The strong reduction of NPRR signals by TNT-mediated n-syb cleavage is consistent with the idea that these signals reflect the release of NPRRs from DCVs.

We have tested the generalizability of the principles used to generate NPRRs by (1) constructing a surrogate NP reporter $NPRR^{ANP}$ as well as a multi-peptide-producing endogenous *Drosophila* NP reporter $NPRR^{dTK}$ (Figure 2-3); (2) characterized NPRR signals in response to varying intensities of electrical stimulation; and (3) recorded NPRR signals in two different classes of NMJ motor neurons containing DCVs with or without SVs, respectively (Figure 4). These experiments revealed, to our surprise, that NPRR responses exhibit cell-type specific characteristics (Figure 4). As NPRRs are applied to other neuropeptides and cell types, a systematic characterization of neuropeptide release properties in different peptidergic neurons should become possible, furthering our understanding of neuropeptide biology.

The method described here can, in principle, be extended to an *in vivo* setting. This would open the possibility of addressing several important unresolved issues in the study of NP function *in vivo*. These include the "which" problem (which neuron(s) release(s) NPs under particular behavioral conditions?); the "when" problem (when do these neurons release NPs relative to a particular behavior or physiological event?); the "where" problem (are NPs released from axons, dendrites or both?); and the "how" problem (how is NP release regulated?). The application of NPRRs to measuring NP release dynamics in awake, freely behaving animals may yield answers to these important long-standing questions.

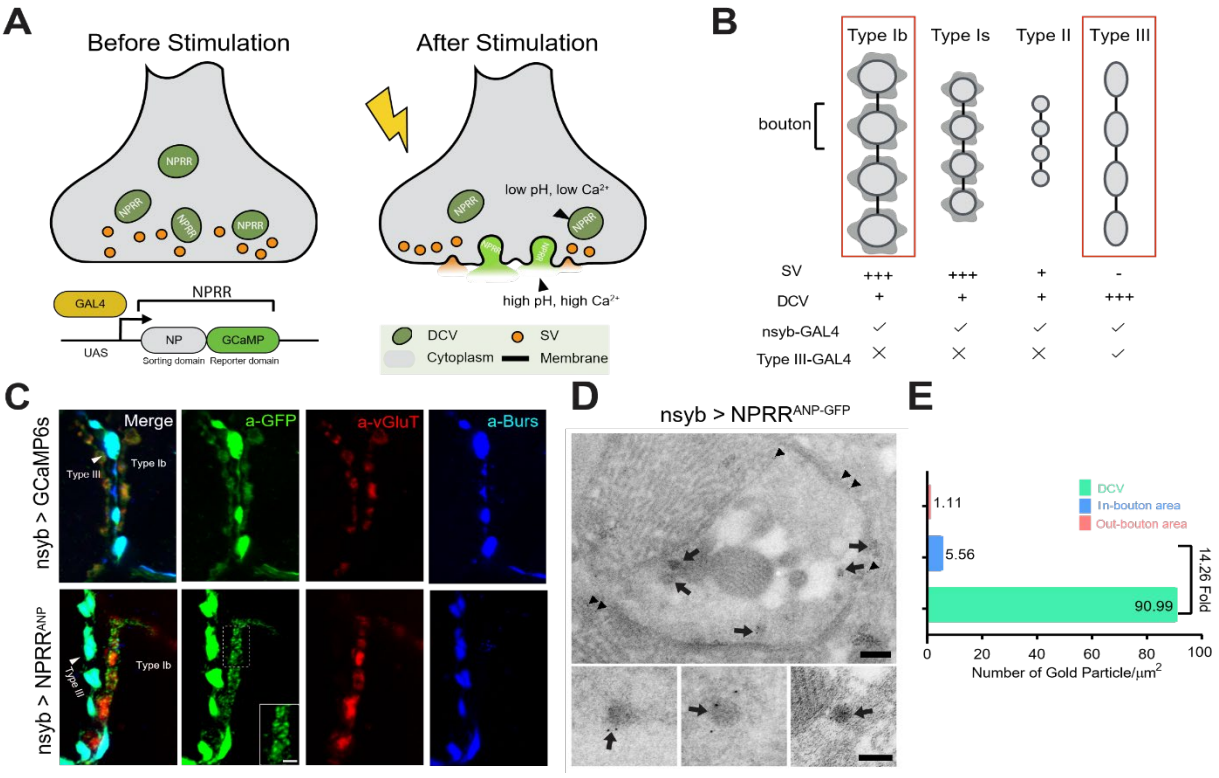

Figure 1: **Localization of an NPRR.**

(A) Schematic illustrating the principle of NPRRs (**N**euro**p**eptide **R**elease **R**eporters). NPRR molecules in the DCV lumen (low pH/low calcium, *left*) exhibit increased fluorescence when released by fusion into the extracellular space (neutral pH/high calcium, *right*). NPRR fluorescent signal is expected to decay following diffusion into the synaptic cleft. New NPRR-containing DCVs are produced by synthesis and transport from the soma, not by recycling. NP: Neuropeptide. DCV: Dense Core Vesicle. SV: Synaptic Vesicle. **(B)** Distinct motor neuron subtypes at the *Drosophila* NMJ (muscle 12/13) have different proportions of DCVs vs. SVs. The GAL4 driver R57C10-Gal4 (nsyb-GAL4) labels all subtypes, while R20C11-GAL4 selectively labels only Type III neurons, which lack SVs ("Type III-GAL4"). Light grey circles, black lines and dark grey shading represent boutons, inter-bouton intervals and subsynaptic reticulum, respectively. The studies in this paper focus on Type Ib neurons and Type III neurons (in red rectangles). **(C)** Triple immunolabeling for GFP (green), Bursicon (blue) and vGluT (red), in flies containing nsyb-GAL4 driving UAS-GCaMP6s *(upper)*, or $NPRR^{ANP}$ (*lower*). Type Ib and Type III boutons are indicated. Scale bar, 5 μm. Inset image ($NPRR^{ANP}$, a-GFP channel) shows details of puncta distribution of $NPRR^{ANP}$ in Type Ib neuron. Scale bar, 2 μm. **(D)** TEM images of boutons immunolabeled with anti-GFP (5 nm gold particle-conjugated) to detect nsyb>$NPRR^{ANP\text{-}GFP}$, which has an identical structure to $NPRR^{ANP}$, but is a GFP rather than GCaMP6s fusion to improve antigenicity. Note strong labeling in DCVs (arrows) and the neuronal plasma membrane (arrowheads). Scale bar, 200 nm. Lower panel shows representative images of labeled DCVs. Scale bar,100 nm. **(E)** Quantification for TEM images in **(D)**.

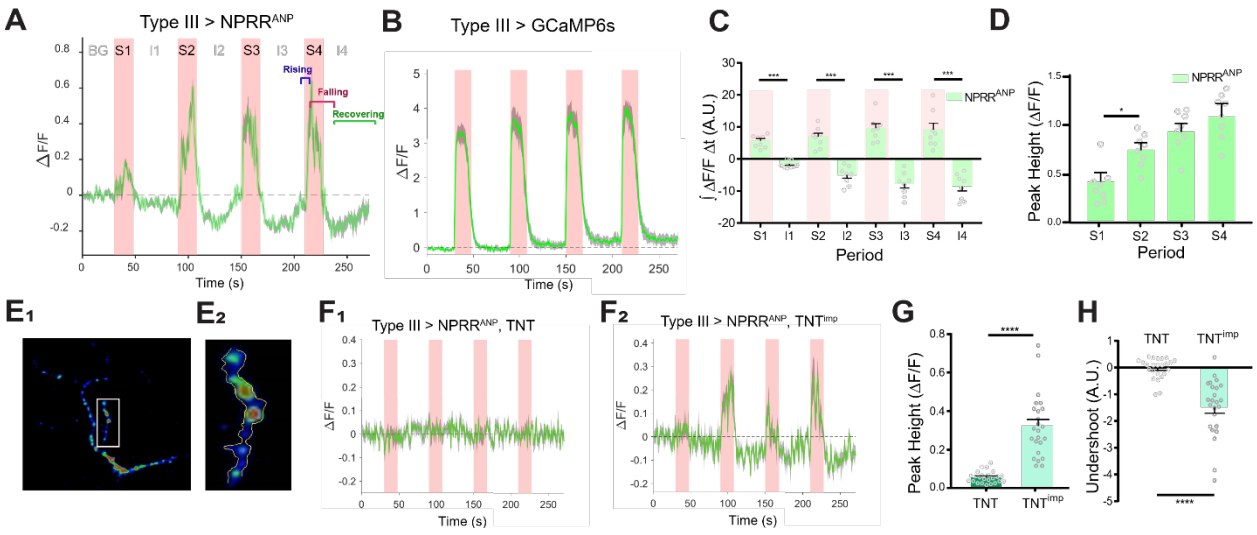

Figure 2: NPRR specifically reports neuropeptide release.

(A) Trace from a representative experiment showing changes in NPRR^{ANP} fluorescence intensity (ΔF/F) in Type III motor neurons at the larval NMJ evoked by electrical stimulation. BG: background. S1-S4: Stimulation trials 1-4. I1-I4: Inter-stimulation Intervals (ISIs) 1-4. Green line: ΔF/F averaged across all boutons in the field of view. Grey shading: s.e.m envelope. Red bar: electrical stimulation trials (70 Hz). The three typical phases of the response are indicated in S4. The peak height of the response on the first trial is characteristically lower (see also **(D)**), and may reflect competition with unlabeled DCVs in the readily releasable pool. **(B)** ΔF/F traces in control flies expressing cytoplasmic GCaMP6s in Type III neurons. **(C)** Integrated NPRR^{ANP} ΔF/F values during trials S1-4 and intervals I1-4. A.U.: arbitrary units. $n = 8$. ***, $P<0.001$. **(D)** Average NPRR^{ANP} ΔF/F peak heights for trials S1-4. $n = 8$. *, $P<0.05$. Plotted values in (**C-D**) are mean±s.e.m. **(E$_1$-E$_2$)** Representative selection of ROIs (yellow). Details see **Materials and methods**. Scale bar, 5 µm. **(F)** NPRR^{ANP} ΔF/F response are abolished in Type III GAL4>UAS-NPRR^{ANP} flies bearing UAS-TNT (**F$_1$**) but not UAS-TNT^{imp} (**F$_2$**). **(G)** Average peak heights of NPRR^{ANP} ΔF/F in combined stimulation trials (S1-4) from (**F**). ****, $P<0.0001$. **(H)** Average "undershoot," defined as the integrated ΔF/F during ISIs I1-4 (see (**C**)). In **C-D** and **G-H**.

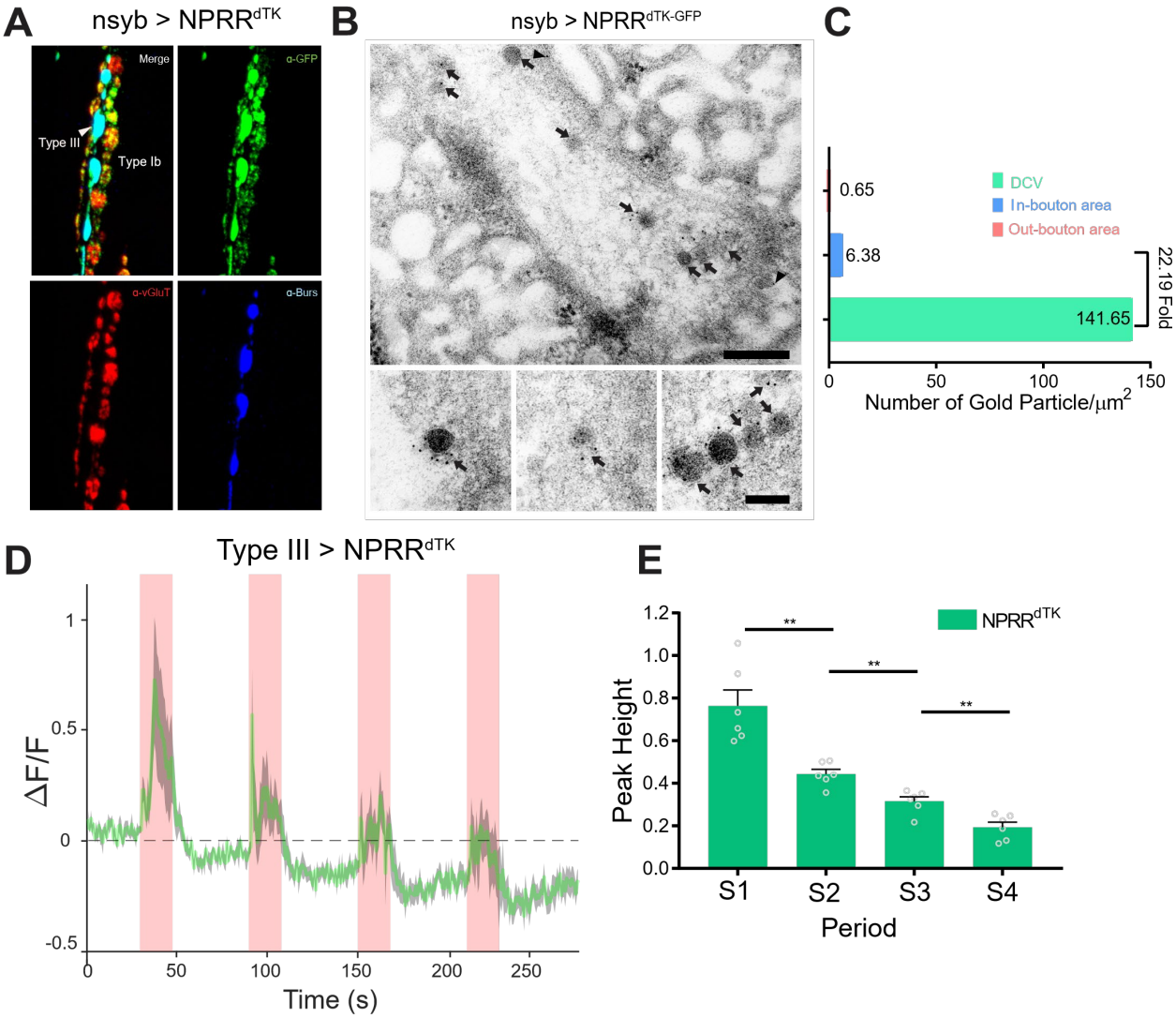

Figure 3: Application of the NPRR approach to a *Drosophila* neuropeptide.

(A) Triple immunolabeling for GFP (green), Bursicon (blue) and vGluT (red) in Type III-GAL4>UAS-NPRR^{dTK} flies. Scale bar, 5 µm. **(B)** TEM images of boutons immunolabeled against GFP (5 nm gold) in nsyb-GAL4>UAS-NPRR$^{dTK\text{-}GFP}$ flies. Note strong labeling in DCVs (arrows) and bouton plasma membrane (arrowheads). Scale bar, 200 nm. Lower panel shows representative images of labeled DCVs. Scale bar,100 nm. **(C)** Quantification of TEM images in **(B)**. **(D)** NPRR^{dTK} ΔF/F curve; stimulation conditions as in **Figure 2A**. **(E)** Average NPRR^{dTK} ΔF/F peak height above pre-stimulation baseline (corrected; see **Materials and methods**) for stimulation trials S1-4. $n = 6$. **, $P<0.01$.

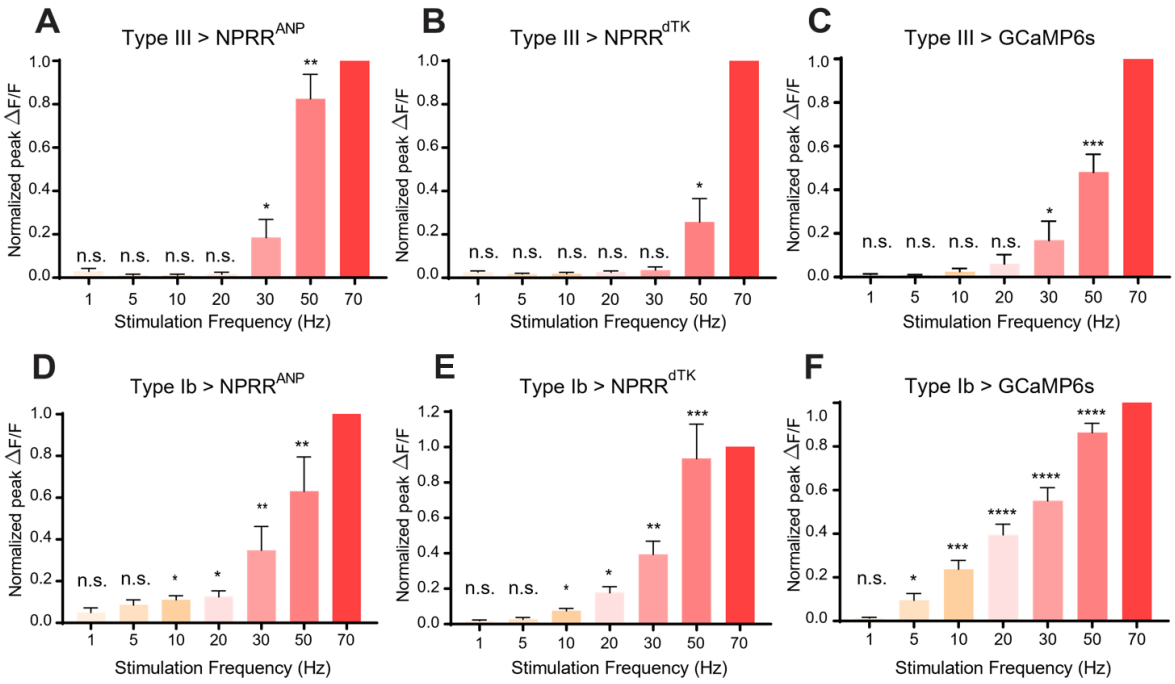

Figure 4: NPRR reveals distinct cell-type specific peptide release properties.

For each preparation, a series of stimulation trials were delivered at frequencies from 1 Hz to 70 Hz, as indicated. In-stimulation response peaks were normalized to 70 Hz. The normalized peaks of NPRRs or calcium responses (measured with cytosolic GCaMP6s) were pooled and plotted for both Type III **(Figure 4A-C)** and Type Ib **(Figure 4D-F)** neurons. Responses were compared to zero. *n* = 6-12. n.s., not significant. *, *P*<0.05. **, *P*< 0.01. ***, *P*< 0.001. ****, *P*<0.0001.

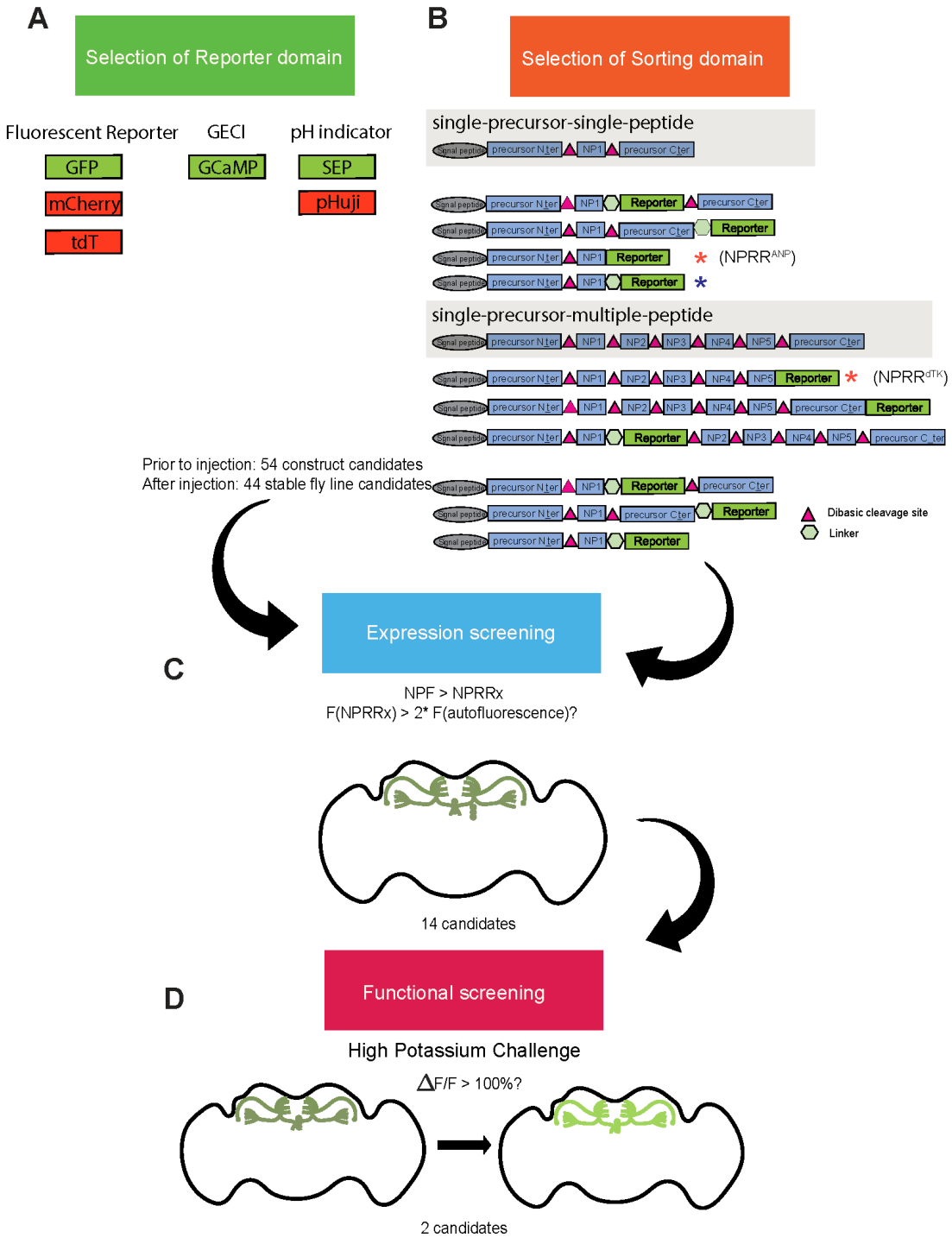
A
Selection of Reporter domain
Fluorescent Reporter
GFP
mCherry
tdT
GECI
GCaMP
pH indicator
SEP
pHuji
B
Selection of Sorting domain
single-precursor-single-peptide
single-precursor-multiple-peptide
Reporter
(NPRR^ANP)
(NPRR^dTK)
Dibasic cleavage site
Linker
Prior to injection: 54 construct candidates
After injection: 44 stable fly line candidates
C
Expression screening
NPF > NPRRx
F(NPRRx) > 2* F(autofluorescence)?
14 candidates
D
Functional screening
High Potassium Challenge
ΔF/F > 100%?
2 candidates

Figure 1—figure supplement 1: NPRR screening pipeline.
A series of reporter-neuropeptide precursor fusions were designed, codon-optimized for *Drosophila*, cloned into expression vectors under the control of the GAL4 upstream activator sequence (UAS), and used to generate transgenic flies. **(A)** Candidate reporters interrogated included (constitutive) fluorescent reporters, genetically encoded calcium indicators (GECI) and pH indicators (pHluorins). **(B)** Sorting domain candidates included different truncated versions of rat Atrial Natriuretic Peptide (ANP; single-precursor-single-peptide) and *Drosophila* tachykinin (dTK; single-precursor-multiple-peptide) precursors. 52 constructs were built and injected. 44 of 54 were successfully integrated as transgenic lines, while 8 were excluded due to lethality or unstable expression. **(C-D)** Candidate UAS-NPRR lines were crossed with an NPF-Gal4 driver line and selected based on their expression in NPF terminals in the adult fly brain. The raw fluorescence intensity of each NPRR candidate was measured using the same microscope parameters (laser power, HV, offset value). 14 candidates passed this screening. (**C**) We screened the performance of difference NPRRs (signal-to-noise contrast) by measuring fluorescence before and immediately after 70mM high-potassium challenge in an *ex vivo* explant preparation of adult fly brains. The post/pre KCl fluorescence ratio is defined as ΔF/F. We arbitrarily set the threshold as 100%. 2 NPRRs with highest ΔF/F passed the final round of screening.
Red asterisks indicate the candidates selected for the studies in **Figure 2** and **Figure 3**. Blue asterisk indicates original ANP-GFP fusion)(Burke et al., 1997; Rao et al., 2001).

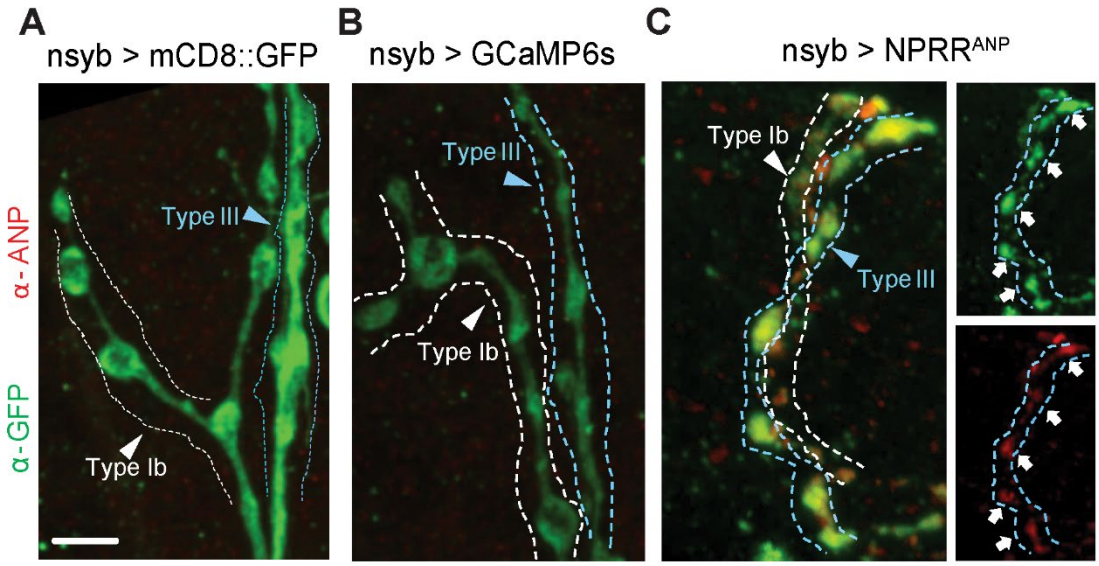

Figure 1—figure supplement 2: Exogeneous neuropeptide ANP dictates the expression pattern of NPRR^{ANP}.

Membrane-bound mCD8::GFP fusion **(A)**, cytosolic GCaMP6s (**B**) and NPRR^{ANP} (**C**) were expressed pan-neuronally in the larval NMJ and stained for both ANP (red) and NPRR (green, anti-GFP). **(C)** Note co-localization of ANP and GFP. Scale bar, 5 μm.

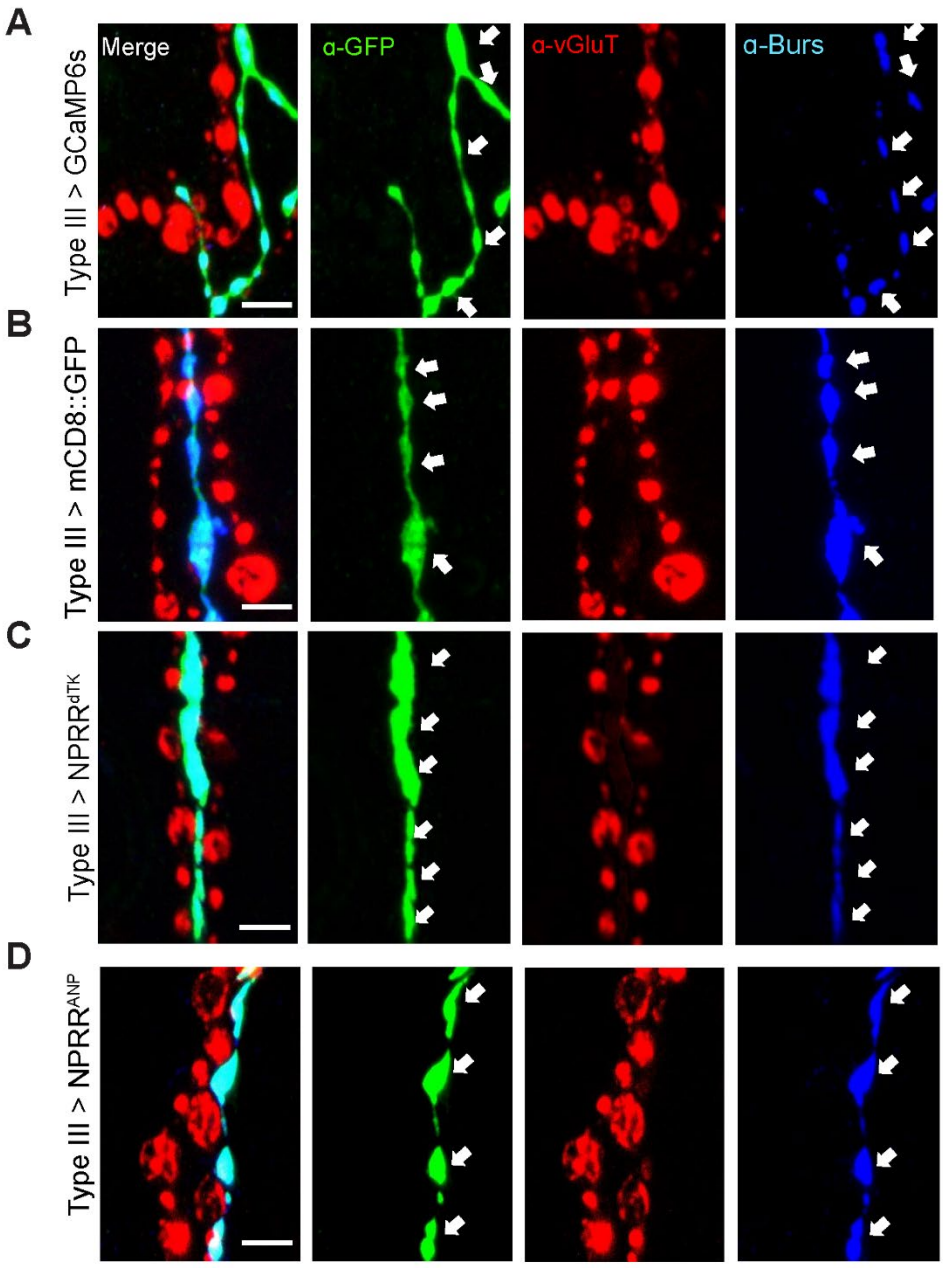

Figure 1—figure supplement 3: Expression of different reporters in Type III neurons in the larval NMJ.

A GAL4 line (R20C11-GAL4, named Type III-GAL4 in this report) allows specific expression in Type III neurons. Expression patterns of **(A)** conventional GCaMP, **(B)** membrane-bound GFP, **(C)** NPRR^{dTK} and **(D)** NPRR^{ANP} using Type III-GAL4. Arrows indicate boutons in Type III neurons, which contain the neuropeptide Bursicon. Note that anti-vGluT stains other types of motor neurons, which are not labeled by the Type III-specific driver used in this experiment. Scale bar, 5 μm.

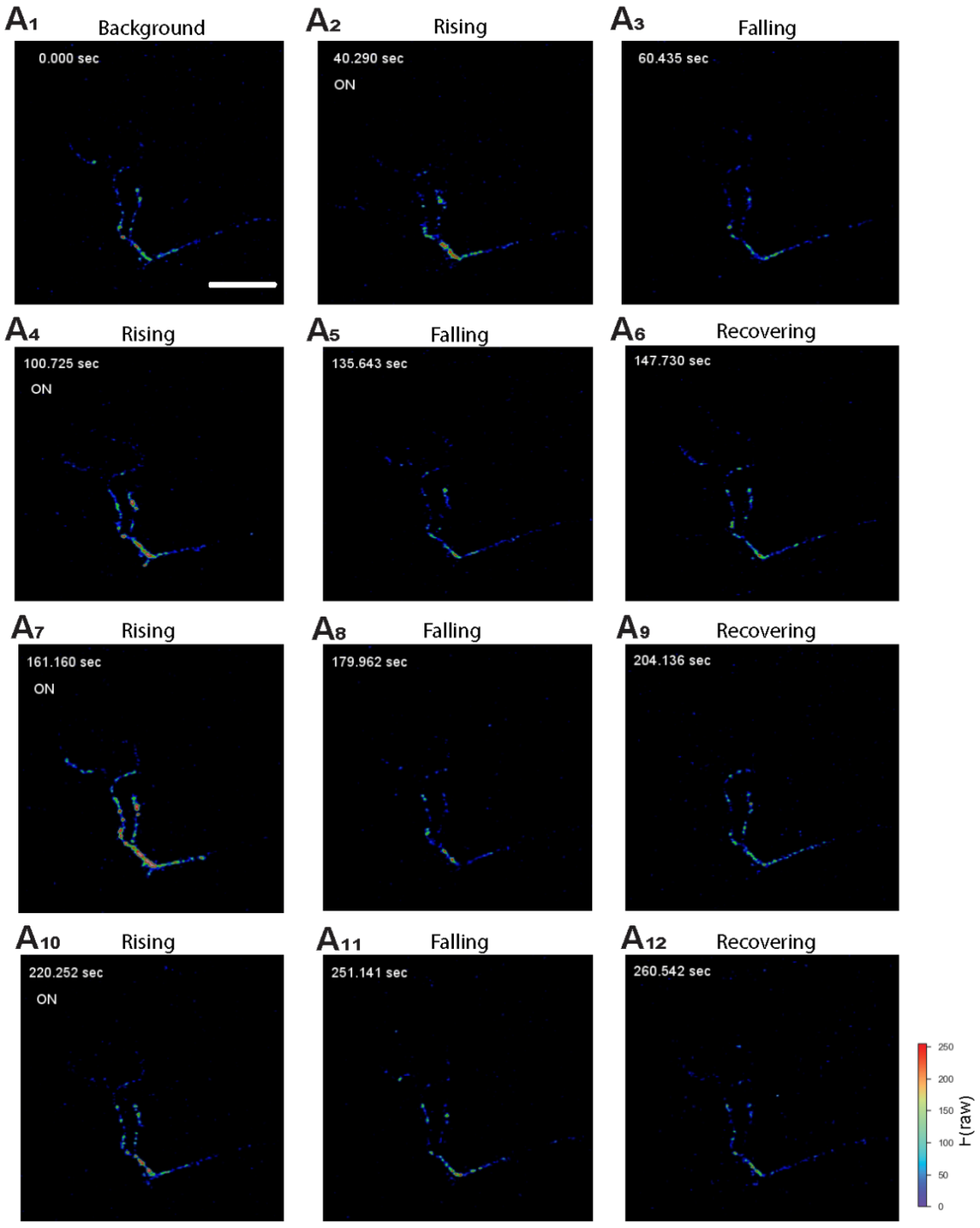

Figure 2—figure supplement 1: Activation of NPRR^{ANP} *in situ*.
Representative still frames (**A$_1$-A$_{12}$**) from video recordings of NPRR^{ANP}-expressing Type III neurons at the larval NMJ. "On" (**A$_{2,4,7,10}$**) represents the onset of electrical pulses. Color bar: Raw fluorescence intensity. Scale bar, 50 µm.

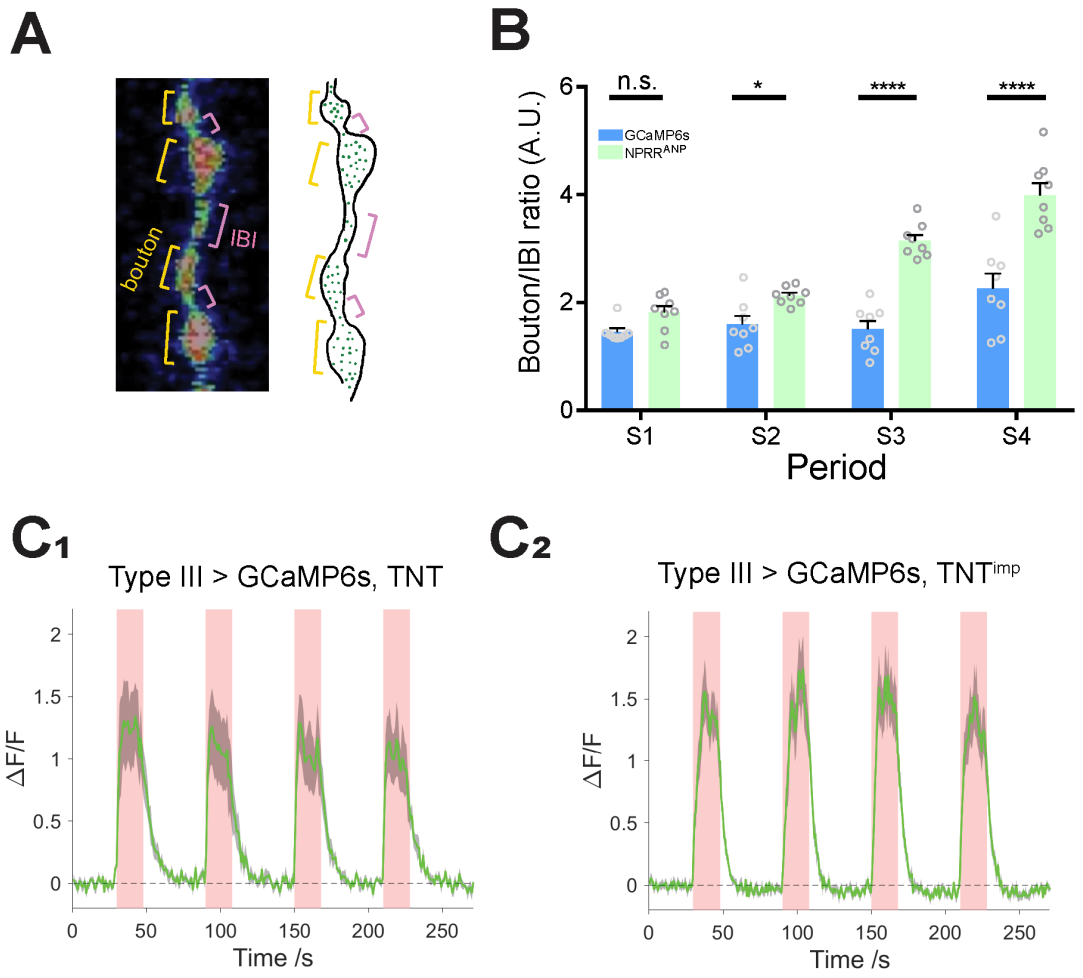

Figure 2—figure supplement 2: NPRR specifically reports neuropeptide release.
(A) Left: Segmentation of Type III neurons into boutons (orange) and inter-bouton intervals (IBIs, red). Right: Schematic illustrating DCV distribution in Type III neurons, based on photomicrograph to the left. Green dots, DCVs. **(B)** Average time-integrated ratio of ΔF/F in boutons/IBIs (**Materials and Methods**), within each stimulation periods. n.s., not significant. *, $P<0.05$. ***, $P< 0.001$. ****, $P<0.0001$.**(C)** TNT does not affect GCaMP6s ΔF/F kinetics. n = 6-7. GCaMP6s peak magnitudes were reduced slightly in TNT **(C_1)** in comparison to TNT^{imp} **(C_2)** preparations, perhaps reflecting partial vulnerability of the cytosolic GCaMP6s reporter to TNT-mediated cleavage and degradation. NPRRs are expected to be protected from TNT by the DCV membrane.

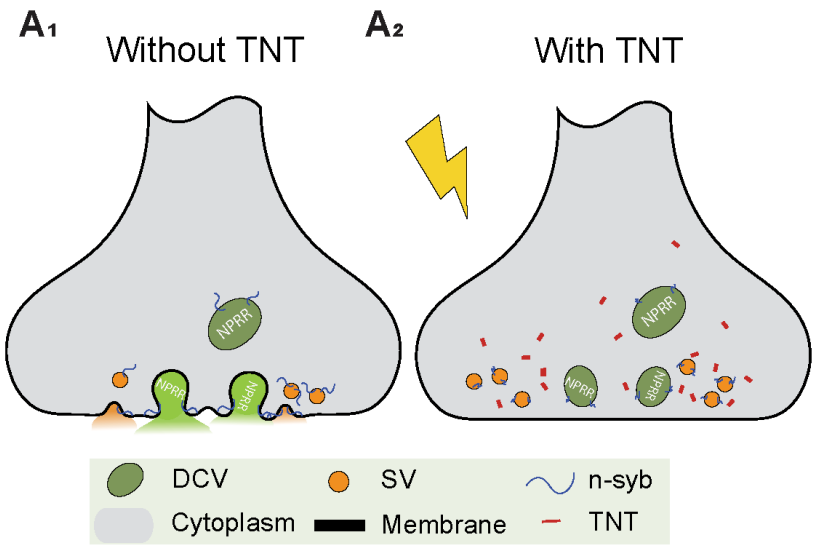

Figure 2—figure supplement 3: Blocking DCV fusion using Tetanus Toxin.
(A1, A2) Tetanus toxin (TNT) blocks vesicle fusion by cleavage of n-synaptobrevin (n-syb).

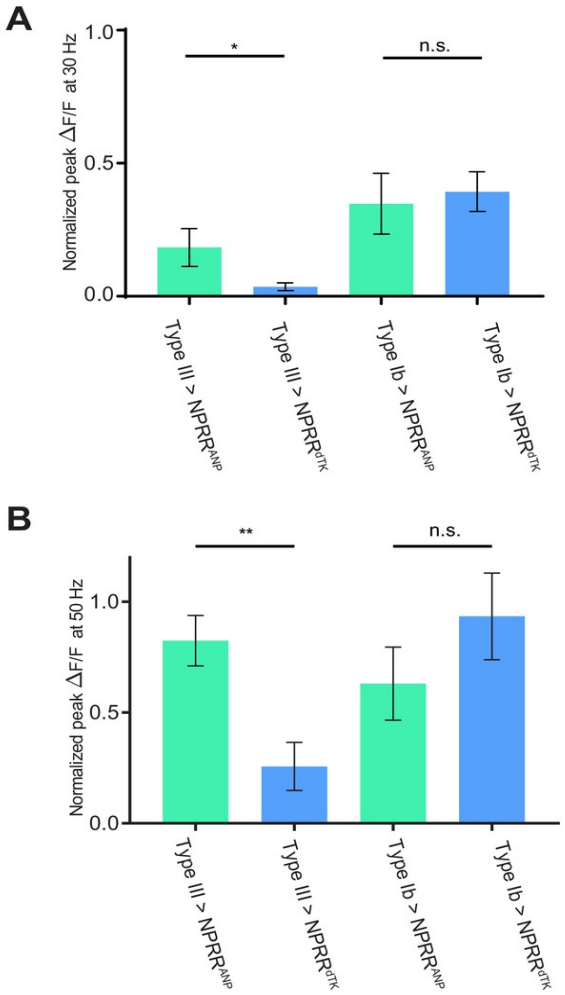

Figure 4—figure supplement 1: Comparison of NPRR response at 30 and 50 Hz.
Normalized ΔF/F peaks in at 30 Hz **(A) and** 50 Hz **(B)** electrical stimulation in Figure 4A, B, D, E are replotted and compared. n = 6-7. *, P<0.05. **, P<0.01. n.s., not significant.

Current techniques for neuropeptide release measurement

	Chemical specificity	Genetic specificity	Spatial specificity	Temporal dynamics	Signal relative to background
Microdialysis	Low	NA	Brain region	minutes-days	High
Antibody-coated microprobe	High	NA	Brain region	minutes-days	High
GFP-tagged propeptide imaging	High	Yes	Neuron of interest	~seconds	Low
NPRR	High	Yes	Neuron of interest	~subseconds	High

Supplementary Table. 1: Current techniques for neuropeptide release measurement.
Summary of current techniques used for neuropeptide release, including microdialysis, antibody-coated microprobes, GFP-tagged propeptide imaging and NPRR. NA, "not applicable"

	$NPRR^{ANP\text{-}GFP}$ (Ib)	$NPRR^{dTK\text{-}GFP}$
average gold particles per DCV	0.71	1.11
gold within DCV area [μm^{-2}]	90.99	141.65
gold within bouton area [μm^{-2}]	5.56	6.38
gold outside bouton area [μm^{-2}]	1.11	0.65
controls		
gold per imaged area [μm^{-2}]	2.18	2.47
background (internal control) [μm^{-2}]	0.57	0.52
background (biological control) [μm^{-2}]	0.25	-
SNR (gold/DCV area vs. background)	159.6	272.4

Supplementary Table. 2: Stereological labeling estimates
Stereological labeling estimations of $NPRR^{ANP\text{-}GFP}$ and $NPRR^{dTK\text{-}GFP}$, respectively, in Type Ib neurons, or in Type Ib and Type III neurons. Biological controls and internal controls are described in Materials and methods. SNR: Signal-to-Noise Ratio.

Key Resources Table

Reagent type (species) or resource	Designation	Source or reference	Identifiers	Additional information
Genetic reagent (*D. melanogaster*)	UAS-NPRR^{ANP} (attp2)	this paper		See Materials and methods, subsection Construction of transgenic animals.
Genetic reagent (*D. melanogaster*)	UAS-NPRR^{dTK} (attp2)	this paper		Same as above.
Genetic reagent (*D. melanogaster*)	UAS-TNT^{imp}	Bloomington Drosophila Stock Center	BDSC:28840; FLYB:FBti0038575; RRID:BDSC_28840	Flybase symbol: w[*]; P{w[+mC]=UAS TeTxLC. (-)V}A2
Genetic reagent (*D. melanogaster*)	UAS-TNT	Bloomington Drosophila Stock Center	BDSC:28838; FLYB:FBti0038527; RRID:BDSC_28838	Flybase symbol: w[*]; P{w[+mC]=UAS TeTxLC.tnt}G2
Genetic reagent (*D. melanogaster*)	w; +; UAS-GCaMP6s (su(Hw)attp1)	Hoopfer et al., 2015		
Antibody	anti-GFP (chicken polyclonal)	Aveslab	Aveslab: GFP-1020; RRID:AB_2307313	(1:250:Immuno-EM, 1:1000: IHC)
Antibody	anti-ANP (rabbit polyclonal)	abcam	abcam #14348	(1:500)

Materials and Methods

Fly strains

All experimental flies were reared on a 12/12-hour day-night cycle at 25°C. Standard chromosomal balancers and genetic strategies were used for all crosses and for maintaining mutant lines. The following strains were obtained from Bloomington Stock Center (Indiana University): R20C11-Gal4 (#48887), R57C10-Gal4 (#39171), UAS-mCD8::GFP (#32185), UAS-TNT (#28838), UAS-TNT^{imp} (#28840). UAS-opGCaMP6s was made by Barret Pfeiffer (Gerald Rubin's lab, Janelia Farm) (Hoopfer, Jung, Inagaki, Rubin, & Anderson, 2015).

Construction of transgenic animals

All PCR reactions were performed using PrimeSTAR HS DNA polymerase (Takara #R045Q). All constructs were verified via DNA sequencing (Laragen).

To construct UAS-NPRR^{ANP}, Drosophila codon-optimized ANP and GCaMP6s were synthesized using gBlocks service (Integrated DNA Technologies), and subcloned into pJFRC7 vector (from Addgene #26220)(Pfeiffer et al., 2010) using Gibson cloning. UAS-dTK-NPRR is built in a similar way except the dTK fragment was cloned from the *Drosophila* brain cDNA. NPRRdTK-GFP and NPRRANP-GFP were built similarly except *Drosophila* codon-optimized GFP was used for the subcloning. All the vectors were injected and integrated into attP2 or attp40 sites (Bestgene Inc).

Expression screening of NPRR candidates

Adult fly brains were dissected in chilled PBS and fixed in 4 % formaldehyde for 55 min at room temperature. After three 10 min rinses with PBS, the brains were cleared with Vectashield (#1000, Vectorlabs), mounted, and used for native fluorescence measurements. We trace the NPF neuron somata and arborization as ROIs. We selected regions next to NPF neurons and measured its fluorescent intensity as a reference, which represents background autofluorescence. Candidates whose fluorescence reached at least 2-fold higher than reference were selected for functional screening.

Functional screening of NPRR candidates

For the baseline fluorescence measurement, we crossed NPF-Gal4 to the candidate lines and generated NPF-Gal4 > NPRRx (x = candidate label) flies for tests. The dissected adult fly brains were mounted on a petri dish and immersed in *Drosophila* imaging saline (108 mM NaCl, 5 mM KCl, 2 mM $CaCl_2$, 8.2 mM $MgCl_2$, 4 mM $NaHCO_3$, 1 mM NaH_2PO_4, 5 mM trehalose, 10 mM sucrose, 5 mM HEPES, pH 7.5). To deliver high potassium challenge, High-K imaging saline was perfused (43 mM NaCl, 70 mM KCl, 2 mM $CaCl_2$, 8.2 mM $MgCl_2$, 4 mM $NaHCO_3$, 1 mM NaH_2PO_4, 5 mM trehalose, 10 mM sucrose, 5 mM HEPES, pH 7.5). Live imaging series were acquired using a Fluoview FV3000 Confocal laser scanning biological microscope (Olympus) with a 40×, 0.8 N.A. (Numerical Aperture) water immersion objective (Olympus). Candidates whose post-stimulation fluorescence reached at least 2-fold of baseline fluorescence (measured as averaged pre-stimulation fluorescence) were selected for *in vivo* tests at NMJ. For each candidate line, at least 3 brains were tested and fold-change of each was averaged.

Immunocytochemistry (ICC)

Cells were fixed in 4 % formaldehyde or Bouin's solution for 30 min at room temperature. After three 15 min rinses with PBS, tissues were incubated with primary antibodies overnight at 4 °C. Following three 15 min rinses with PBS, tissues were incubated with secondary antibody for 2 hours at room temperature. Following three 15 min rinses, tissues were cleared with Vectashield (#1000, Vectorlabs) and mounted. Confocal serial optical sections were acquired using a Fluoview FV3000 Confocal laser scanning biological microscope (Olympus) with a 60×, 1.30 N.A. silicone oil objective (Olympus). All image processing and analyses were done using ImageJ (National Institute of Health).

The following primary antibodies were used: Chicken anti-GFP (1:250-1:1000, Aveslab #1020), Rabbit anti-ANP (1:500, abcam #14348), Guinea pig anti-vGluT(Goel & Dickman, 2018) (1:1500), Rabbit anti-syt1(Littleton, Bellen, & Perin, 1993) (1:500) and Rabbit anti-Bursicon (1:2000, a gift from Dr. Benjamin White).

The following secondary antibodies were used: Alexa Fluor 488 Goat anti-Chicken IgY (#A11039, Invitrogen), Alexa Fluor 488 Goat anti-Rabbit IgG (#A11008, Invitrogen), Alexa Fluor 568 Goat anti-Rabbit IgG(H+L) (#A11011, Invitrogen), Alexa Fluor 633 Goat anti-Rabbit IgG(H+L) (#A21070, Invitrogen), Alexa Fluor 488 Goat anti-Guinea Pig IgG(H+L) (#A11073, Invitrogen), Alexa Fluor 568 Goat anti-Guinea Pig IgG(H+L) (#A11075, Invitrogen), Alexa Fluor 568 Goat anti-Mouse IgG(H+L) (#A11004, Invitrogen) and Alexa Fluor 633 Goat anti-Mouse IgG(H+L) (#A21050, Invitrogen).

Electron microscopy

Drosophila tissues were fixed in 4% formaldehyde in PBS and stored at 4°C until preparation by high-pressure freezing (HPF) and freeze-substitution (FS) (Buser & Drubin, 2013; Buser & Walther, 2008). Tissues were cryoprotected in 2.3 M sucrose for 45 minutes, transferred to 200 µm deep planchettes and high-pressure frozen in an EMPact2 with RTS (Leica, Vienna, Austria). FS was carried out in an AFS2 (Leica, Vienna, Austria) in methanol containing 5% water, 0.05% glutaraldehyde and 0.1% uranyl acetate (-90 °C, 3 h; -90 to -80 °C, 10 h; -80 °C, 4 h; -80 to 4 °C, 24 h). Samples were washed once in methanol containing 5% water, infiltrated with hard grade LR White (Electron Microscopy Sciences, Hatfield, PA, USA) at 4 °C ([LR White] : [methanol containing 5% water] 1:1, 24 h; 100% LR White, 3x 24 h) and polymerized in a fresh change of LR

White using a Pelco BioWave (Ted Pella, Inc., Redding, CA, USA) set to 750 W, 95 °C for 45 minutes.

60 nm thin sections (UCT ultramicrotome, Leica, Vienna, Austria) were picked up on formvar-coated 50 mesh copper grids. The sections were blocked for 3 minutes in blocking buffer (PBS with 0.5% bovine serum albumin, which was used for all antibody dilutions), incubated in anti-GFP antibody (1:500, Aveslab #1020) for 5 minutes, washed 3 times in blocking buffer, incubated in rabbit anti chicken antibody (1:50, MP Biomedicals #55302) for 5 minutes, washed 3 times on blocking buffer, incubated on protein A - 5nm gold (1:50, Utrecht, Netherlands), and washed 3 times in PBS and 3 times in distilled water. The sections were stained in uranyl acetate or uranyl acetate and Reynolds lead citrate depending on the desired contrast and imaged at 80 kV in a Zeiss EM10C (Zeiss, Oberkochen, Germany) using a CCD camera (Gatan, Pleasanton, CA, USA).

Labeling density was estimated using stereological methods(Griffiths & Hoppeler, 1986). Cross-sections through boutons were recorded and the following parameters were measured: total image area, total number of gold particles, number of visible dense core vesicles (DCV), number of gold particles within a 50 nm radius of the DCV center, bouton area (grid intersection estimate), gold within the bouton cytoplasm, gold within 20 nm of the bouton plasma membrane, gold outside of the bouton (mainly sER). Background labeling was estimated using internal controls (labeling on blank resin and on muscle fibers) and a biological control (non-GFP expressing genotype). Occasional obvious, large gold aggregates were disregarded. Background was consistently below 0.6 gold/μm^2 in independently repeated labeling experiments.

Electrical Stimulation

The dissection of third-instar larvae was performed in zero-calcium HL3 saline. The CNS was removed to avoid spontaneous motor neuron activity. To minimize muscle contraction induced by electrical stimulation of motor neurons, the larval body walls were slightly stretched and incubated in HL3 saline supplemented with 10 mM glutamate for 5 mins after dissection to desensitize postsynaptic glutamate receptors. Samples were then shifted to HL3 saline containing 1mM glutamate and 1.5mM Ca^{2+}. Motor nerves were sucked into a glass micropipette with a stimulation electrode. In Figure 2 and Figure 3, to induce maximum dense core vesicle release at type III motor neuron terminals, 4 repetitive bursts (70 Hz stimulation for 18-20s with pulse width of 1ms) with intervals of 40-42s were programmed and triggered with a Master-9 stimulator (A.M.P.I., Israel) connected to an iso-flex pulse stimulator (A.M.P.I., Israel). The stimulation intensity was tested and set to double the intensity required to induce muscle contraction by a single pulse stimulation.

In Figure 4, stimulation trials were delivered with the same duration, but with a series of frequencies spanning 1 Hz to 70 Hz.

Calcium imaging

A Nikon A1R confocal microscope with resonant scanner and NIS Element software were used to acquire live Ca^{2+} imaging on third instar larvae, bathed with 1 mM glutamate added in 1.5 mM Ca^{2+} HL3 saline. Type III motor neuron terminals in abdominal segments from A2 to A5 were imaged using a 60x APO 1.4 N.A. water immersion objective with 488 nm excitation laser. A 5-min period was used for time-lapse imaging at a resonance frequency of 1 fps (512 x 512 pixels or 1024 x 1024 pixels), with z-stacks (step length varying from 1 to 1.5 μm) covering the depth of entire type III motor neuron terminals. The repetitive electrical stimulation of 70 Hz was delivered during the

imaging session. Samples with severe muscle contractions were abandoned due to imaging difficulties. Maximum intensity projection (MIP) and image registration were conducted using Image J. Plugins including Image Stabilizer (K. Li, CMU) and Template Matching (Q. Tseng) were used for compensating drifting and correcting movement induced by electrical stimulations. ROIs were manually selected by tracing the outer edge of each neuron based on the baseline fluorescence. If the fluorescence was too weak to trace, we established a reference stack by empirically adjusting the contrast on a duplicate of the raw image stack. We used the reference stack for ROI selection and projected the selected ROIs back onto to the raw image stack for measurement. For frames in which the sample movement could not be automatically corrected, we manually outlined the ROIs used for measurements. Preparations with severe movement or deformation artifacts were abandoned to avoid unreliable measurements. Each ROI represent a traceable neuronal branch except Figure 2—figure supplement 2B, in which the ROIs were further manually partitioned into boutons and IBIs (Inter-Bouton Intervals) based on morphology. Fluorescence change were normalized to the pre-stimulation background except for Figure 3E, for which the data in each trial was normalized to the average $\Delta F/F$ during a 5 seconds period just before stimulation was initiated. No sample size is predetermined based on statistics. Ca^{2+} imaging data were acquired from at least 6 independent NMJs from at least 5 animals.

Statistical Analysis

Data are presented as mean ± s.e.m. All data analysis was performed with Graphpad Prism 6, Microsoft Excel and custom Matlab codes. Mann-Whitney U test was used for comparison except in Figure 4, where One-sample T test was used for comparison with a specified value (0).

References

Ales, E., Tabares, L., Poyato, J. M., Valero, V., Lindau, M., & Alvarez de Toledo, G. (1999). High calcium concentrations shift the mode of exocytosis to the kiss-and-run mechanism. *Nat Cell Biol*, *1*(1), 40-44. https://doi.org/10.1038/9012

Barg, S., Olofsson, C. S., Schriever-Abeln, J., Wendt, A., Gebre-Medhin, S., Renstrom, E., & Rorsman, P. (2002). Delay between fusion pore opening and peptide release from large dense-core vesicles in neuroendocrine cells. *Neuron*, *33*(2), 287-299. https://doi.org/Doi 10.1016/S0896-6273(02)00563-9

Bargmann, C. I., & Marder, E. (2013). From the connectome to brain function. *Nature Methods*, *10*(6), 483-490. https://doi.org/10.1038/Nmeth.2451

Barykina, N. V., Subach, O. M., Doronin, D. A., Sotskov, V. P., Roshchina, M. A., Kunitsyna, T. A., Malyshev, A. Y., Smirnov, I. V., Azieva, A. M., Sokolov, I. S., Piatkevich, K. D., Burtsev, M. S., Varizhuk, A. M., Pozmogova, G. E., Anokhin, K. V., Subach, F. V., & Enikolopov, G. N. (2016). A new design for a green calcium indicator with a smaller size and a reduced number of calcium-binding sites. *Sci Rep*, *6*, 34447. https://doi.org/10.1038/srep34447

Burke, N. V., Han, W. P., Li, D. Q., Takimoto, K., Watkins, S. C., & Levitan, E. S. (1997). Neuronal peptide release is limited by secretory granule mobility. *Neuron*, *19*(5), 1095-1102. https://doi.org/10.1016/S0896-6273(00)80400-6

Buser, C., & Drubin, D. G. (2013). Ultrastructural imaging of endocytic sites in Saccharomyces cerevisiae by transmission electron microscopy and immunolabeling. *Microsc Microanal*, *19*(2), 381-392. https://doi.org/10.1017/S1431927612014304

Buser, C., & Walther, P. (2008). Freeze-substitution: the addition of water to polar solvents enhances the retention of structure and acts at temperatures around -60 degrees C. *J Microsc*, *230*(Pt 2), 268-277. https://doi.org/10.1111/j.1365-2818.2008.01984.x

Chen, T. W., Wardill, T. J., Sun, Y., Pulver, S. R., Renninger, S. L., Baohan, A., Schreiter, E. R., Kerr, R. A., Orger, M. B., Jayaraman, V., Looger, L. L., Svoboda, K., & Kim, D. S. (2013). Ultrasensitive fluorescent proteins for imaging neuronal activity. *Nature*, *499*(7458), 295-300. https://doi.org/10.1038/nature12354

Fremeau, R. T., Troyer, M. D., Pahner, I., Nygaard, G. O., Tran, C. H., Reimer, R. J., Bellocchio, E. E., Fortin, D., Storm-Mathisen, J., & Edwards, R. H. (2001). The expression of vesicular glutamate transporters defines two classes of excitatory synapse. *Neuron*, *31*(2), 247-260. https://doi.org/10.1016/S0896-6273(01)00344-0

Goel, P., & Dickman, D. (2018). Distinct homeostatic modulations stabilize reduced postsynaptic receptivity in response to presynaptic DLK signaling. *Nat Commun*, *9*(1), 1856. https://doi.org/10.1038/s41467-018-04270-0

Gorczyca, M., & Budnik, V. (2006). Anatomy of the Larval Body Wall Muscles and NMJs in the third instar larval stage. *The Fly Neuromuscular Junction: Structure and Function*, *75*, 367.

Griffiths, G., & Hoppeler, H. (1986). Quantitation in immunocytochemistry: correlation of immunogold labeling to absolute number of membrane antigens. *Journal of Histochemistry & Cytochemistry*, *34*(11), 1389-1398.

Hentze, J. L., Carlsson, M. A., Kondo, S., Nassel, D. R., & Rewitz, K. F. (2015). The Neuropeptide Allatostatin A Regulates Metabolism and Feeding Decisions in Drosophila. *Sci Rep*, *5*, 11680. https://doi.org/10.1038/srep11680

Hokfelt, T., Broberger, C., Xu, Z. Q., Sergeyev, V., Ubink, R., & Diez, M. (2000). Neuropeptides--an overview. *Neuropharmacology*, *39*(8), 1337-1356.

Hoopfer, E. D., Jung, Y., Inagaki, H. K., Rubin, G. M., & Anderson, D. J. (2015). P1 interneurons promote a persistent internal state that enhances inter-male aggression in Drosophila. *Elife*, *4*. https://doi.org/10.7554/eLife.11346

Insel, T. R., & Young, L. J. (2000). Neuropeptides and the evolution of social behavior. *Curr Opin Neurobiol*, *10*(6), 784-789.

Kempf, C., Staudt, T., Bingen, P., Horstmann, H., Engelhardt, J., Hell, S. W., & Kuner, T. (2013). Tissue Multicolor STED Nanoscopy of Presynaptic Proteins in the Calyx of Held. *Plos One*, *8*(4). https://doi.org/ARTN e6289310.1371/journal.pone.0062893

Kendrick, K. M. (1990). Microdialysis measurement of in vivo neuropeptide release. *J Neurosci Methods*, *34*(1-3), 35-46.

Koon, A. C., & Budnik, V. (2012). Inhibitory control of synaptic and behavioral plasticity by octopaminergic signaling. *J Neurosci*, *32*(18), 6312-6322. https://doi.org/10.1523/JNEUROSCI.6517-11.2012

Levitan, E. S., Lanni, F., & Shakiryanova, D. (2007). In vivo imaging of vesicle motion and release at the Drosophila neuromuscular junction. *Nat Protoc*, *2*(5), 1117-1125. https://doi.org/10.1038/nprot.2007.142

Lin, M. Z., & Schnitzer, M. J. (2016). Genetically encoded indicators of neuronal activity. *Nat Neurosci*, *19*(9), 1142-1153. https://doi.org/10.1038/nn.4359

Littleton, J. T., Bellen, H. J., & Perin, M. S. (1993). Expression of synaptotagmin in Drosophila reveals transport and localization of synaptic vesicles to the synapse. *Development*, *118*(4), 1077-1088.

Loveall, B. J., & Deitcher, D. L. (2010). The essential role of bursicon during Drosophila development. *BMC Dev Biol*, *10*, 92. https://doi.org/10.1186/1471-213X-10-92

McNabb, S. L., & Truman, J. W. (2008). Light and peptidergic eclosion hormone neurons stimulate a rapid eclosion response that masks circadian emergence in Drosophila. *Journal of Experimental Biology*, *211*(14), 2263-2274. https://doi.org/10.1242/jeb.015818

Menon, K. P., Carrillo, R. A., & Zinn, K. (2013). Development and plasticity of the Drosophila larval neuromuscular junction. *Wiley Interdiscip Rev Dev Biol*, *2*(5), 647-670. https://doi.org/10.1002/wdev.108

Miesenbock, G., De Angelis, D. A., & Rothman, J. E. (1998). Visualizing secretion and synaptic transmission with pH-sensitive green fluorescent proteins. *Nature*, *394*(6689), 192-195. https://doi.org/10.1038/28190

Mitchell, K. J., Pinton, P., Varadi, A., Tacchetti, C., Ainscow, E. K., Pozzan, T., Rizzuto, R., & Rutter, G. A. (2001). Dense core secretory vesicles revealed as a dynamic Ca2+ store in neuroendocrine cells with a vesicle-associated membrane protein aequorin chimaera. *Journal of Cell Biology*, *155*(1), 41-51. https://doi.org/10.1083/jcb.200103145

Nassel, D. R., & Winther, A. M. (2010). Drosophila neuropeptides in regulation of physiology and behavior. *Prog Neurobiol*, *92*(1), 42-104. https://doi.org/10.1016/j.pneurobio.2010.04.010

Pfeiffer, B. D., Ngo, T. T. B., Hibbard, K. L., Murphy, C., Jenett, A., Truman, J. W., & Rubin, G. M. (2010). Refinement of Tools for Targeted Gene Expression in Drosophila. *Genetics*, *186*(2), 735-U488. https://doi.org/10.1534/genetics.110.119917

Rao, S., Lang, C., Levitan, E. S., & Deitcher, D. L. (2001). Visualization of neuropeptide expression, transport, and exocytosis in Drosophila melanogaster. *J Neurobiol*, *49*(3), 159-172.

Schaible, H. G., Jarrott, B., Hope, P. J., & Duggan, A. W. (1990). Release of immunoreactive substance P in the spinal cord during development of acute arthritis in the knee joint of the cat: a study with antibody microprobes. *Brain Res*, *529*(1-2), 214-223.

Shakiryanova, D., Tully, A., & Levitan, E. S. (2006). Activity-dependent synaptic capture of transiting peptidergic vesicles. *Nat Neurosci*, *9*(7), 896-900. https://doi.org/10.1038/nn1719

Sturman, D. A., Shakiryanova, D., Hewes, R. S., Deitcher, D. L., & Levitan, E. S. (2006). Nearly neutral secretory vesicles in Drosophila nerve terminals. *Biophys J*, *90*(6), L45-47. https://doi.org/10.1529/biophysj.106.080978

Sweeney, S. T., Broadie, K., Keane, J., Niemann, H., & O'Kane, C. J. (1995). Targeted expression of tetanus toxin light chain in Drosophila specifically eliminates synaptic transmission and causes behavioral defects. *Neuron*, *14*(2), 341-351.

Taghert, P. H., & Veenstra, J. A. (2003). Drosophila neuropeptide signaling. *Adv Genet*, *49*, 1-65.

Tian, L., Hires, S. A., & Looger, L. L. (2012). Imaging neuronal activity with genetically encoded calcium indicators. *Cold Spring Harb Protoc*, *2012*(6), 647-656. https://doi.org/10.1101/pdb.top069609

Umezaki, Y., Yasuyama, K., Nakagoshi, H., & Tomioka, K. (2011). Blocking synaptic transmission with tetanus toxin light chain reveals modes of neurotransmission in the PDF-positive circadian clock neurons of Drosophila melanogaster. *J Insect Physiol*, *57*(9), 1290-1299. https://doi.org/10.1016/j.jinsphys.2011.06.004

van den Pol, A. N. (2012). Neuropeptide transmission in brain circuits. *Neuron*, *76*(1), 98-115. https://doi.org/10.1016/j.neuron.2012.09.014

Winther, A. M. E., Siviter, R. J., Isaac, R. E., Predel, R., & Nassel, D. R. (2003). Neuronal expression of tachykinin-related peptides and gene transcript during postembryonic development of Drosophila. *Journal of Comparative Neurology*, *464*(2), 180-196. https://doi.org/10.1002/cne.10790

Wong, M. Y., Cavolo, S. L., & Levitan, E. S. (2015). Synaptic neuropeptide release by dynamin-dependent partial release from circulating vesicles. *Mol Biol Cell*, *26*(13), 2466-2474. https://doi.org/10.1091/mbc.E15-01-0002

Xia, X., Lessmann, V., & Martin, T. F. (2009). Imaging of evoked dense-core-vesicle exocytosis in hippocampal neurons reveals long latencies and kiss-and-run fusion events. *J Cell Sci*, 75-82. https://doi.org/10.1242/jcs.034603

Xu, T., Binz, T., Niemann, H., & Neher, E. (1998). Multiple kinetic components of exocytosis distinguished by neurotoxin sensitivity. *Nat Neurosci*, *1*(3), 192-200. https://doi.org/10.1038/642

Xu, T., & Xu, P. (2008). Differential Regulation of Small Clear Vesicles and Large Dense-Core Vesicles. In Z.-W. Wang (Ed.), *Molecular Mechanisms of Neurotransmitter Release* (pp. 327-339). Humana Press. https://doi.org/10.1007/978-1-59745-481-0_16

Zandawala, M., Yurgel, M. E., Texada, M. J., Liao, S., Rewitz, K. F., Keene, A. C., & Nassel, D. R. (2018). Modulation of Drosophila post-feeding physiology and behavior by the neuropeptide leucokinin. *PLoS Genet*, *14*(11), e1007767. https://doi.org/10.1371/journal.pgen.1007767

Zhu, D., Zhou, W., Liang, T., Yang, F., Zhang, R. Y., Wu, Z. X., & Xu, T. (2007). Synaptotagmin I and IX function redundantly in controlling fusion pore of large dense core vesicles. *Biochem Biophys Res Commun*, *361*(4), 922-927. https://doi.org/10.1016/j.bbrc.2007.07.083

Chapter 3

IMAGING NEUROPEPTIDE LOCALIZATION AND RELEASE IN MAMMALIAN CELLS WITH NOVEL GENETICALLY ENGINEERED REPORTERS

Summary

Neuropeptides are essential to the regulation of a variety of developmental, physiological, and behavioral functions. However, the subcellular localization and release properties of neuropeptides are less understood. Here we report the development of two sets of genetically engineered reporters: Neuropeptide Localization and Expression reporters (NPLER) and Neuropeptide Release Reporters (NPRR) and their applications in N46, a novel peptidergic cell line. The investigation of two neuropeptides of interest, NPY and NkB reveals previously unexplored differences in the sorting, routing, and release processes. Furthermore, we transformed PC12 cells with NPLER to generate a prototypical generic platform that potentially accelerates large-scale RNAi screening.

Introduction

Neuropeptides play significant roles in modulating neuronal activities (Hökfelt et al., 2003; Nusbaum et al., 2017; van den Pol, 2012). In mammals, over 100 neuropeptides are discovered and studied (Russo, 2017; van den Pol, 2012). It is generally accepted that (1) each neuropeptide owns its unique expression pattern throughout the brain and some peripheral endocrine cells; (2) each neuropeptide has distinct functions; (3) each peptidergic neuron/cell usually contains more than one type of neuropeptide. However, these studies offered limited insight as (1) mainly focused on cell lines originated from peripheral tissues, such as pancreas and adrenal glands; (2) only very few neuropeptides were studied. Many fluorescent protein-fused neuropeptide reporters were generated,

but they functioned mostly as proxies for secretory granule properties. There is a huge gap between the current strategies to develop novel tools or platforms, and the ambition of demystifying the complexity of neuropeptides. In this study, we established a prototypic platform that contains an adequate cell line and two sets of genetically engineered reporters: Neuropeptide Localization and Expression Reporters (NPLERs) and Neuropeptide Release Reporters (NPRRs). Two neuropeptides of interest, Neurokinin B (NkB) and Neuropeptide Y (NPY), were studied in this platform. We provided lines of evidence that NkB and NPY have distinct localization and routing destinations, and their subdomains function differently. NPRR studies prove that physiologically relevant stimuli, such as PACAP, triggers NPY release. Lastly, we tested the potential of transforming a canonical cell line to a generalized platform for studies of exogenous neuropeptides and regulations.

Results

A novel cell line for neuropeptide imaging

We selected two neuropeptides of interest for this study: Neurokinin B (NkB) and Neuropeptide Y (NPY), for their well-characterized physiological functions and strong clinical significance. NPY plays an essential role in feeding (Hökfelt et al., 2008; Luquet et al., 2005), energy balance (Loh et al., 2015) and stress (Heilig, 2004; Hirsch & Zukowska, 2012). NPY receptor antagonists were heavily invested to battle obesity and diabetes (Williams et al., 2020; Yulyaningsih et al., 2011), but none has survived to the New Drug Application (NDA) phase. NkB (Tac2) was mostly associated with ovulatory cycles (Hall, 2019) and airway diseases (Piedimonte, 1995). NK3R antagonists are but recent studies uncovered NkB functions in the central brain, such as coordination of a pleiotropic brain state caused by chronic social isolation (Zelikowsky et al., 2018).

We therefore sought to find cell lines that endogenously express NkB and/or NPY. Hypothalamic cells are known for enriched expression of neuropeptides (Parker & Bloom, 2012). Previous efforts of immortalizing hypothalamic cells result in a wide collection of neuropeptidergic cell lines (Belsham et al., 2004). Each cell line has a unique neuropeptide expression profile, characterized at the mRNA level by RT-PCR (Belsham et al., 2004). We resorted to the profiles and shortlisted 5 hypothalamic cell lines based on their expression of NkB or NPY, including 2 embryonic cell lines (mHypoE-N7, mHypoE-N46) and 3 adult cell lines (mHypoA-2/29, mHypoA-2/32, mHypoA-59) (Figure 1A). MIN-6β, an insulinoma cell line, was also included because of its popular use in the investigation of secretory granule release (Figure 1A) (Rutter et al., 2006; Varadi et al., 2005). We employed immunocytochemistry with NkB and NPY antibodies for further validations, the results were generally consistent with RT-PCR (Figure 1B). We next asked if these cell lines sort and transport neuropeptides properly. We modified NPY-GFP, a canonical secretory granule marker, by replacing its human NPY fragment with mouse NPY, all else unaltered. To distinguish the new reporter from NPY-GFP, we named it NPLER$^{NPYfl\text{-}GFP}$ (details discussed later) (Figure 1C). Transfection of this new reporter gave rise to fluorescence in all cell lines, but only the embryonic cell lines (mHypoE-N7 and mHypoE-N46) showed nicely colocalized double-labelings of GFP and NPY (Figure 1D$_1$). In mHypoE-N7 cells, the majority of fluorescence resides in the peri-nucleus region, likely ER and golgi apparatus. Little fluorescence was seen in the processes. mHypoE-N46 cells, on the contrary, possessed dispersed fluorescent puncta throughout the cell, strongly indicative of appropriate sorting and trafficking of the NPLER transgene. Parallel experiment of mHypoE-N46 cells without NPLER$^{NPYfl\text{-}GFP}$ suggested that the green fluorescence was not contributed by cell autofluorescence (Figure 1D$_2$). Therefore, mHypoE-N46 cells (N46 cells in the following context)

were chosen as the NPY reporter testbed. Moreover, N46 cell line was the only candidate that endogenously expresses both NPY and NkB, supported by both RT-PCR data and immunocytochemistry (Figure 1A-B). It is likely that N46 cells also makes ways for NkB reporter screenings.

We then asked if N46 cells can release neuropeptides. High potassium challenge triggers neuropeptide release in fruit flies (Bulgari et al., 2018; Ding et al., 2019), neuroblastoma cell line (Ou et al., 1998) and hypothalamic explant (Dube et al., 1992; Gamber et al., 2005). High potassium stimulation triggers intense depolarization and massive neuropeptide release (Cavadas et al., 2002; Wang et al., 2016), resulting in the decrease of intracellular neuropeptide load (Figure 1B). We therefore designed a KCl stimulation experiment in which two parallel groups of cells were incubated in control buffer and high potassium buffer, respectively (Figure 2C). The cells were stained against NPY or NkB subsequently. NPY staining in control cells have significantly higher fluorescent intensity (****P<0.0001, Mann Whitney *U* test) (Figure 2D). NkB staining showed similar results, yet the difference between control and KCl challenged group was smaller (*P<0.05, Mann Whitney *U* test). The decrease of intracellular fluorescence reflects the release of primed neuropeptides to the extracellular spaces. We conclude that N46 cells are capable of releasing NkB and NPY.

Design, screening, and validation of NPLERs

We previously described the development and application of Neuropeptide Release Reporters (NPRRs) (Ding et al., 2019; Han & Ding, 2022) in *drosophila*. A genetically encoded NPRR should contain at least (1) a reporter domain that reflects the physico-chemical contrast between the

intravesicular milieu and the extracellular space and (2) a sorting domain that ensures its selective trafficking into DCVs (Figure $3A_1$). We reasoned that the configuration of *Drosophila* NPRR is applicable to mammals, as neuropeptides and their processing enzymes are highly evolutionarily conserved (Hoyle, 1998).

In parallel, we propose a set of sister reporters to visualize the intracellular expression and localization of neuropeptides. These new Neuropeptide Localization and Expression Reporters (NPLERs) were designed to share the same sorting domain with NPRRs (Figure $3A_2$), but do not experience fluorescent rise upon DCV fusion (Figure 3B). An appropriate NPLER reporter domain should have high brightness, high photostability and pH-invariant fluorescence. Therefore, the pKa of NPLER reporter domain falls between 3 and 5.5. NPRRs, on the contrary, entail reporter domains of higher pKa (5.5-7.4) to capitalize on the pH sensitivity (Figure 3C). We identified 8 NPLER reporter domain candidates and ~10 NPRR reporter domain candidates, based on the brightness/pKa profiles and cell line expression screening. Many widely used exocytosis markers and vesicle fusion reporters contain enhanced GFP (eGFP) fragments, we included them as reference NPLER reporter domains (Figure 3D), even though its pKa is higher than 5.5 (eGFP:~6.0). Other candidates include three GFP mutants (mTurqoise2 (mTq2), Gamillus, mVenus), mCherry and mKO2. NPRR reporter domain candidates are comprised of some latest pH-sensitive sensors, such as pHmScarlet variants (Liu et al., 2021) and novel pHluorins (unpublished data), and some genetically engineered calcium indicators (GECIs), such as GCaMP6s (Chen et al., 2013), low calcium affinity GCaMP6 derivatives(de Juan-Sanz et al., 2017) and B-GECO-1 (Zhao et al., 2011) (Figure 3D).

NPY prepropeptide contains 3 domains, a 28-aa signal peptide at N terminus, NPY domain, and a CPON domain (C peptide of NPY). It was proposed that the signal peptide of NPY is sufficient for DCV sorting process (El Meskini et al., 2001), we therefore renamed it signal/sorting peptide to highlight its potential dual functions (Figure $3E_1$). NkB signal peptide was too renamed in this study to avoid confusion, although its role in DCV sorting remains unclear (Figure $3E_2$). We designed three versions of NPY sorting domains, including the full length (NPY_{fl}), the CPON-depleted fragment that truncates at the 64^{th} amino acid (NPY_{64}) and 28-aa signal/sorting peptide only fragment (NPY_{28}) (Figure $3E_1$). All reporter domains were concatenated at the C-terminus of sorting domains, an empirical practice from the *Drosophila* NPRR screening to ensure strong fluorescent brightness of reporters (Ding et al., 2019). The combinations of both domain candidates, together with variation of linker sequence in some cases, result in a pool of ~30 $NPLER^{NPY}$ candidates. mTurqoise2 and mVenus and mCherry outperform others as best reporter domains. NkB sorting domains were designed with similar strategies, though NkB prepropeptide encompasses four domains. We assumed that the best reporter candidates from $NPLER^{NPY}$ screening function equally well for NkB, and generated 12 $NPLER^{NkB}$ candidates with all possible combinations (Figure $3E_2$).

We next asked if the various compositions of sorting domains lead to differences in localization and expression of reporters. We compared four reporters: $NPLER^{NPYfl\text{-}GFP}$, $NPLER^{NPYfl\text{-}mTq2}$, $NPLER^{NPY64\text{-}mTq2}$ and $NPLER^{NPY28\text{-}mTq2}$ via antibody staining against mTq2 or GFP (Figure $4A_1$). Expression of reporters was observed in all groups, as compared with the non-transfected control (Figure $4A_2$). We then compared two reporters without full-length NPY prepropeptide as their sorting domains. N46 cells transfected with either $NPLER^{NPY28\text{-}mTq2}$ (CMV-NPY_{28}-mTq2) (Figure $4B_1$) or $NPLER^{NPY64\text{-}mTq2}$ (CMV-NPY_{64}-mTq2) (Figure $4B_2$) showed perfect colocalization of NPY

staining and GFP staining (Figure 4B). It was not surprising in the case of NPLER$^{NPY64\text{-}mTq2}$, as the sorting domain contains the entire NPY peptide reactive to the antibody. Nevertheless, NPLER$^{NPY28\text{-}mTq2}$ does not contain NPY fragment in its design. NPY staining signals were solely contributed by endogenous NPY. Colocalization of endogenous NPY and NPLER$^{NPY28\text{-}mTq2}$ suggest that the 28-aa signal peptide of NPY is sufficient to drive the proper sorting and trafficking of a reporter domain in N46 cells. The sorting/trafficking function of NPY signal peptide in the hypothalamic cell line is consistent with the reports in corticotrope tumor cells and PC12 cells (El Meskini et al., 2001).

In all reporters with sorting domain variations, we noticed that some cells showed a perinucleus fluorescent patch (indicated by red triangle, Figure 4A$_1$), while some do not (white triangle, Figure 4A$_1$). The former may suggest accumulation of immature NPLER molecules in ER or Golgi apparatus. We counted the ratio of cells showing such accumulation over all transfected cells. Around 50-65% of cells showed such "perinucleus cap" (NPLER$^{NPYfl\text{-}GFP}$: 20/38, 52.6%; NPLERNPY$^{64\text{-}mTq2}$: 27/44, 61.4%; NPLER$^{NPY28\text{-}mTq2}$: 23/55, 51.1%). The accumulation may result from the overexpression of CMV-driven NPLER in some cells. We further compared the subcellular distribution of these two NPLER^{NPY} candidates with organelle-specific markers that label ER or Golgi apparatus (ER: Calreticulin, TGN: TGN-38) (Figure 4C-D). The strong NPLER fluorescence hindered us from accurate quantification of overlap (Manders Coefficients), we turned to the processes of the cells. A small fraction of NPLER signals overlap with either ER or Golgi marker in the processes, and no statistically significant difference was found between NPLER$^{NPY64\text{-}mTq2}$ and NPLER$^{NPY28\text{-}mTq2}$ (Figure 4C$_3$, D$_3$).

To further compare the subcellular trafficking and distribution of NPLER^{NPY} candidates, reporters with different length of sorting domains were paired in all possible combinations and co-transfected

in N46 cells (Figure 5). Direct comparisons between NPY_{fl} vs. NPY_{64} (Figure 5A), NPY_{fl} vs. NPY_{28} (Figure 5B) and NPY_{64} vs. NPY_{28} (Figure 5C) all showed highly colocalized distribution in the processes, while the extent of retention near the perinucleus region differ. We conclude that all tested sorting domains of NPY, including the signal/sorting peptide only version, can route NPLERs in an efficient fashion, as how neuropeptides are processed.

We subsequently tested mTq2-based $NPLER^{NkB}$ candidates that vary in sorting domains (Figure 6A). Native fluorescence of two longer versions, $NPLER^{NkBfl\text{-}mTq2}$ ($NPLER^{NkB\text{-}1}$) and $NPLER^{NkB91\text{-}mTq2}$ ($NPLER^{NkB\text{-}2}$), exhibited fluorescent puncta in the processes, while the two shorter ones did not. Instead, the mesh-shaped pattern in $NPLER^{NkB79\text{-}mTq2}$ ($NPLER^{NkB\text{-}3}$) highly suggested ER retention. The signal peptide only $NPLER^{NkB\text{-}4}$ barely presented signals (Figure 6B). The distribution of $NPLER^{NkB\text{-}3}$ led to the hypothesis that the C-terminus domains of NkB proprepeptide are involved in proper sorting and trafficking downstream of ER processing. Therefore, we investigated the cellular organelle distribution of two best candidates $NPLER^{NkB\text{-}1}$ and $NPLER^{NkB\text{-}2}$ via organelle-specific marker labeling (ER: Calreticulin, TGN: TGN-38) (Figure 6C). Quantification with Manders Overlap Coefficient (MOC) showed no significant difference between two candidates in the Golgi apparatus (Figure $6C_2$), yet a much higher fraction of $NPLER^{NkB\text{-}2}$ was found in ER, suggesting that $NPLER^{NkB\text{-}1}$ release from ER to the downstream more efficiently (Figure $6C_1$). Taken together, we believe that the full-length sorting domain is required for an optimal $NPLER^{NkB}$.

NPLER reveals distinct routing properties of NkB and NPY

The NPLER functions as a proxy for neuropeptide localization, which allowed us to ask how NPY and NkB distribute in a cell. Double labeling of neuropeptides is challenging, as most efficient

neuropeptide antibodies are generated from rabbits. In the case of NPY, staining with antibodies of mouse or goat origins fail to show puncta pattern. We co-transfected two NPLERs, NPLER$^{NPYfl\text{-}mCherry}$ and NPLER$^{NkBfl\text{-}mTq2}$ (Figure 7A) in N46 cells. Surprisingly, they did not colocalize, particularly in the processes of the cells (Figure 7B). To test if the pattern results from the peculiarity of N46 cells, we performed a parallel experiment with the rat pheochromocytoma PC12 cells, a canonical cell line for studying neuromodulation, via co-transfection of the same reporters (Figure 7A). The NPLER^{NPY} puncta were distinct from the NPLER^{NkB} puncta (Figure 7C). Moreover, the relative scarcity of the latter reporter coincided with the expression profile of PC12 cells, which express high level of NPY but no NkB (Figure 7D).

Unlike small-molecule neurotransmitters, neuropeptides are routed into dense core vesicles for release (van den Pol, 2012). DCVs were identified via electron microscopy and named for the enhanced electron density in the vesicle lumen (De Camilli & Jahn, 1990). They also bear heterogeneity in sizes and molecular machineries, resulting in a panel of many DCV markers, notably members of the chromogranin and secretogranin families (De Camilli & Jahn, 1990; Huttner et al., 1991; Taupenot et al., 2003). These markers were mostly found in chromaffin cells, but were later found commonly shared by other cell types (Montero-Hadjadje et al., 2007; Winkler & Fischer-Colbrie, 1992). The availability of antibodies targeting some of them, in this case Chromogranin A (ChgA), Chromogranin B (ChgB), Secretogranin II (ScgII), Secretogranin III (ScgIII) and Secretogranin V (ScgV), allowed us to ask if NPY and NkB enter DCVs, and if so, of what kind. We tried to test the expression of DCV markers via antibody staining in N46 cells, but observed inconclusive fluorescent pattern caused by high background. Therefore, we used PC12 cells instead and transfected with NPLER$^{NPYfl\text{-}mTq2}$ (Figure 8A) or NPLER$^{NkBfl\text{-}mTq2}$ (Figure 8G), respectively.

NPLER^{NPY} puncta colocalize with DCV markers including ChgA, ChgB, ScgII and ScgIII. All of them label NPLER^{NPY} puncta to some extent, not perfectly ((Figure 8B-E, white triangles: colocalization, arrows: no colocalization). We did not see ScgV staining in PC12 cells (Figure 8F). In comparison, only a small fraction of NPLER^{NkB} puncta colocalize with ChgB (Figure 8I) but not the others (Figure 8H, J,K). The majority of NPLER^{NkB} seem not being labeled by any of the used DCV markers. It is likely that the NkB reporter is routed into a unique group of DCVs that are not labeled by the panel of markers in this study. Alternatively, these puncta may be transported to other cellular organelles like lysosomes. Further investigations using other DCV and organelle markers may help resolve the identity of NPLER^{NkB} routing destinations. Taken together, we conclude that NPLER^{NPY} and NPLER^{NkB} are routed in N46 and PC12 cells, suggesting that these two neuropeptides employ different sorting and trafficking mechanisms.

Visualizing NPY release with NPRR^{NPY}

Both N46 cells and PC12 cells can release neuropeptides under high potassium conditions (Figure 2D-E) (Chen et al., 1997). We conducted a mini-screen for more physiologically relevant secretagogues based on previous reports in bovine adrenal chromaffin cells (Podvin et al., 2015). The incubation with 100nM Pituitary adenylate cyclase-activating polypeptides (PACAP) in both N46 cells and PC12 cells caused the significantly decrease of anti-NPY fluorescence (Figure 9A-B), indicating the presence and efficiency of PACAP-triggered release of NPY.

Though the expression profiles of neuropeptides are well-characterized in many cell types, it remains largely unknown that how they are released. Our previous work in *Drosophila* (Ding et al., 2019), as well as the success of various similar reporters for imaging synaptic vesicles and secretory

granules (Gandasi et al., 2015; Miesenböck et al., 1998; Rutter et al., 2006), motivated us to generate neuropeptide release reporters (NPRRs) in mammalian cells. The engineering of NPLERs gained us an understanding of proper design of a sorting domain. We then surveyed various pH-sensitive fluorescent proteins and genetically engineered calcium indicators (GECIs) to select a proper reporter domain (Figure 3D). The best candidate CMV-NPY_{64}-mVSEP was a combination of a NPY-containing sorting domain and a novel pH sensitive fluorescent protein (Figure $9C_1$). The pH sensitivity profile of mVSEP provided a huge contrast between intravesicular microenvironment (pH=5.5) and extracellular spaces (pH=7.4) (Figure $9C_2$). We named the reporter $NPRR^{NPY}$. KCl-evoked release of $NPRR^{NPY}$ was observed as the brightening of sparse puncta in N46 cells (Figure 9D, orange triangles). The dynamics exhibited a relatively long release phase suggested by the "fat tail" of fluorescence curve (Figure 9E). PACAP-evoked release in N46 cells showed similar pattern (Figure 9F, orange triangles), but the peaks were sharper (Figure 9G). These results collectively suggest that the neuropeptide release dynamics may vary with different stimuli. PACAP-evoked release in PC12 cells (Figure 9H, orange triangles) were not as strong and experienced a rapid decay unlike in N46 cells (Figure 9I). We were surprised by the observation, as PACAP incubation experiments suggested a stronger release in PC12 cells rather than in N46 cells (Figure 9A-B). One explanation is the time scale difference between the incubation experiment (30 mins) and live imaging (90 seconds per trial). While the imaging focused on the puncta with fluorescent change, we observed that a large fraction of fluorescent blobs in PC12 cells remained stable in our imaging trials (Figure 9H). PC12 cells may adopt an asynchronous, slow-release mode. We attempted to prolong the length of recording, yet the weak adherence of PC12 cells gave rise to uncorrectable motion artifacts. Nevertheless, we demonstrated that the NPRR dynamics was dependent on both stimulation protocols and cell types.

An NPLER-based RNAi screening platform

RNA interference (RNAi) is a widely recognized approach for sequence-specific silencing via regulating mRNA stability (Wilson & Doudna, 2013). It is used both as a powerful gene knock-down tool in model organisms (Agrawal et al., 2003; Svoboda, 2020), and as a promising therapeutic strategy (Aagaard & Rossi, 2007; Setten et al., 2019). Cell line-based RNAi screen entails selection of a proper cell system and quantitative measurements such as qPCR of a targeted gene. We proposed to facilitate the screening by establishing an NPLER-based platform that (1) visualizes the efficacy of knock-down and (2) establishes a universally applicable cell line.

PC12 cells do not express NkB (Figure 7D$_2$). The introduction of NPLER$^{NkBfl\text{-}mTq2}$, however, showed DCV-like puncta (Figure 7C) which are partially labeled by marker ChgB (Figure 8I), suggesting that at least some NPLER^{NkB} molecules were routed correctly. We therefore designed two siRNAs targeting different regions of NkB gene (Figure 10A), either of which was co-transfected with NPLER^{NkB} (Figure 10B). Cells were double stained with GFP antibody (against the reporter domain of NPLER) and NkB antibody (against the sorting domain of NPLER). We calculated the ratio of NkB staining between the successfully transfected cells and the non-transfected cells. The mean ratios of no siRNA, siRNA^{Scramble} and siRNA$^{NkB\text{-}1}$ are between 1.6-1.8 (1.848, 1.679, 1.677) with no statistically significant differences, while the ratio in siRNA$^{NkB\text{-}2}$ (1.149) is significantly lower in siRNA^{Scramble} control (Figure 10C)), suggesting the high efficiency of NkB knock-down by siRNA$^{NkB\text{-}2}$. We reasoned that the siRNA interrupted the NPLER expression via targeting its NkB fragment in the sorting domain, by which the reporter domain would too be affected. We further quantified the fluorescent intensity of reporter domain of transfected cells. The reporter domain fluorescence in siRNA$^{NkB\text{-}2}$ is significantly lower than in control group, consistent with the findings

in NkB staining. NPLER^{NkB}-PC12 cell system provides a prototypical model for initial RNAi screening to an exogenous neuropeptide with a well-established cell line. It is possible that such practice is universally applicable to other neuropeptides.

Discussion

Here we described the development of two collections of sister reporters, NPLERs (Neuropeptide Localization and Expression Reporter) and NPRRs (Neuropeptide Release Reporter). Proof-of-concept experiments with NPLERs against NPY and NkB reveal their differences in sorting and routing. N46, a novel embryonic hypothalamic cell line, as well as the canonical PC12 cells, were used as testbeds for the reporters (Table 1). This allowed us to uncover previously unexplored cell type specificity in terms of neuropeptide processing. We further visualized NPY release dynamics in response to PACAP, a physiologically relevant stimulus and showed the distinct properties of release in N46 and PC12 cells. Lastly, we transformed PC12 cells to a potentially generalizable RNAi screening platform by introducing an NPLER for an exogenous neuropeptide. These results collectively contribute to a deeper understanding of neuropeptide pathways, and provide a powerful model platform to facilitate the explorations of neuropeptide-targeting therapeutics.

Though we provide compelling evidence on the proper sorting and trafficking of these reporters, it is likely that their strong expression may cause protein overload in the secretory pathways. Transfection of NPLER^{NPY} candidates in cells that endogenously express NPY sometimes result in a perinucleus “cap” (Figure 5), a phenomenon not observed with NPLER^{NkB}. Given that NkB was relatively sparse in compared to NPY in N46 cells (Figure 2A) and showed no staining in PC12 cells (Figure 7D), it is possible that the NPLER^{NPY} is competing with endogenous NPY for the secretory

capacities. Detailed mechanisms are unknown and await further investigations. A potential solution to this problem is to employ knock-in techniques such as CRISPR-Cas9 (Doudna & Charpentier, 2014; Hsu et al., 2014) to insert the reporter to a genetic locus to fine-tune the expression to an appropriate level.

We also attempted to image NkB release but failed due to their low baseline expression. Unlike NPLER^{NkB} that are compatible with immunocytochemistry to amplify the fluorescent intensity, NPRRs are designed for live imaging that entails higher baseline fluorescence for the identification of puncta. The use of high laser power bleached the fluorophores and hindered long-term imaging. A new fluorescent protein with optimized pH sensitivity, brightness and better resistance to photobleaching will be pivotal to the next-generation NPRR. Moreover, we failed to generate the red version of NPRRs due to the failure of capturing fluorescent contrast. New pH-sensitive red fluorescent proteins will be a powerful addition to the NPRR collection. An ideal yet undone experiment is to simultaneously image NPY and NkB release, and track their fluorescent change to multiple types of stimuli. It is tempting to investigate if the routing differences unveiled by the NPLER studies also lead to any differences in release dynamics.

We also exploited the use of NPLERs for RNAi screening by integrating NPLER^{NkB} to PC12 cells, which do not endogenously express NkB. It is shown that the efficacy of siRNA could be visualized with NPLER brightness, and PC12 cells may function as a generic testbed for an exogenous neuropeptide. These advantages may accelerate large-scale, imaging-based neuropeptide siRNA screening. Though we are too aware of its relatively low sensitivity in relation to the traditional RT-

PCR approach, which is reasonable due to the differences in the amplification process. We still believe that the imaging-based platform serves as an alternative strategy for preliminary screenings.

In the long term, we hope that NPLER/NPRR platform will better the understanding of neuropeptide biology. Its *in vivo* applications will uncover the dynamic neuromodulation of behaviorally and physiologically relevant neural circuits. The platform may ultimately work as a hypothesis generator for the discoveries of novel therapeutics for treating human diseases.

A

RT-PCR results (from suppliers)

	Hypothalamic					Insulinoma
	mHypoE-N7	mHypoE-N46	mHypoA-2/29	mHypoA-2/32	mHypoA-59	MIN6beta
NPY	-	+	+	-	++	?
NkB	++	++	very weak	strong	-	?
Insulin	-	+	-	-	-	++

B

IHC results

	Hypothalamic					Insulinoma
	mHypoE-N7	mHypoE-N46	mHypoA-2/29	mHypoA-2/32	mHypoA-59	MIN6beta
NPY	very weak/-	+	weak	-	+	+
NkB	strong	+	weak	+	+	weak
Insulin	-	very weak	-	-	very weak/-	++

C

D₁

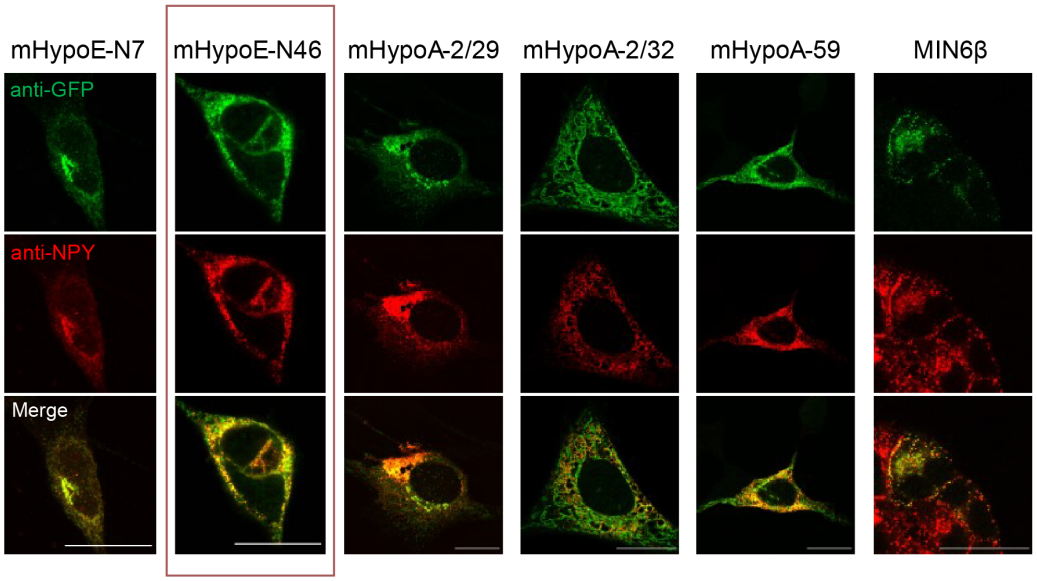

D₂

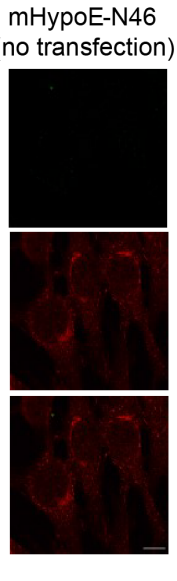

Figure 1: A novel cell line for design, screening, and validation of neuropeptide reporters.

(A) RT-PCR profiles were used as references to shortlist a collection of hypothalamic cell lines to study the neuropeptides of interest (details in Introduction); an insulinoma cell line was acquired in parallel due to its popularity in neuropeptide research (Gandasi et al., 2015; Makhmutova et al., 2017; Varadi et al., 2005). **(B)** Antibody staining-based screening of candidate cell lines yield similar results as in RT-PCR experiments yet provide extra neuropeptide expression profile in insulinoma cells. **(C,D$_1$)** Expression pattern screening of candidate cell lines with a fiduciary neuropeptide reporter NPLER$^{NPYfl\text{-}GFP}$ that follows similar design as human NPY-GFP (see **Materials and Methods** for details). **(D$_2$)** is a no-transfection control for mHypoE-N46. GFP/NPY double staining of cell lines result in a good candidate mHypoE-N46 (highlighted in red box, "N46" is used in the following contexts), which shows 1) fluorescent puncta and 2) perfect colocalization of NPLER and NPY staining pattern, both highly suggestive of proper neuropeptide trafficking. Scale bar, 10 μm.

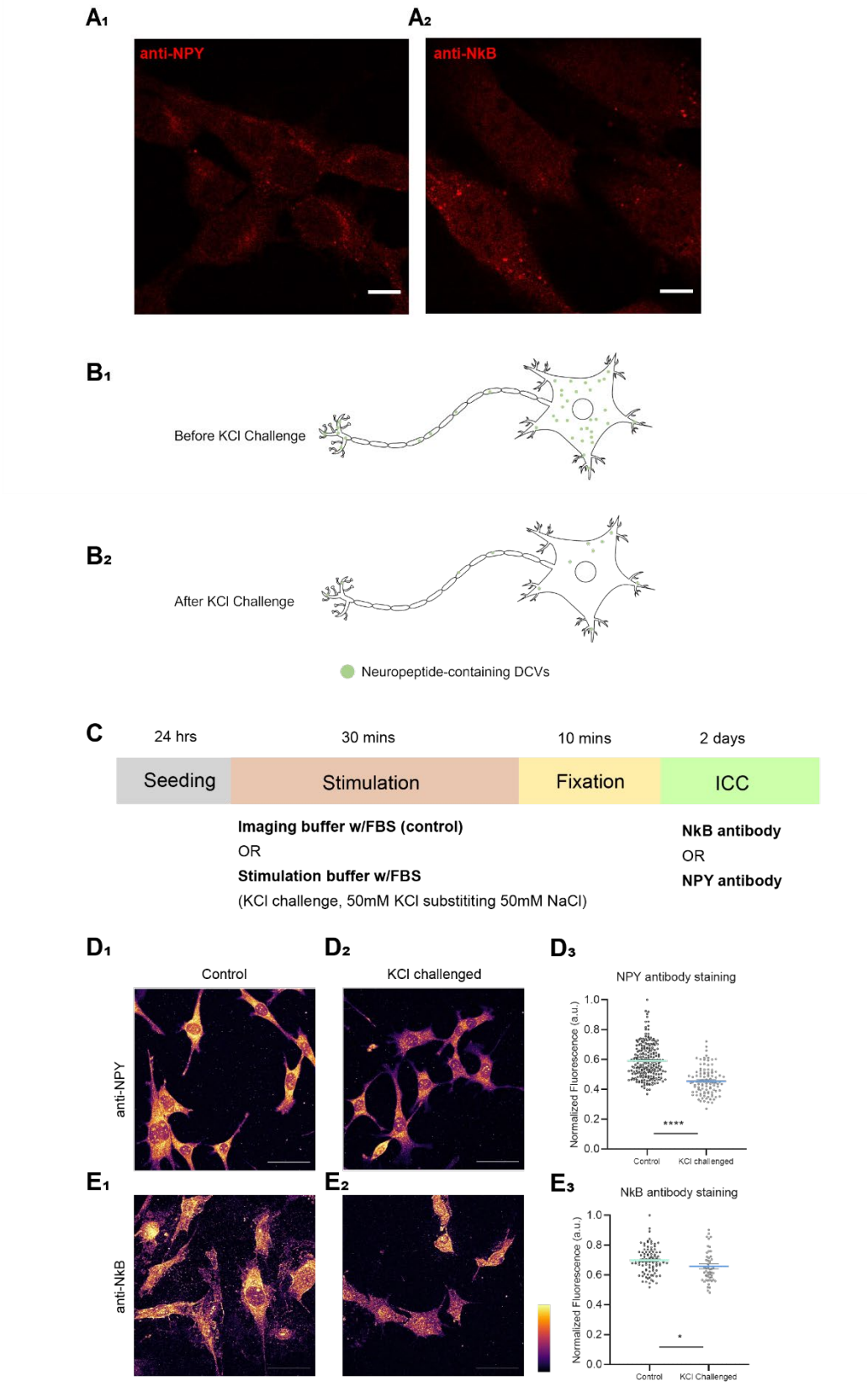

Figure 2: N46 cells express and release NPY and NkB.

(A_1) NPY and **(A_2)** NkB staining of N46 cells. **(B)** KCl-stimulation model. KCl challenge strongly depolarizes the cells and triggers massive neuropeptide release. Neuropeptide-containing DCVs in the control cells **(B_1)** will be mobilized, primed and released by KCl stimulation **(B_2)**. **(C)** Experimental procedure for KCl challenge experiment. N46 cells were seeded and grown for 24 hours, following incubation in FBS-supplemented buffer or stimulation buffer (with 50mM K^+ replacing 50mM Na^+) for 30 minutes. Cells were subsequently fixed and stained with neuropeptide antibody. **(D)** NPY staining of control **(D_1)** and KCl challenged **(D_2)** N46 cells. Quantification **(D_3)** show statistically significant reduction of NPY signals in KCl challenged group (N=102-224), implying the cells release endogenous NPY upon strong activation. **(E)** NkB staining of control **(E_1)** and KCl challenged **(E_2)** N46 cells. Quantification **(E_3)** reaches similar conclusions (N=53-96) as in **(D_3)**. (*P<0.05, ****P<0.0001, Mann-Whitney *U* test). Images in **(D_1, D_2, E_1, E_2)** were normalized and pseudo-colored to highlight contrasts.

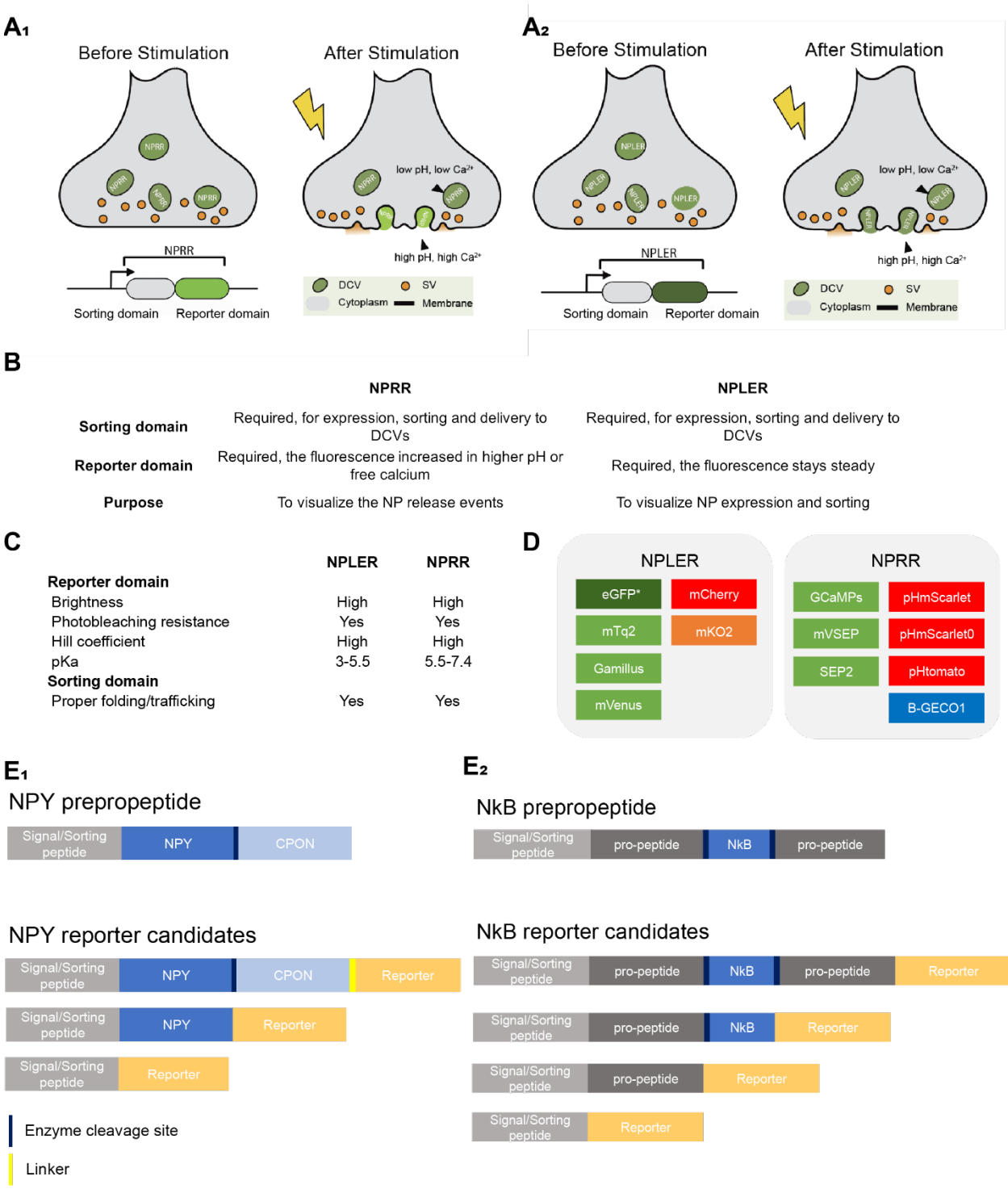

Figure 3: Neuropeptide Localization and Expression Reporters (NPLERs) and Neuropeptide Release Reporters (NPRRs).

(A_1) Principles of Neuropeptide Release Reporter (NPRR), adapted from studies in Chapter 2 (Ding et al., 2019; Han & Ding, 2022), **(A_2)** Principles of Neuropeptide Localization and Expression Reporter (NPLER). **(B)** Summary of similarities and contrasts between NPRR and NPLER. The design of sorting domain is interchangeable. The choice of reporter domain and design purposes are different. **(C)** Rationales of reporter domain selection were used to comply with principles in **(B)**. **(D)** Candidate reporter domains were selected based on **(C)**. **(E)** Candidate sorting domains were designed following the mapping of neuropeptide prepropeptide domains, the concatenation of reporter domain to the C terminus was an empirical inference from the *Drosophila* screening (Ding et al., 2019). Candidate reporters were generated for two neuropeptides of interest, Neuropeptide Y (NPY) **(E_1)** and Neurokinin B **(E_2)**.

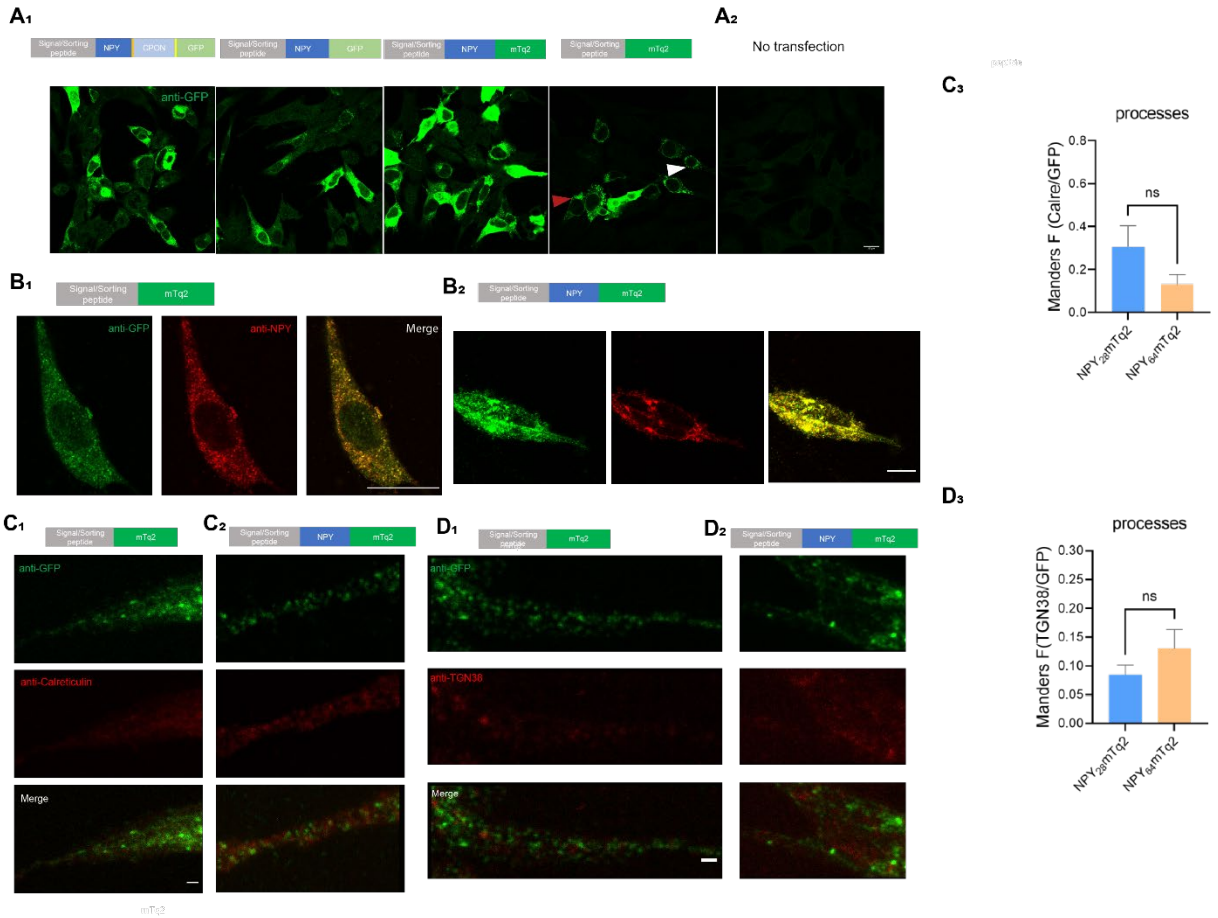

Figure 4: Comparison of NPLER^{NPY} candidates with variations in the sorting domain.

(A) Comparisons between NPLER^{NPY} with various configurations of sorting domains (A_1) and non-transfected blank control (A_2). Red triangle points to a cell with perinucleus accumulation, white triangle points to a cell without. **(B_1)** Configuration of NPLER$^{NPY28\text{-}mTq2}$ (CMV-NPY_{28}-mTq2). Transfected N46 cells show perfect colocalization of NPLER$^{NPY28\text{-}mTq2}$ and NPY, note that the reporter transgene does not contain NPY fragment. NPY staining signals are completely contributed by endogenous NPY. **(B_2)** Configuration of NPLER$^{NPY64\text{-}mTq2}$ (CMV-NPY_{64}-mTq2), transfected N46 cells show perfect colocalization of NPLER$^{NPY64\text{-}mTq2}$ and NPY, note that the reporter transgene contains the antigen reactive to NPY antibody. Scale bar, 10 µm. **($C_{1\text{-}2}$)** GFP/Calreticulin double-labeling of NPLER$^{NPY28\text{-}mTq2}$ transfected cell, similarly for NPLER$^{NPY64\text{-}mTq2}$, **(C_3)** Comparison of overlap between Calreticulin and GFP immunofluorescence in NPLER$^{NPY64\text{-}mTq2}$ and NPLER$^{NPY28\text{-}mTq2}$ (N=7-8, ns: not significant, Mann-Whitney *U* test). **($D_{1\text{-}2}$)** GFP/TGN38 double-labeling of NPLER$^{NPY28\text{-}mTq2}$ transfected cell, similarly for NPLER$^{NPY64\text{-}mTq2}$, **(C_3)** Comparison of overlap between TGN38 and GFP immunofluorescence in NPLER$^{NPY64\text{-}mTq2}$ and NPLER$^{NPY28\text{-}mTq2}$ (N=13-14, ns: not significant, Mann-Whitney *U* test).

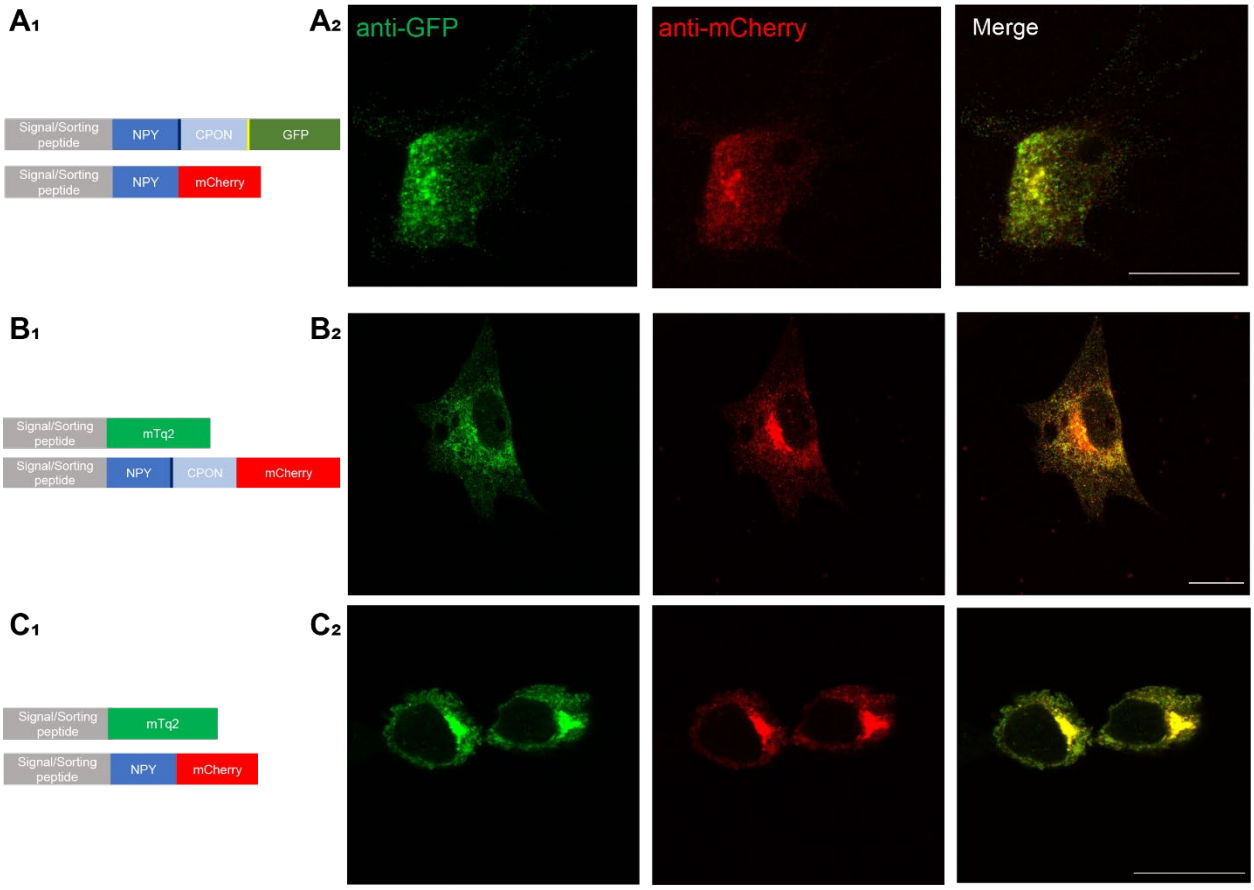

Figure 5: NPLER^{NPY} candidates with various sorting domains show similar subcellular pattern.

Green and red NPLERs with different sorting domains were co-transfected in several ways. **(A_1, B_1, C_1)** illustrate transgenes used for transfection in **(A_2, B_2, C_2)**. Comparisons of green and red channels in **(A_2, B_2, C_2),** respectively, show similar subcellular patterns. Scale bar, 10 µm.

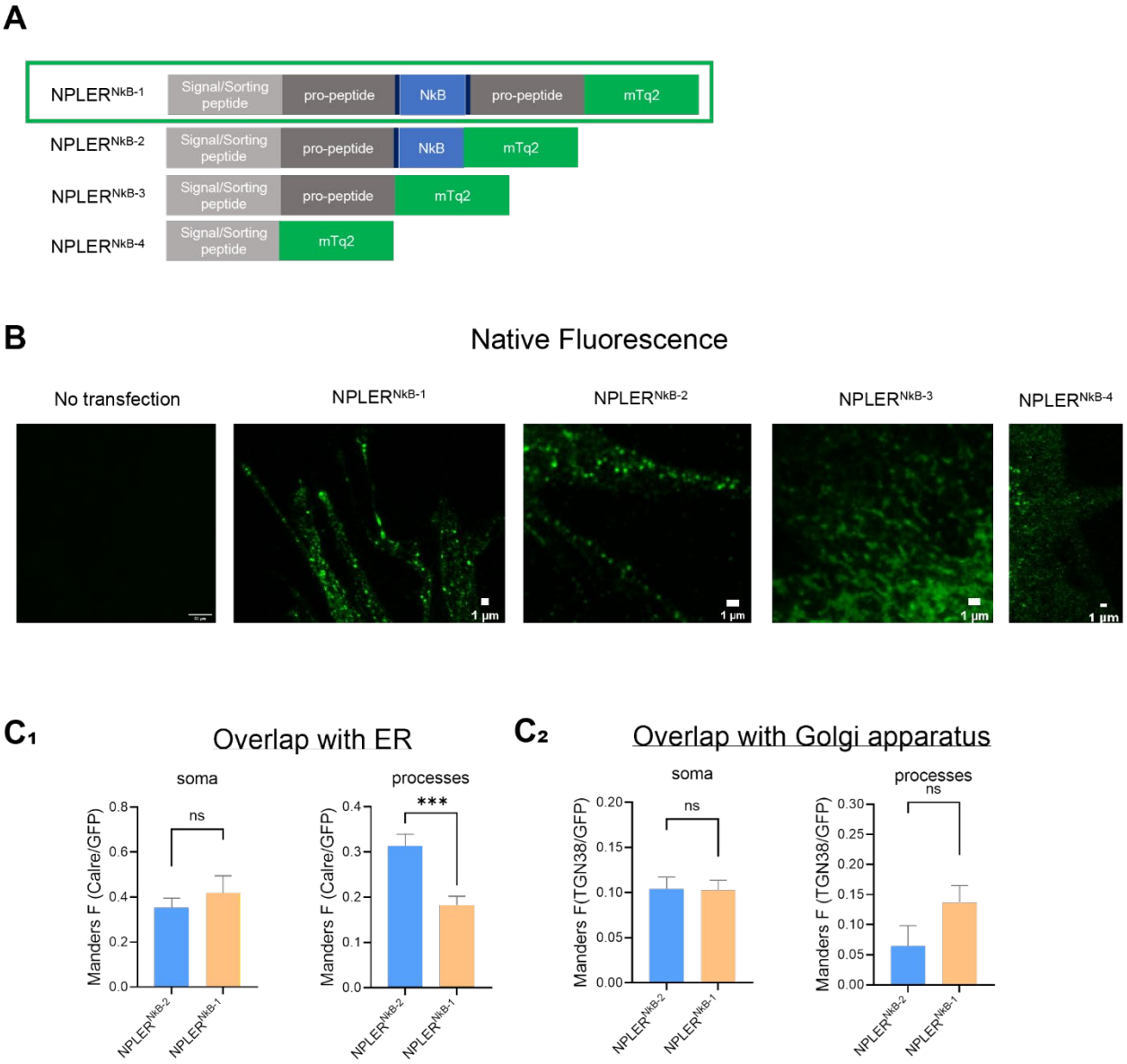

Figure 6: NPLER^{NKB} reporter requires full-length sorting domain for optimal performance.

(A) Illustration of various designs of NPLER^{NkB} candidates, which differ in the configuration of sorting domains. The best candidate full-length version NPLER^{NkB-1} is highlighted in green box. **(B)** Native fluorescence screening of NPLER^{NkB} candidates in N46 cells. NPLER^{NkB-1} and NPLER^{NkB-2} exhibit fluorescent puncta in the processes that suggest proper vesicular trafficking, while NPLER^{NkB-3} and NPLER^{NkB-4} do not. Scale bar, 1 µm except in control (10 µm). **(C)** Further comparisons between NPLER^{NkB-1} and NPLER^{NkB-2} were assisted by double labeling with an ER marker (Calreticulin) or a golgi marker (TGN38). Overlaps between the reporter and the organelle marker were quantified with the Manders' overlap coefficients. NPLER^{NkB-2} show higher level of overlap with ER, suggesting higher ER retention and lower efficiency of trafficking. Data are plotted as mean±s.e.m. (***P<0.001, Student's t-test).

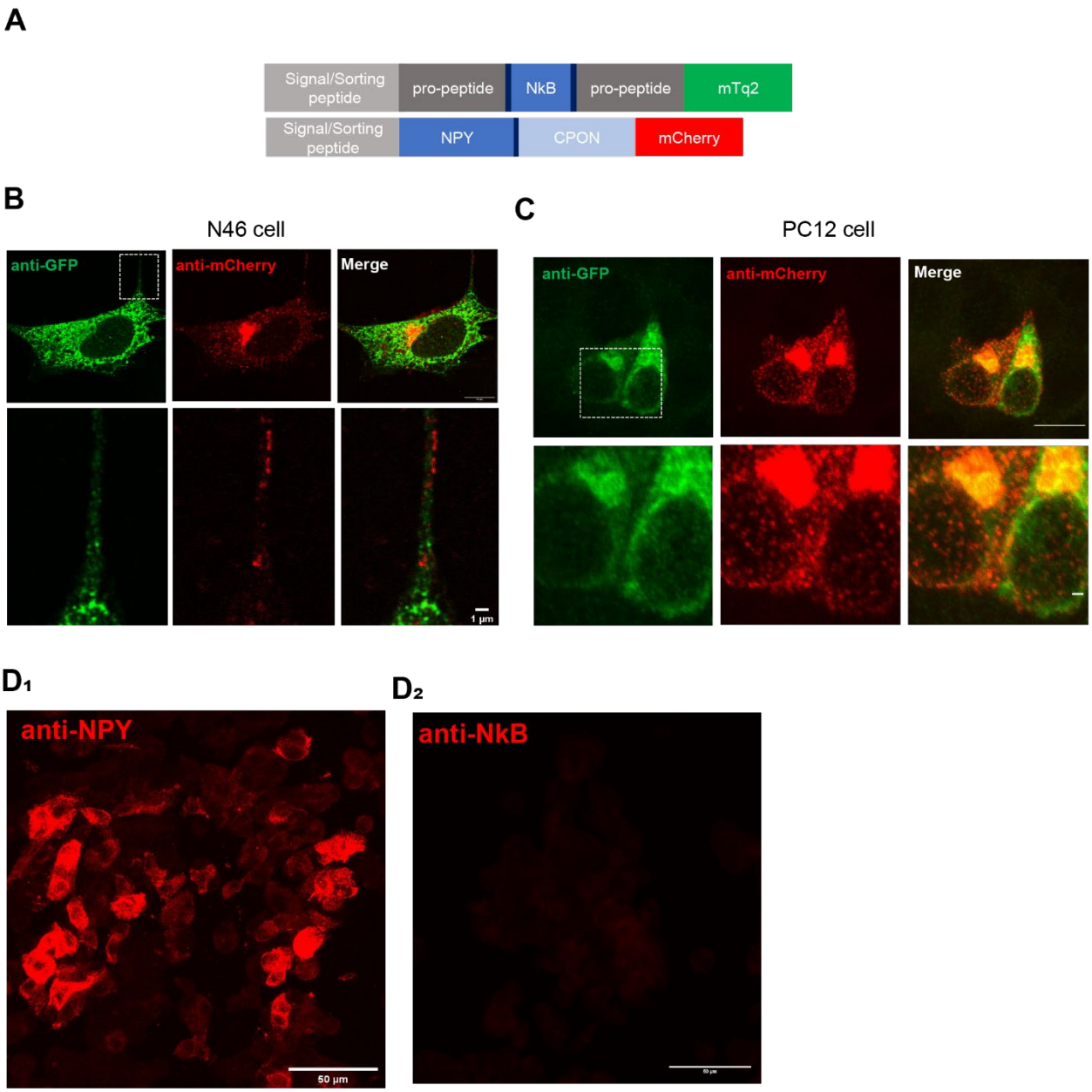

Figure 7: NPLER^{NPY} and NPLER^{NkB} are routed differently in N46 and PC12 cells.

(A) Illustration of NPLER$^{NkB\text{-}1}$ (CMV-NkB$_{full}$-mTq2) and NPLER$^{NPYfl\text{-}mCherry}$ (CMV-NPY$_{full}$-mCherry). They were co-transfected in the cell line for experiments in **(B,C)**. **(B)** Two-color staining of co-transfected N46 cells. NPLER$^{NkB\text{-}1}$ and NPLER^{NPYfl} show different subcellular patterns (upper) and do not colocalize in the processes (lower). **(C)** Two-color staining of co-transfected PC12 cells, with similar observations in **(B)**. Scale bar, 10 µm (upper) and 1 µm (lower). **(D)** PC12 cells express endogenous NPY **(D$_1$)** but not NkB **(D$_2$)**. Scale bar, 50 µm

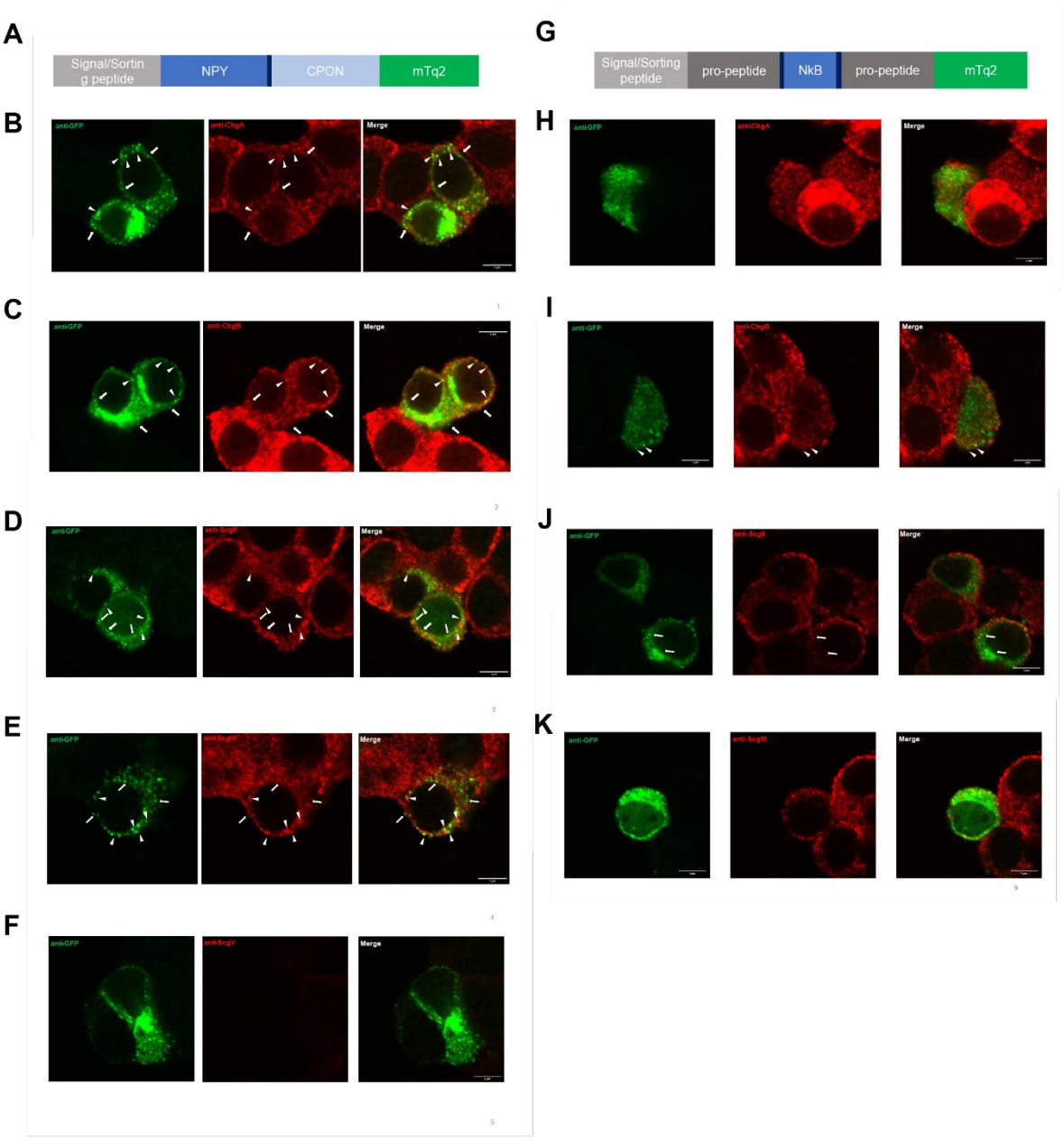

L

	ChgA	ChgB	ScgII	ScgIII	ScgV
PC12 cell	+	+	+	+	-
Overlap					
NPY^{+} DCV	+	+	+	+	N/A
NkB^{+} DCV	-	+	-	-	N/A

Figure 8: Difference in DCV entry of $NPLER^{NPY}$ and $NPLER^{NkB}$ in PC12 cells.

(A) Illustration of $NPLER^{NPYfl\text{-}mTq2}$ (CMV-NPY_{full}-mTq2). PC12 cells transfected with **(A)** were fixed and co-stained, respectively, with multiple canonical DCV markers, including Chromogranin A **(B)**, Chromogranin B **(C)**, Secretogranin II **(D)**, Secretogranin III **(E)** and Secretogranin V **(F)**. Similarly, PC12 cells transfected with $NPLER^{NkB\text{-}1}$ (CMV-NkB_{full}-mTq2, illustrated in **(G)**) were co-stained with the same panel of DCV markers **(H-K)** except Secretogranin V, as it showed no expression in PC12 cells **(F)**. White triangles indicate colocalization of DCV markers with NPLERs, yet white arrows point to NPLER fluorescent not labeled by a DCV marker. Scale bar, 50 μm. **(L)** summarizes the presence/absence of DCV markers in PC12 cells, as well as the presence of their overlap with NPY and NkB NPLERs, respectively.

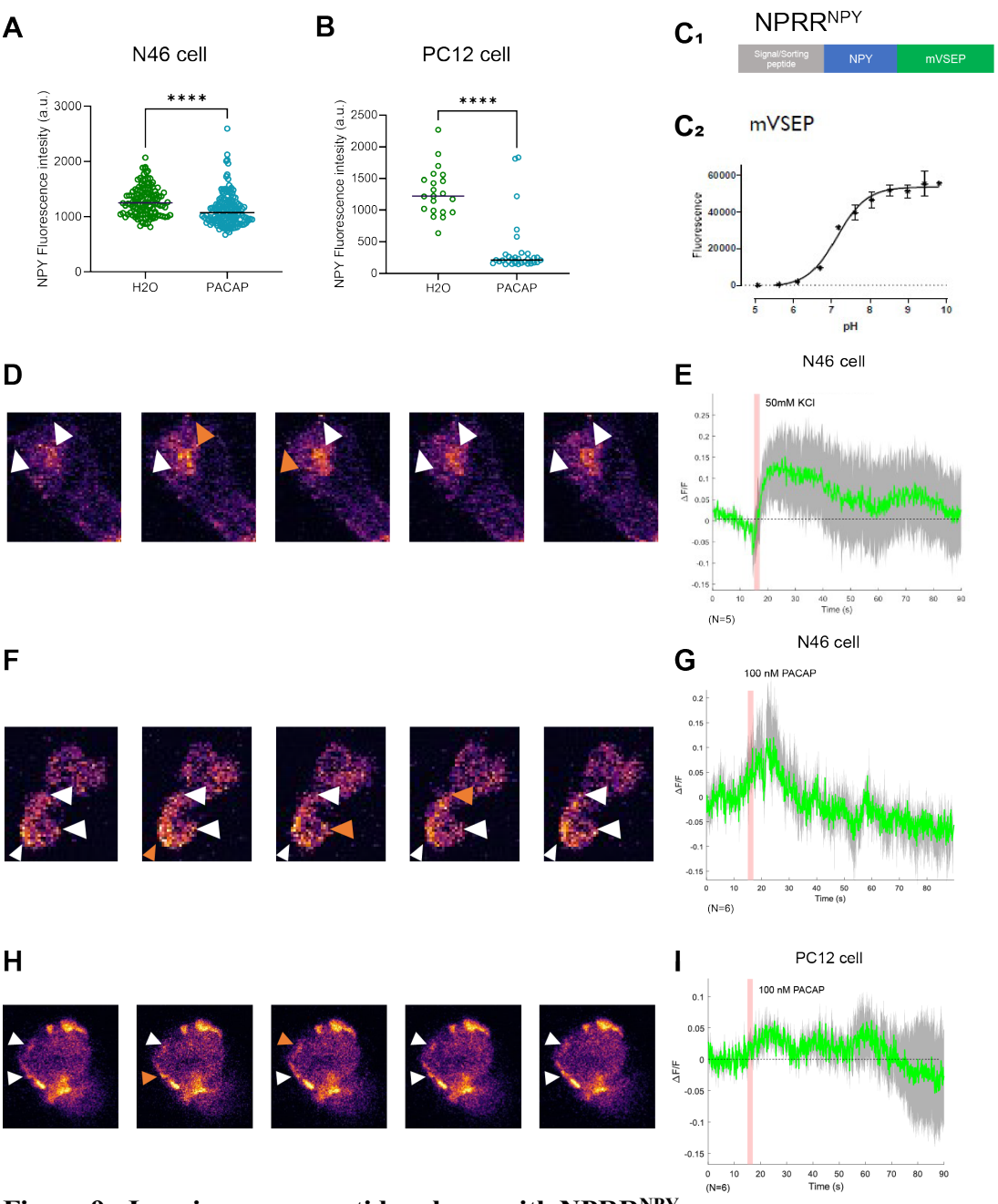

Figure 9: Imaging neuropeptide release with NPRR^{NPY}.

(A-B) Cells treated with 30 min incubation in either solvent (H_2O) or 100 nM PACAP were fixed and used for NPY antibody staining, the fluorescent intensity of each cell was individually measured, both in **(A)** N46 (N=121-134) and **(B)** PC12 (N=21-31). Data were pooled for comparison (****P<0.0001, Mann-Whitney *U* test). **(C1)** Illustration of NPRR^{NPY} configuration. **(C2)** Characterization of a novel pHluorin mVSEP that constitutes the reporter domain of NPRR^{NPY}. Similar case was seen in PC12 cells. N46 cells transfected with NPRR^{NPY} were imaged with KCl stimulation **(D-E)** or PACAP stimulation **(F-G)**, similarly transfected PC12 cells were imaged with

PACAP stimulation **(H-I)**, KCl stimulation caused PC12 cells dislodge and hindered live imaging. Images in **(D,F,H)** are pseudo-colored to highlight contrast. Triangles point to regions of interest, while orange triangles indicate the onset of releasing events.In **(E,G,I)**, red bar indicates the introduction of stimuli, pooled trials are presented as mean±s.e.m. (N=5-6, shown in figures).

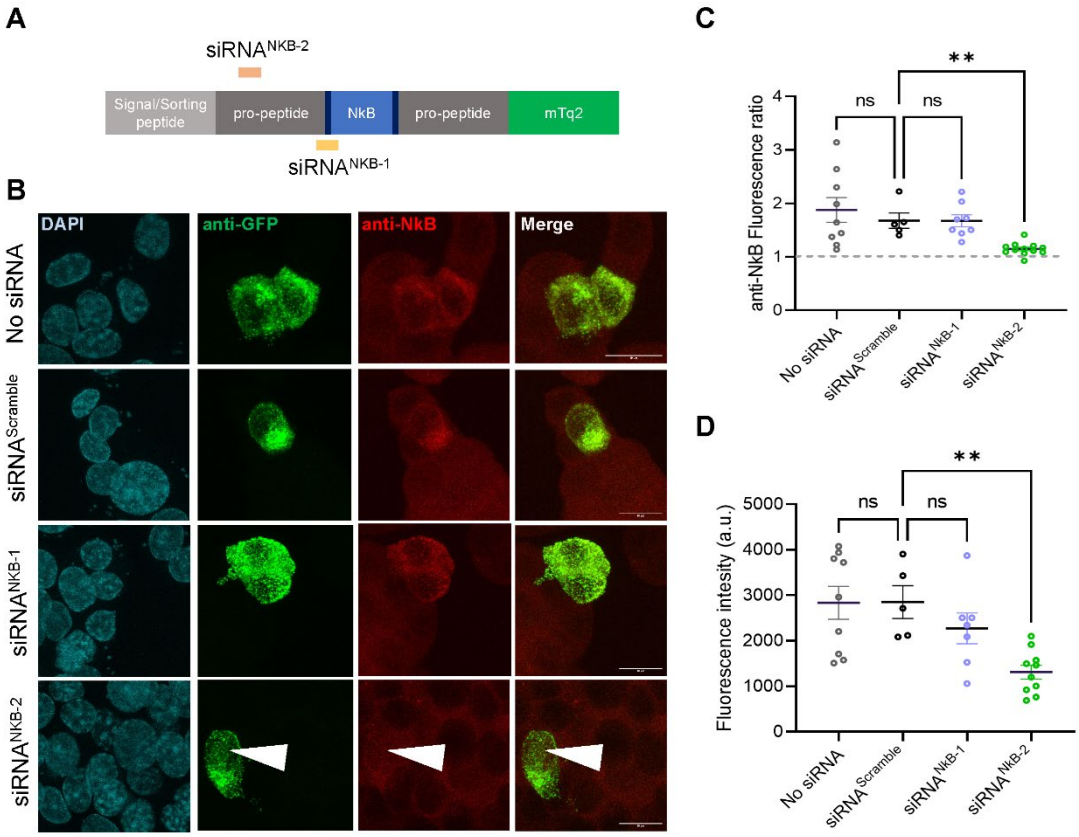

Figure 10: An NPLER-based RNAi screening platform.

(A) The targeting regions of NkB siRNAs, in reference to the NPLER^{NkB-1}. **(B)** 3-color confocal imaging of PC12 cells transfected with siRNAs. All groups show positive correlation of GFP channel and NkB channel except in siRNA^{NkB-2}. White arrows point to a representative cell that shows NkB reduction when transfected, suggesting the knock-down effect of NkB by the siRNA. **(C)** Images were quantified in each group to compare the anti-NkB fluorescence ratio between NPLER transfected or non-transfected cells in the same experiment. The ratio of siRNA^{NkB-2} is statistically lower than the siRNA^{Scramble} (N=5-12) **(D)** The absolute fluorescent intensity of transfected cells was quantified and compared for each group (N=5-10) (**P<0.01, Kruskal-Wallis test).

	Origin	Growth	Maintenance	Adherence	Transfection efficiency*	Expression of NP	Prescence of DCV
N46	Mouse embryonic hypothalamic cell	Fast	Easy	High	10-20%	Yes	?
PC12	Rat pheochromocytoma cell	Slow	Hard	Low	5-10%	Yes	Yes

Table 1: Comparison of N46 cells and PC12 cells.

Materials and Methods

Cell culture

Hypothalamic cell lines (Cedarlane Laboratories), MIN-6β cells (Addexbio Technologies) and PC12 cells (ATCC) were maintained at 37 ℃ under 5% CO_2. Hypothalamic cell lines were maintained in high-glucose Dulbecco's modified essential medium containing 10% fetal bovine serum, 100 units/ml penicillin, and 0.1 mg/ml streptomycin as suggested by the cell line supplier. MIN-6β cells were maintained similarly except 15% fetal bovine serum was added. PC12 cells were grown in Dulbecco's modified essential medium containing 5% calf serum, 5% horse serum, 100 units/ml penicillin, and 0.1 mg/ml streptomycin. In every passage, a fraction of cells was stored in liquid nitrogen for further use. All cells were discarded after 10 times of passage. JetPRIME® Versatile DNA/siRNA transfection reagent (Polyplus transfection) was used in all cell transfection experiments.

Molecular cloning

All PCR reactions were performed using PrimeSTAR HS DNA polymerase (Takara #R045Q). To construct NPRR and NPLER candidates, sorting domain fragments were cloned from mouse cDNA library (OriGene Technologies) or synthesized using gBlocks service (Integrated DNA Technologies), while reporter domains were cloned from commercially available plasmids that contain DNA fragments encoding fluorescent proteins (Addgene). Human NPY-GFP (Addgene #74629) was used as a reference transgene. All fragments were subcloned into pCMV or pAAV backbone using Gibson Assembly approach. All constructs were verified via DNA sequencing (Laragen). Candidate plasmids that pass preliminary cell line screening underwent Maxiprep, pCMV plasmids were prepared with Pureyield System (Promega A2393) and pAAV plasmids with Nucleobond® Xtra Maxi EF (Takara #740424.10).

Immunocytochemistry (ICC)

Cells were seeded in 24-well plates that were prepared in advance to have a piece of poly D-lysine (PDL) coated cover glass (Carolina Biological Supply 633029) that were in each well. After 24 hours of transfection, cells were quickly rinsed with PBS and fixed in 4 % paraformaldehyde for 10 min at room temperature. After two 5-min rinses with PBS and one 5-min rinse with 0.1% PBST, cells were blocked for 3 minutes in PBST with 5% normal goat serum, and subsequently incubated in primary antibodies overnight at 4 °C with gentle shaking. Following three 10-min rinses with PBS, cells were incubated in secondary antibodies for 2 hours at room temperature with gentle shaking. Cover glasses with cells on top were carefully dried with Kimwipe and inverted placed on a slide with a tiny drop of mounting media (Vectashield with DAPI, Vector Laboratories; Slowfade, Thermo Scientific S36963). To prevent cover glasses from gliding, electric tapes were cut in tiny strips and placed on both sides of the glass. Confocal serial optical

sections were acquired using an Fluoview FV3000 Confocal laser scanning biological microscope (Olympus) with a 60×, 1.30 N.A. silicone oil objective (Olympus). All image processing and analyses were performed using ImageJ (National Institute of Health).

The following primary antibodies were used: Chicken anti-GFP (1:2000, Aveslab #1020), Rabbit anti-NkB (1:500, Thermo Scientific PA116745), Rabbit anti-NPY (1:500, BMA Biomedicals T4070), Mouse anti-dsRed (1:500, Takara #632543), Rabbit anti-dsRed (1:500, Takara #632496), Rabbit anti-NPY (1:500, BMA Biomedicals T4070), Rabbit anti-NPY (1:500, Cell Signaling Technology 11976S), Rabbit anti-ChgA (1:500, SYSY #259003), Rabbit anti-ChgB (1:500, SYSY #259103), Rabbit anti-ScgII (1:500, Proteintech 20357-1-AP) , Rabbit anti-ScgIII (1:500, Proteintech 10954-1-AP), Rabbit anti-ScgV (1:500, Proteintech 10761-1-AP), Rabbit anti-Calreticulin (1:500, Novus Biologicals NB600-103SS), Rabbit anti-TGN38 (1:500, Novus Biologicals, #NBP1-03495SS), Mouse anti-TGN38 (1:500, BD #610898).

The following secondary antibodies were used: Alexa Fluor 488 Goat anti-Chicken IgY (#A11039, Invitrogen), Alexa Fluor 488 Goat anti-Rabbit IgG (#A11008, Invitrogen), Alexa Fluor 568 Goat anti-Rabbit IgG(H+L) (#A11011, Invitrogen), Alexa Fluor 568 Goat anti-Mouse IgG(H+L) (#A11004, Invitrogen) and Alexa Fluor 633 Goat anti-Mouse IgG(H+L) (#A21050, Invitrogen).

RNAi experiments

All siRNA probes were purchased or synthesized (Integrated DNA Technologies), and transfected using JetPRIME® Versatile DNA/siRNA transfection reagent (Polyplus transfection) to yield the final concentration of 50 μM. Transfection efficiency was estimated with fluorescently labeled TYE

563 siRNA control provided (Integrated DNA Technologies) prior to each batch of experiments. $siRNA^{Scramble}$ was a negative control from the same supplier. Antisense sequences of used siRNA are shown below.

$siRNA^{NkB-1}$: ACGUUUCUGUGGAAGUGAUGUCUCCUU

$siRNA^{NkB-2}$: AAGCUGAGGGCGAGGACAGCCGCAAAC

Live imaging

Cells were seeded in 24 well plates that were prepared in advance to have 2-3 pieces of PDL-coated cover glass (Warner Instruments 64-0700, 64-0720) placed in each well. After 24-34 hour of transfection, cover glasses were transferred to a customized perfusion chamber and bathed in imaging solutions. The imaging solution used for imaging experiments of hypothalamic cell lines consisted of (in mM): 140 NaCl, 4 KCl, 2 $CaCl_2$, 1 $MgCl_2$, 10 glucose, and 10 HEPES at pH 7.3 as in (Belsham et al., 2004). stimulation solution consisted of (in mM): 94 NaCl, 50 KCl, 2 $CaCl_2$, 1 $MgCl_2$, 10 glucose, and 10 HEPES at pH 7.3 was used for KCl stimulation. Imaging solution for PC12 cell lines contains (in mM):130 NaCl, 5 KCl, 0.33 Na_2HPO_4, 0.44 KH_2PO_4, 4.2 $NaHCO_3$, 5.6 glucose, 0.8 $MgCl_2$, and 10 HEPES at pH 7.4 as in (Bauerfeind et al., 1995). KCl stimulation of PC12 was performed with imaging solution altered with (in mM) 85 NaCl, 50 KCl, all else equal. Perfusion of imaging and stimulation solution was assisted with a peristaltic pump (Cole-Parmer EW-78001-72), while secretagogue PACAP (Tocris, #1186), was prepared at 1000X concentration (100 nM) and injected locally into the imaging solution. Time-lapse images were acquired using an Fluoview FV3000 Confocal laser scanning biological microscope (Olympus) with a 60×, 0.90 N.A. water objective (Olympus). Resonant scanning mode was used, sampling speed was tuned to 8-10Hz with adjustments in number of averaging, zoom-in factors and size of

imaging window. Image J Plugins including Image Stabilizer (K. Li, CMU) and Template Matching (Q. Tseng) were used for compensating minor x-y drifting. Image series with z-drift were discarded.

Statistical analysis

All data analysis was performed with Graphpad Prism 9, Microsoft Excel and custom Matlab codes. Mann-Whitney *U* test was used for comparison in most cases. Data underwent normality tests in advance if parametric comparisons were needed (Kolmogorov-Smirnov test, Shapiro-Wilk test, D'Agostino & Pearson test). Bonferroni correction was used for multiple comparisons.

References

Aagaard, L., & Rossi, J. J. (2007). RNAi therapeutics: Principles, prospects and challenges. *Advanced Drug Delivery Reviews*. https://doi.org/10.1016/j.addr.2007.03.005

Agrawal, N., Dasaradhi, P. V. N., Mohmmed, A., Malhotra, P., Bhatnagar, R. K., & Mukherjee, S. K. (2003). RNA Interference: Biology, Mechanism, and Applications. *Microbiology and Molecular Biology Reviews*, *67*(4), 657–685. https://doi.org/10.1128/mmbr.67.4.657-685.2003

Bauerfeind, R., Jelinek, R., & Huttner, W. B. (1995). Synaptotagmin I- and II-deficient PC12 cells exhibit calcium-independent, depolarization-induced neurotransmitter release from synaptic-like microvesicles. *FEBS Letters*, *364*(3), 328–334. https://doi.org/10.1016/0014-5793(95)00419-A

Belsham, D. D., Cai, F., Cui, H., Smukler, S. R., Salapatek, A. M. F., & Shkreta, L. (2004). Generation of a Phenotypic Array of Hypothalamic Neuronal Cell Models to Study Complex Neuroendocrine Disorders. *Endocrinology*, *145*(1), 393–400. https://doi.org/10.1210/EN.2003-0946

Bulgari, D., Jha, A., Deitcher, D. L., & Levitan, E. S. (2018). Myopic (HD-PTP, PTPN23) selectively regulates synaptic neuropeptide release. *Proceedings of the National Academy of Sciences of the United States of America*, *115*(7), 1617–1622. https://doi.org/10.1073/pnas.1716801115

Cavadas, C., Silva, A. P., Cotrim, M. D., Ribeiro, C. A. F., Brunner, H. R., & Grouzmann, E. (2002). Differential secretion of catecholamine and neuropeptide Y in response to KCl from mice chromaffin cells. *Annals of the New York Academy of Sciences*, *971*, 335–337. https://doi.org/10.1111/j.1749-6632.2002.tb04489.x

Chen, T. W., Wardill, T. J., Sun, Y., Pulver, S. R., Renninger, S. L., Baohan, A., Schreiter, E. R., Kerr, R. A., Orger, M. B., Jayaraman, V., Looger, L. L., Svoboda, K., & Kim, D. S. (2013). Ultrasensitive fluorescent proteins for imaging neuronal activity. *Nature*, *499*(7458), 295–300. https://doi.org/10.1038/nature12354

Chen, X., Dimaggio, D. A., Han, S. P., & Westfall, T. C. (1997). Autoreceptor-induced inhibition of neuropeptide Y release from PC-12 cells is mediated by Y2 receptors. *American Journal of Physiology - Heart and Circulatory Physiology*, *273*(4 42-4). https://doi.org/10.1152/ajpheart.1997.273.4.h1737

De Camilli, P., & Jahn, R. (1990). Pathways to regulated exocytosis in neurons. *Annual Review of Physiology*, *52*(1), 625–645. https://doi.org/10.1146/annurev.ph.52.030190.003205

de Juan-Sanz, J., Holt, G. T., Schreiter, E. R., de Juan, F., Kim, D. S., & Ryan, T. A. (2017). Axonal Endoplasmic Reticulum Ca2+ Content Controls Release Probability in CNS Nerve Terminals. *Neuron*, *93*(4), 867-881.e6. https://doi.org/10.1016/j.neuron.2017.01.010

Ding, K., Han, Y., Seid, T. W., Buser, C., Karigo, T., Zhang, S., Dickman, D. K., & Anderson, D. J. (2019). Imaging neuropeptide release at synapses with a genetically engineered reporter. *ELife*, *8*. https://doi.org/10.7554/elife.46421

Doudna, J. A., & Charpentier, E. (2014). The new frontier of genome engineering with CRISPR-Cas9. *Science*. American Association for the Advancement of Science.

https://doi.org/10.1126/science.1258096

Dube, M. G., Sahu, A., Kalra, P. S., & Kalra, S. P. (1992). Neuropeptide Y release is elevated from the microdissected paraventricular nucleus of food-deprived rats: an in vitro study. *Endocrinology*, *131*(2), 684–688. https://doi.org/10.1210/endo.131.2.1639015

El Meskini, R., Jin, L., Marx, R., Bruzzaniti, A., Lee, J., Emeson, R. B., & Mains, R. E. (2001). A signal sequence is sufficient for green fluorescent protein to be routed to regulated secretory granules. *Endocrinology*, *142*(2), 864–873. https://doi.org/10.1210/endo.142.2.7929

Gamber, K. M., Macarthur, H., & Westfall, T. C. (2005). Cannabinoids augment the release of neuropeptide Y in the rat hypothalamus. *Neuropharmacology*, *49*(5), 646–652. https://doi.org/10.1016/j.neuropharm.2005.04.017

Gandasi, N. R., Vestö, K., Helou, M., Yin, P., Saras, J., & Barg, S. (2015). *Survey of Red Fluorescence Proteins as Markers for Secretory Granule Exocytosis*. https://doi.org/10.1371/journal.pone.0127801

Hall, J. E. (2019). Neuroendocrine Control of the Menstrual Cycle. *Yen & Jaffe's Reproductive Endocrinology: Physiology, Pathophysiology, and Clinical Management: Eighth Edition*. Elsevier Inc. https://doi.org/10.1016/B978-0-323-47912-7.00007-X

Han, Y., & Ding, K. (2022). Imaging Neuropeptide Release at *Drosophila* Neuromuscular Junction with a Genetically Engineered Neuropeptide Release Reporter. *Methods in Molecular Biology*, *2417*, 193–203. https://doi.org/10.1007/978-1-0716-1916-2_15

Heilig, M. (2004). The NPY system in stress, anxiety and depression. *Neuropeptides*. https://doi.org/10.1016/j.npep.2004.05.002

Hirsch, D., & Zukowska, Z. (2012). NPY and stress 30 years later: The peripheral view. *Cellular and Molecular Neurobiology*. https://doi.org/10.1007/s10571-011-9793-z

Hökfelt, T., Bartfai, T., & Bloom, F. (2003). Neuropeptides: Opportunities for drug discovery. *Lancet Neurology*. https://doi.org/10.1016/S1474-4422(03)00482-4

Hökfelt, T., Stanic, D., Sanford, S. D., Gatlin, J. C., Nilsson, I., Paratcha, G., Ledda, F., Fetissov, S., Lindfors, C., Herzog, H., Johansen, J. E., Ubink, R., & Pfenninger, K. H. (2008). NPY and its involvement in axon guidance, neurogenesis, and feeding. *Nutrition*. https://doi.org/10.1016/j.nut.2008.06.010

Hoyle, C. H. V. (1998). Neuropeptide families: Evolutionary perspectives. *Regulatory Peptides*. https://doi.org/10.1016/S0167-0115(97)01073-2

Hsu, P. D., Lander, E. S., & Zhang, F. (2014). Development and applications of CRISPR-Cas9 for genome engineering. *Cell*. https://doi.org/10.1016/j.cell.2014.05.010

Huttner, W. B., Gerdes, H. H., & Rosa, P. (1991). The granin-(chromogranin/secretogranin) family. *Trends in Biochemical Sciences*, *16*(C), 27–30. https://doi.org/10.1016/0968-0004(91)90012-K

Liu, A., Huang, X., He, W., Xue, F., Yang, Y., Liu, J., Chen, L., Yuan, L., & Xu, P. (2021). pHmScarlet is a pH-sensitive red fluorescent protein to monitor exocytosis docking and fusion steps. *Nature Communications*, *12*(1), 1–12. https://doi.org/10.1038/s41467-021-21666-7

Loh, K., Herzog, H., & Shi, Y. C. (2015). Regulation of energy homeostasis by the NPY system.

Trends in Endocrinology and Metabolism. https://doi.org/10.1016/j.tem.2015.01.003

Luquet, S., Perez, F. A., Hnasko, T. S., & Palmiter, R. D. (2005). NPY/AgRP neurons are essentials for feeding in adult mice but can be ablated in neonates. *Science*, *310*(5748), 683–685. https://doi.org/10.1126/science.1115524

Makhmutova, M., Liang, T., Gaisano, H., Caicedo, A., & Almaça, J. (2017). Confocal imaging of neuropeptide Y-pHluorin: A technique to visualize insulin granule exocytosis in intact murine and human islets. *Journal of Visualized Experiments*, *2017*(127). https://doi.org/10.3791/56089

Miesenböck, G., De Angelis, D. A., & Rothman, J. E. (1998). Visualizing secretion and synaptic transmission with pH-sensitive green fluorescent proteins. *Nature*, *394*(6689), 192–195. https://doi.org/10.1038/28190

Montero-Hadjadje, M., Vaingankar, S., Elias, S., Tostivint, H., Mahata, S. K., & Anouar, Y. (2007). Chromogranins A and B and secretogranin II: evolutionary and functional aspects. *Acta Physiologica*, *192*(2), 309–324. https://doi.org/10.1111/j.1748-1716.2007.01806.x

Nusbaum, M. P., Blitz, D. M., & Marder, E. (2017). Functional consequences of neuropeptide and small-molecule co-transmission. *Nature Reviews Neuroscience*. https://doi.org/10.1038/nrn.2017.56

Ou, X. M., Partoens, P. M., Wang, J. M., Walker, J. H., Danks, K., Vaughan, P. F., & De Potter, W. P. (1998). The storage of noradrenaline, neuropeptide Y and chromogranins in and stoichiometric release from large dense cored vesicles of the undifferentiated human neuroblastoma cell line SH-SY5Y. *International Journal of Molecular Medicine*, *1*(1), 105–112. https://doi.org/10.3892/ijmm.1.1.105

Parker, J. A., & Bloom, S. R. (2012). Hypothalamic neuropeptides and the regulation of appetite. *Neuropharmacology*. https://doi.org/10.1016/j.neuropharm.2012.02.004

Piedimonte, G. (1995). Tachykinin peptides, receptors, and peptidases in airway disease. *Experimental Lung Research*. Ihttps://doi.org/10.3109/01902149509031765

Podvin, S., Bundey, R., Toneff, T., Ziegler, M., & Hook, V. (2015). Profiles of secreted neuropeptides and catecholamines illustrate similarities and differences in response to stimulation by distinct secretagogues. *Molecular and Cellular Neuroscience*, *68*, 177–185. https://doi.org/10.1016/j.mcn.2015.06.008

Russo, A. F. (2017). Overview of Neuropeptides: Awakening the Senses? *Headache*, *57*(Suppl 2), 37–46. https://doi.org/10.1111/head.13084

Rutter, G. A., Loder, M. K., & Ravier, M. A. (2006). Rapid three-dimensional imaging of individual insulin release events by Nipkow disc confocal microscopy. *Biochemical Society Transactions*, *34*(5), 675–678. https://doi.org/10.1042/BST0340675

Setten, R. L., Rossi, J. J., & Han, S. ping. (2019). The current state and future directions of RNAi-based therapeutics. *Nature Reviews Drug Discovery*. https://doi.org/10.1038/s41573-019-0017-4

Svoboda, P. (2020). Key Mechanistic Principles and Considerations Concerning RNA Interference. *Frontiers in Plant Science*. https://doi.org/10.3389/fpls.2020.01237

Taupenot, L., Harper, K. L., & O'Connor, D. T. (2003). The Chromogranin–Secretogranin Family.

New England Journal of Medicine, *348*(12), 1134–1149. https://doi.org/10.1056/nejmra021405

van den Pol, A. N. (2012). Neuropeptide Transmission in Brain Circuits. *Neuron*. https://doi.org/10.1016/j.neuron.2012.09.014

Varadi, A., Tsuboi, T., & Rutter, G. A. (2005). Myosin Va transports dense core secretory vesicles in pancreatic MIN6 β-cells. *Molecular Biology of the Cell*, *16*(6), 2670–2680. https://doi.org/10.1091/mbc.E04-11-1001

Wang, X., Hu, R., Liang, J., Li, Z., Sun, W., & Pan, X. (2016). 5-HT7 Receptors Are Not Involved in Neuropeptide Release in Primary Cultured Rat Trigeminal Ganglion Neurons. *Journal of Molecular Neuroscience*, *59*(2), 251–259. https://doi.org/10.1007/s12031-016-0727-6

Williams, D. M., Nawaz, A., & Evans, M. (2020). Drug Therapy in Obesity: A Review of Current and Emerging Treatments. *Diabetes Therapy*. https://doi.org/10.1007/s13300-020-00816-y

Wilson, R. C., & Doudna, J. A. (2013). Molecular Mechanisms of RNA Interference. *Annual Review of Biophysics*, *42*(1), 217–239. https://doi.org/10.1146/annurev-biophys-083012-130404

Winkler, H., & Fischer-Colbrie, R. (1992). The chromogranins A and B: The first 25 years and future perspectives. *Neuroscience*, *49*(3), 497–528. https://doi.org/10.1016/0306-4522(92)90222-N

Yulyaningsih, E., Zhang, L., Herzog, H., & Sainsbury, A. (2011). NPY receptors as potential targets for anti-obesity drug development. *British Journal of Pharmacology*, *163*(6), 1170–1202. https://doi.org/10.1111/j.1476-5381.2011.01363.x

Zelikowsky, M., Hui, M., Gradinaru, V., Deverman, B. E., Anderson, D. J., Karigo, T., Choe, A., Yang, B., Blanco, M. R., Beadle, K., Gradinaru, V., Deverman, B. E., & Anderson, D. J. (2018). The Neuropeptide Tac2 Controls a Distributed Brain State Induced by Chronic Social Isolation Stress. *Cell*, *173*(5), 1265-1279.e19. https://doi.org/10.1016/j.cell.2018.03.037

Zhao, Y., Araki, S., Wu, J., Teramoto, T., Chang, Y. F., Nakano, M., Abdelfattah, A. S., Fujiwara, M., Ishihara, T., Nagai, T., & Campbell, R. E. (2011). An expanded palette of genetically encoded Ca2+ indicators. *Science*, *333*(6051), 1888–1891. https://doi.org/10.1126/science.1208592

Chapter 4

EXPLORING NOVEL THERAPEUTICS WITH GENETICALLY ENGINEERED REPORTERS

Summary

A variety of psychiatric and metabolic disorders are associated with the dysfunction of neuropeptide signaling pathways, whose malfunction can result in a variety of mental illnesses and metabolic disorders. Neuropeptide receptors are druggable targets (typically GPCRs) that have received heavy investment from the pharmaceutical industry. Many of these drugs have failed in the clinic, however, resulting in abandonment of this approach. One potential reason for failure is that each neuropeptide often has multiple, functionally redundant receptors. Therefore, inhibiting just one receptor may not suffice to have any effect. An alternative strategy is to target the *processing/release* of the neuropeptide from neurons, rather than blocking its receptor. We have developed new technology that allows the detection of localization, expression and release of specific neuropeptides. Here we propose to use this technology to develop an *in vitro* platform for high-throughput screening of drug libraries for CRISPR sgRNAs, specific recombinant antibodies and rational design of novel neuropeptide derivatives. In the long term, we expect to develop a large-scale drug screening platform that automates the research and development of neuropeptide-targeted lead compounds.

Introduction

Neuropeptides are a class of neural signaling molecules that play a pivotal role in brain function and human health. Malfunctioning of neuropeptide pathways can potentially result in a variety of mental illnesses triggered by stress, and metabolic disorders, including obesity (Griebel & Holsboer, 2012;

Hökfelt et al., 2003). For example, it is widely believed that disrupted cholecystokinin (CCK), neurokinin (NK) and corticotropin-release factor (CRF) pathways cause depression and anxiety (Bowers et al., 2012; Schank et al., 2012); abnormal neuropeptide Y (NPY) and Agouti-Related Peptide (AGRP) signaling results in feeding disorders which can potentially lead to obesity (Arora & Anubhuti, 2006; Dhillo & Bloom, 2001), Calcitonin gene-related peptide (CGRP) and substance P are thought to be related to the transmission of pain (Hökfelt et al., 2001; Russell et al., 2014). Peripheral dysregulation of neuropeptides, such as PYY, affects satiety sensation (Acuna-Goycolea & Van Den Pol, 2005; Batterham et al., 2003; Pedragosa-Badia et al., 2013). The list goes on. A huge battery of drugs has been developed in the hopes that targeting neuropeptide pathways will lead to novel therapies for neuropsychiatric, neurodegenerative or neurometabolic disorders.

Neuropeptide receptors are druggable targets (typically GPCRs) that have received heavy investment from the pharmaceutical industry (Jacobson, 2015; Tyndall & Sandilya, 2005). Many of these drugs have failed in the clinic, however, resulting in abandonment of this approach by many pharma companies (Eiger et al., 2022). One potential reason for failure is that each neuropeptide often has multiple, functionally redundant receptors (van den Pol, 2012). Therefore, inhibiting just one receptor may not suffice to have any effect. An alternative strategy is to target the *processing/release* of the neuropeptide from neurons, rather than blocking its receptor. We have developed new technology that allows the detection of release of specific neuropeptides (Ding et al., 2019). Here we propose to use this technology to develop an *in vitro* platform for high-throughput screening of drug libraries for inhibitors of specific neuropeptide synthesis/processing and/or release. This proposal is mechanistically testable owing to (1) the characterizations of neuropeptide biogenesis, sorting, trafficking, maturation and release, also (2) the establishment of NPLER/NPRR platforms as a hypothesis generator and testbed (details in Chapter 3). In the long term, we expect to develop a

large-scale drug screening platform that automates the research and development of neuropeptide-targeted lead compounds.

We explored the potential of some latest biotechnologies as new, transformative therapeutics for treating neuropeptide relevant disorders. These techniques regulate the neuropeptide pathway at multiple levels (Figure 1). In this chapter, I will focus on the progress on CRISPR-Cas9 screening, as well as two new protein engineering techniques that alter the binding, trafficking and release properties of neuropeptides. RNAi-based neuropeptide regulation was discussed in Chapter 3.

Results

Regulation of NPY with CRISPR-Cas9 in PC12 cells

CRISPR-Cas9 technology is widely used for genome editing and engineering (Doudna & Charpentier, 2014; Hsu et al., 2014; Jiang & Doudna, 2017). We attempted to integrate NPLER imaging platform with CRISPR-Cas9 to facilitate functional screening of neuropeptide-targeting sgRNAs. We aimed to regulate the expression of Neuropeptide Y (NPY), because (1) we have established a full-fledge NPY screening platform (Chapter 3), and (2) NPY sgRNA candidates are available from databases (details in Materials and Methods). However, the puromycin selection of N46 cells was unsuccessful for the CRISPR construct. We turned to PC12 cells for pilot experiments. The rat origin of PC12 cells removed some sgRNA candidates that only recognize mouse NPY. Fortunately, 1 out of 3 sgRNAs dramatically reduced the fluorescent intensity of NPY antibody staining in PC12 cells (A-B). The median fluorescence of control sgRNA (35.26 unit, n=20) was twice as high as NPY sgRNA (17.54 unit, n=19) (Figure 2B).

CRISPR-Cas9 was designed to interrupt NPY biogenesis at the DNA level (Figure 1). We wondered why the complete removal of NPY staining was not seen. Hypotheses include (1) PC12 cells are diploid. Cas9 may not function as efficiently to interact with two alleles; (2) Residual mRNA or synthesized peptides linger after NPY DNA was disrupted. Further experiments to support or deny these hypotheses will involve the establishment of stable cell line, pinpointing cut site of sgRNAs, and forcing out residual neuropeptide via intense neuronal activations. NPLER-assisted sgRNA screening will be developed based on the mentioned pilot experiments. The antibody-free approach will potentially generalize its implementation to any neuropeptide of choice.

Interference of neuropeptide pathways with novel intravesicular antibodies

Recombinant antibody technology sprung from interfacing molecular biology, protein engineering and immunology to facilitate manipulation of antibody fragments (Boss et al., 1984; Elgundi et al., 2017; Kontermann & Müller, 1999). The idea of assembling heavy and light chains of Fv fragment as a means of antigen binding (Figure 3A), later named scFv (single-chain variable fragment), inspired us to explore the potential of interfering neuropeptide prior to their release from the DCVs. If a scFv binds an neuropeptide with high affinity and specificity, it may be possible to sort the scFv molecules into the DCVs via specific sorting domains uncovered in Chapter 3. Neuropeptides, once scFV-bound, are potentially hindered from binding downstream receptors. In theory, the "competitive binding" model works better for neuropeptides due to their small size and limited epitopes. I named these hypothetical molecules iD-Ab (intra-DCV Antibodies) (Figure 3B).

Commercialized neuropeptide antibodies are mostly polyclonal (specifically, rabbit). Only few antibody sequences were made available. In our desk research, sequences of 6 NPY antibodies were uncovered from various public sources. We identified the motif of these antibodies through parallel

comparisons with other sequences to identify the positions of variable fragments. The heavy and light chain from these fragments were concatenated with designed linkers in between to form NPY iD-Ab candidates #1-6. NPLER^{NPY28mTq2} served as control, as it shared with all iD-Ab candidates the configuration of sorting domains (Figure 3C$_1$). N46 cells were transfected with the control or one of six iD-Abs, stained with anti-NPY antibody, and compared for fluorescent intensity. In the "competitive binding" model, an iD-Ab that efficiently binds NPY within the DCVs will block or reduce the binding with the staining antibody. In another word, low staining fluorescence bode well for good iD-Ab candidates.

Cell death was seen predominantly in #4, also moderately in #2. #1 and #6 candidates showed no significant differences with the control (Figure 3C$_2$). Cells transfected with #2 or #3 have peculiarly strong immunofluorescence. #5 exhibited reduced staining and healthy cell morphology (Figure 3D). Detailed analysis of two candidates, #3 and #5 confirmed that the fluorescence increased and decreased relative to the control group, respectively (Figure 3E). Parallel experiments were performed in PC12 cells (Figure 3F), where no statistically significant difference was seen between #3 and control, #5 again showed reduced immunofluorescence (Figure 3G), implying that iD-Ab #5 may serve as a novel molecule to target NPY at the intravesicular level.

Engineered neuropeptides as next-generation drug candidates

Peptide YY (PYY), together with Neuropeptide Y and pancreatic polypeptide (PP), constitutes the neuropeptide Y (NPY) family of biologically active peptides (Holzer et al., 2012). Though structurally similar with NPY, PYY is expressed exclusively in endocrine cells of the digestive system and preferentially binds a different receptor, NPY2R (Gantz et al., 2007; Rangwala et al., 2019). Physiologically, PYY exerts an anorexigenic effect through (1) indirect inhibition of feeding-

promoting AgRP/NPY neurons in the arcuate nucleus (Acosta et al., 2011; Batterham et al., 2002, 2003; Beutler et al., 2017; Sloth et al., 2007), (2) cause taste aversion (Halatchev & Cone, 2005) Administration of PYY reduces food intake in mouse, rat and human (Batterham et al., 2002; Chelikani et al., 2005; Pittner et al., 2004). Ablation of PYY in mice causes obesity (Boey et al., 2008). The plasma level of PYY is inversely correlated with Body Mass Index in human, as lean group shows higher plasma PYY than the obese group in both pre- and post-prandial conditions (Batterham et al., 2003; Guo et al., 2006). However, research and development of PYY-derived therapeutics fall behind, mostly due to (1) the chemical instability caused by rapid proteolysis and (2) severe sides effects from ascended doses, an indirect result of (1) (Adrian et al., 1986; Toräng et al., 2015). Therefore, we wondered if our established platform would assist the exploration of novel therapeutics.

We first tested if cells in our platform express endogenous PYY. Antibody staining results confirmed that PYY does not express in N46 cells (Figure 4A) and PC12 cells (Figure 4D), consistent with the reported exclusivity of gut expression (Batterham et al., 2003). We then generated an expression plasmid encoding a full-length mouse PYY driven by CAG promoter (CAG-Native PYY). Surprisingly, the PYY staining signals in the transfected N46 cells show strong accumulation in the nucleus and peri-nucleus regions. We reasoned that the embryonic feature of this cell line may result in an underdeveloped, or different neuropeptide sorting machineries for an exogenous neuropeptide, so we performed a parallel experiment in PC12 cells and observed that the majority of fluorescence locate within the nucleus, inferred from the DAPI staining (Figure 4E). The absence of dispersed puncta along the processes, a pattern commonly shared by neuropeptides, led to our belief that PYY does not sort and/or traffic properly in the tested cells. We investigated the structure and domains of PYYs and other neuropeptides, and transformed native PYY with domain swapping and residual

modifications. Expression of the engineered PYY with the same plasmid configuration (CAG-Engineered PYY) removed the abnormal accumulation in N46 cells (Figure 4C) and PC12 cells (Figure 4F). The expression pattern of the engineered PYY, as distributed puncta in soma and processes, highly suggests that the engineering practices enhance the sorting/trafficking of an exogenous neuropeptide.

Intravenous and intraperitoneal administration of PYY reduces body weight (Chelikani et al., 2005, 2007). We therefore adapted the PYY plasmids for AAV expression. In addition, we included a scramble control consists of identical amino acid composition of the neuropeptide but with shuffled sequence. The control is presumably deprived of binding any neuropeptide receptors. All three transgenes were packaged in AAV-PHP.S for peripheral tissue expression (Chan et al., 2017a). CAG promoter was used to enable strong gene expression. 6-month-old aged male mice underwent unilateral retro-orbital viral injection, and single-housed for seven weeks to monitor their body weight change (Figure 5A). All three groups (native PYY, engineered PYY and control) experienced loss of weight in the first three weeks after injection, likely due to some metabolic change by the surgery or viral expression. However, all three groups showed rebound of body weight between week 4 and 7. The control group gained the most weight as expected, while native PYY and engineered PYY did not differ in their weight-loss effect. It is yet immature to conclude that engineering PYY exhibits no superiority, as the immunohistochemical results from the postmortem fat tissue of experimental animals demonstrate that engineered PYY show better distribution pattern than the native counterpart (Figure 5B), a piece of phenomenon seen in cell lines (Figure 4). The inguinal white adipose tissue (IngWAT) does not express PYY endogenously but they can release neuropeptides (Figure 5B) (Wang et al., 2008), exogenous expression of native PYY result in a tangled-fiber pattern while in the case of engineered, PYY staining much resemble the distribution

of secretory granules in adipocytes. We further employed ELISA to measure the released PYY in the blood serum. The engineered PYY group shows a strikingly high level of serum PYY (~8.04 ng/ml) compared to the other two group (~0.48 ng/ml and ~0.41 ng/ml) (Figure 5C). Data were inferred from a parallel standard curve generated with standardized PYY provided (Figure 5C). The difference in serum concentration is likely due to the enhanced expression, or optimized release properties of PYY molecules in non-intestinal tissues after engineering. However, it remains unclear why the elevated PYY level did not lead to weight loss in animals. One possibility is the saturation of PYY created a "ceiling effect" in weight change; another possibility is the usage of AAV-PHP.S may have introduced unknown influence on the metabolic states of animals.

Discussion

The scientific advance and clinical significance of neuropeptides prompted us to explore early-stage therapeutics by integrating multiple cutting-edge biotechnologies to our imaging platform. The progress of our attempts, including CRISPR-Cas9, novel recombinant antibody, neuropeptide engineering, as well as the RNAi approach described previously (Chapter 3), are summarized (Table 1). We yielded at least one good candidate from each category of technology in the preliminary screening and engineering. The NPLER/NPRR imaging platform could further (1) empower large-scale screening of siRNAs, sgRNAs and scFvs that specifically target neuropeptides, and (2) assist rational design of novel neuropeptide derivatives with altered sorting/trafficking efficiencies, release properties and receptor affinities.

In summary, we propose to establish a novel and scalable drug-screening platform to help advance the discovery of new drugs for regulating neuropeptide action in a therapeutic context. It is yet

difficult to estimate the potential market size directly, as the platform is not itself a product for customers, but rather a vehicle to facilitate pharmaceutical R&D processes. Nevertheless, the market size for indications that could be treated with neuropeptide-related drugs is very large, as it includes obesity, stress/anxiety, depression, and chronic pain. The products from our platform will be several drug leads that, respectively, target a specific type of neuropeptide. These leads will undergo further *in vitro* validation, and hopefully in animal studies and for patients.

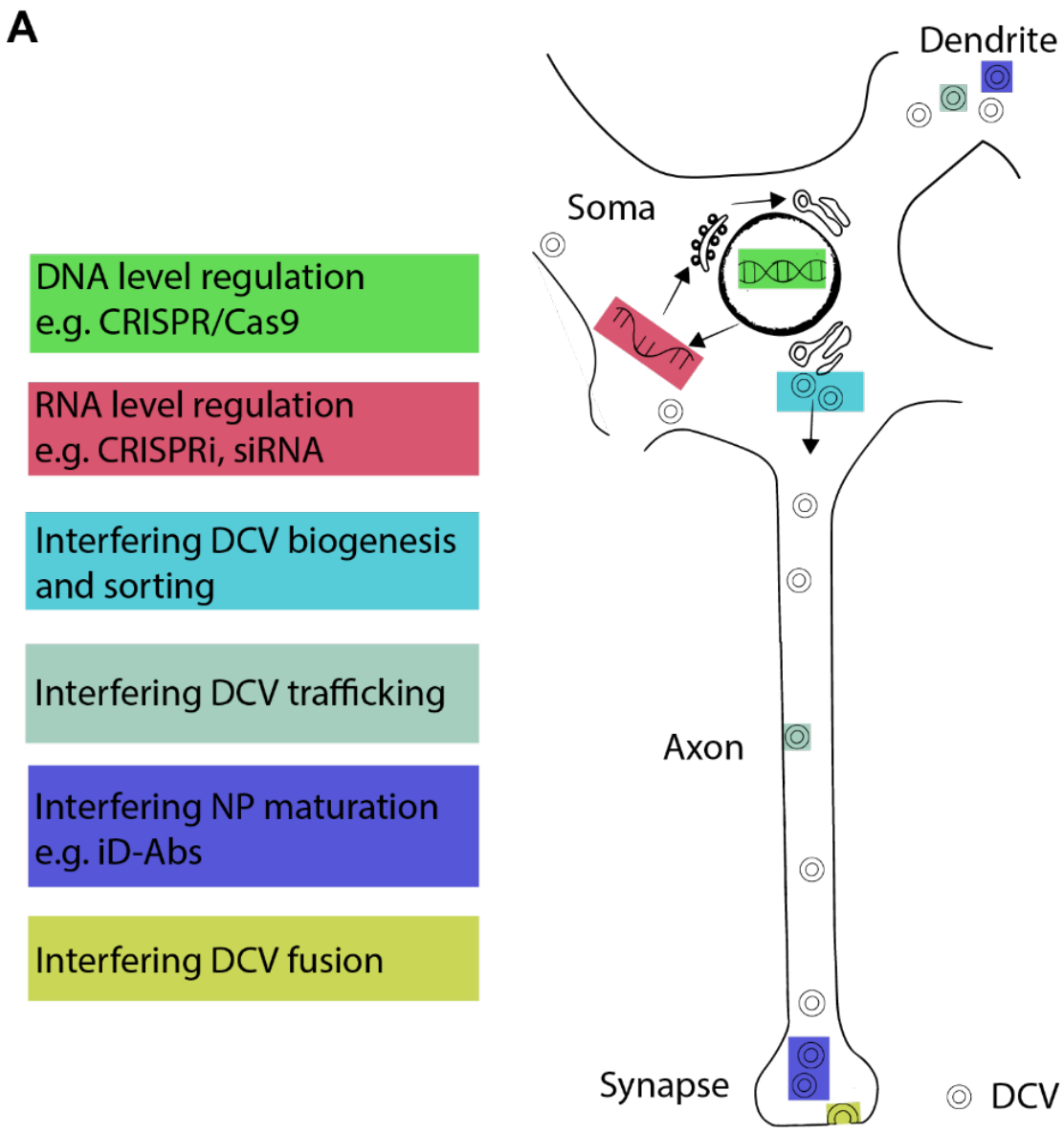

Figure 1: Means to target neuropeptide pathways in a peptidergic neuron.

(A) The complex nature of neuropeptide genesis, sorting, trafficking and release enable multiple ways of targeting neuropeptide pathways. These means are color coded and placed into a peptidergic neuron illustration.

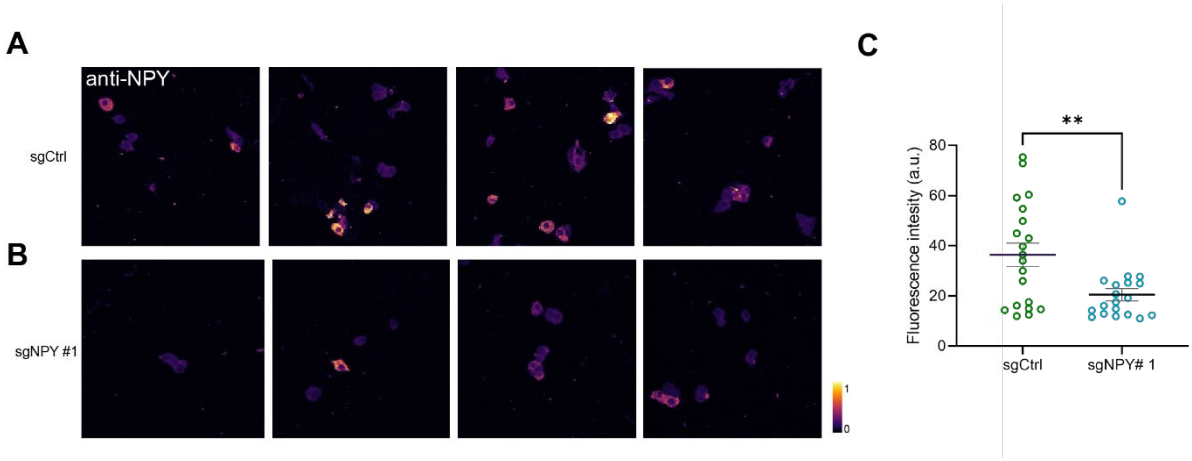

Figure 2: Regulating NPY expression in PC12 cells with CRISPR-Cas9.

(A-B) Example images of PC12 cells transfected with Cas9 and control sgRNA **(A)** or Cas9 and sgRNA targeting Neuropeptide Y **(B)**, details are shown in **Materials and Methods**. Images were pseudo-colored to highlight contrast. **(C)** sgNPY #1 downregulates NPY expression in PC12 cells. Quantification and comparison of fluorescence in intact cells (N=19-20) of **(A,B)**. (**P<0.01, Mann-Whitney *U* test).

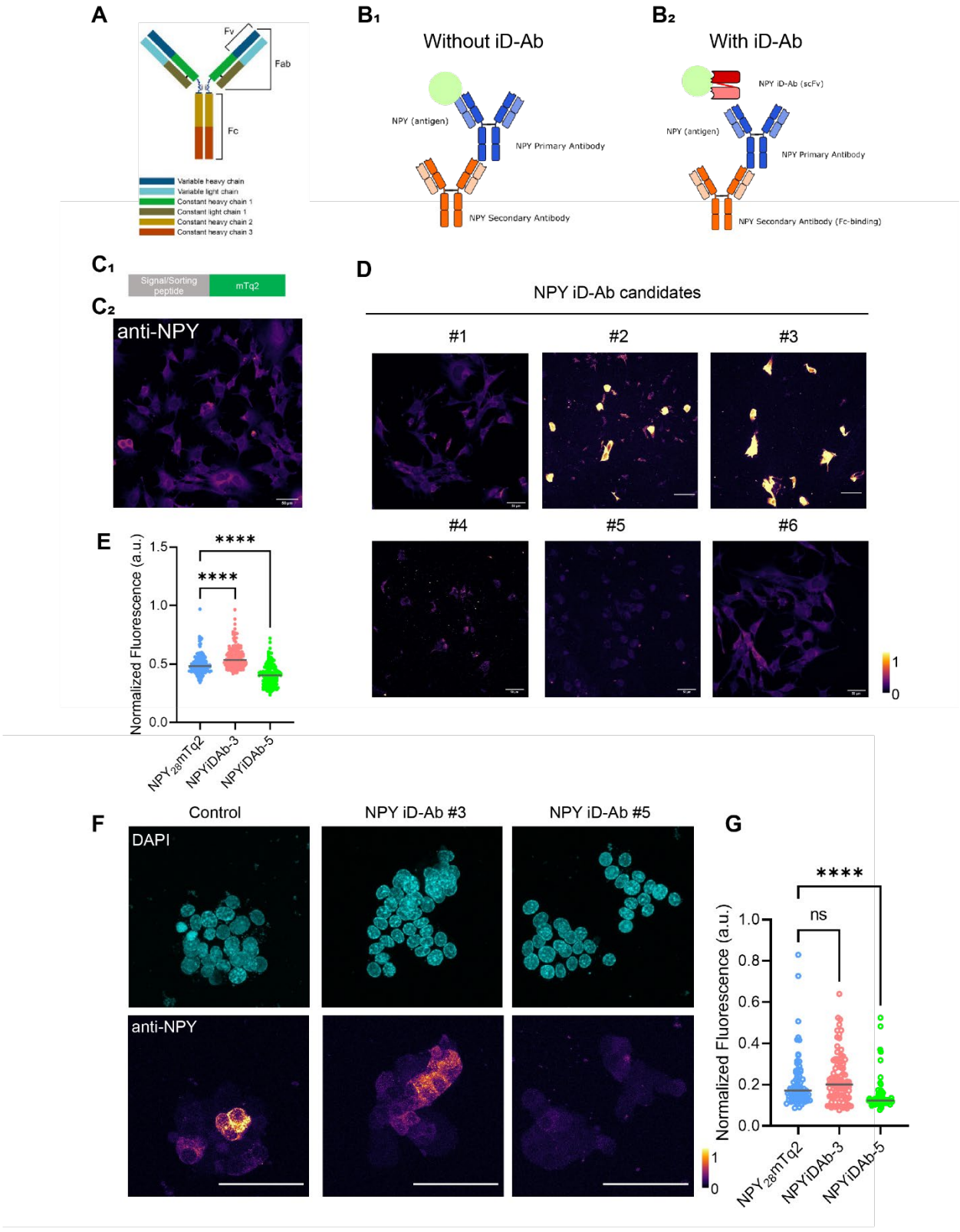

Figure 3: Targeting neuropeptide signaling with intra-DCV Antibodies (iD-Abs).

(A) Illustration of an antibody molecule, which consists of Fab and Fc regions. Fv (variable) regions on the Fab arm recognizes and binds antigen. **(B)** Principle of intra-DCV antibodies (iD-Abs). The canonical primary-secondary antibody binding provides means to visualize and amplify the presence of antigens **(B1)**. If two Fv regions of an antibody are concatenated in lieu of a linker to form a single-chain antibody, and such an antibody is engineered to sort and transport into the DCVs like neuropeptides, it may competitively bind the antigen (neuropeptide) **(B2)** to block or attenuate its interaction with downstream GPCR receptors. These engineered single-chain antibody candidates were named intra-DCV antibody (iD-Ab). **(C)** N46 cells were transfected with $NPLER^{NPY}$ (CMV-NPY_{28}mTq2) **(C1)** and stained for NPY as control **(C2)** for further iD-Ab candidate screening. **(D)** 6 iD-Abs that potentially target NPY were tested via immunocytochemistry, similar to **(C2)**. Among all candidates, #4 exhibited toxicity to N46 cells, #1 and #6 showed no difference, #2 and #3 had increased staining signals and cell morphology was abnormal in the former case. #5 showed decreased anti-NPY signals, making it a potential good candidate for NPY signaling interruption. **(E)** Quantification of two candidates of interest, iD-Ab #3 and #5, as well as their comparisons with control in **(C1)** confirmed the significance of the increase/decrease of fluorescence. (****P<0.0001, Mann-Whitney *U* test). **(F)** Validation of iD-Ab #3 and #5 in PC12 cells and corresponding quantifications of comparisons **(G)**, with #3 showing no change of fluorescence, but #5 decreased as in N46 cells in **(D,E)** (ns: not significant, ****P<0.0001, Mann-Whitney *U* test). Scale bar, 50 μm.

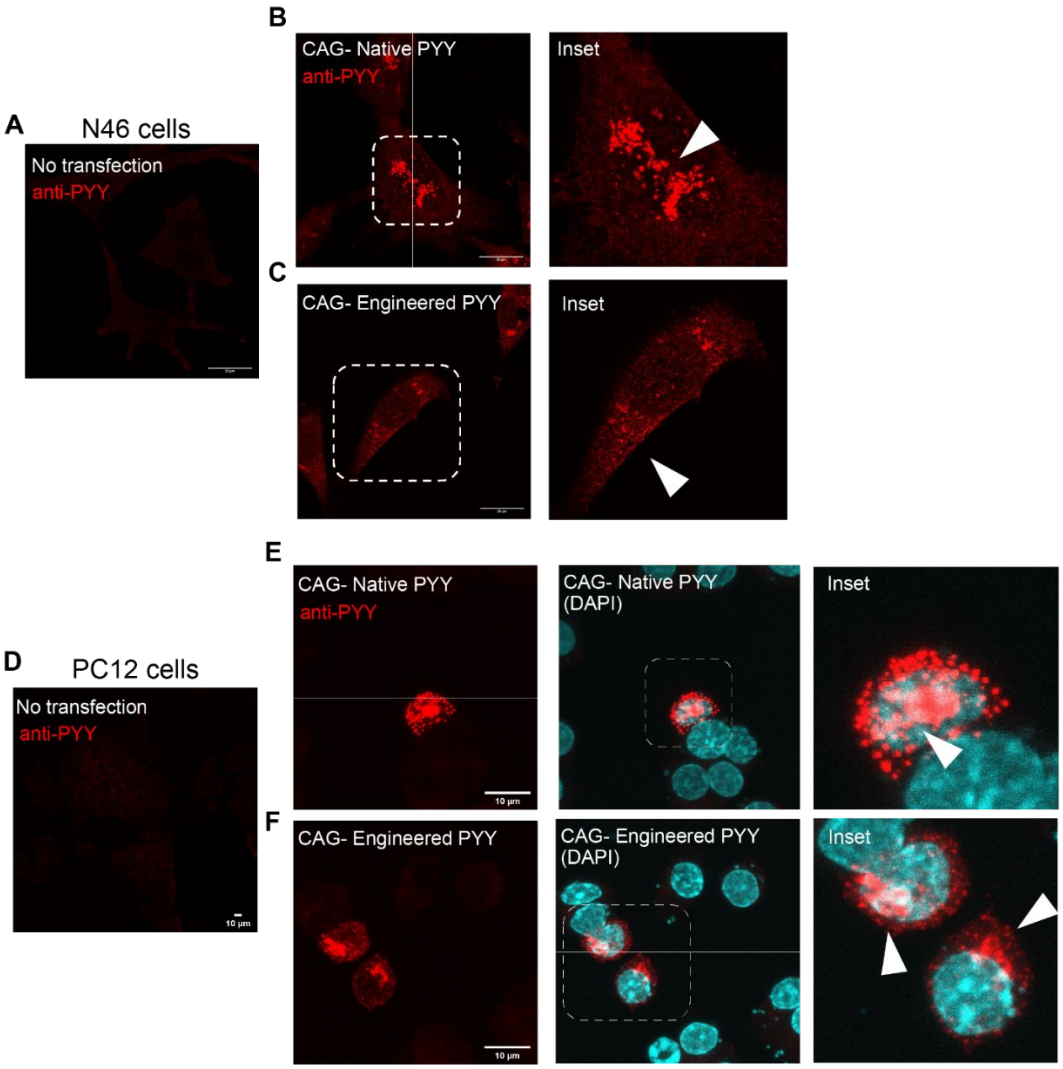

Figure 4: Neuropeptide engineering reduces organelle retention of Peptide YY (PYY) in cell lines.

(A) N46 cells do not express endogenous PYY. **(B)** Exogenous expression of PYY in its native form result in strong accumulation of stained signals at the center of cells, likely in ER, golgi apparatus or nucleus. **(C)** Engineered PYY attenuates accumulation of stained signals in **(B)**. Similar case was seen in PC12 cells, as endogenous PYY was also not seen **(D)**, exogenous expression exhibits a nucleus patch **(E)**, as referenced by the DAPI staining. **(F)** The size of the patch reduces dramatically with engineered PYY expression. Demonstrative regions of interest were indicated with arrow signs. Scale bar, 10 µm.

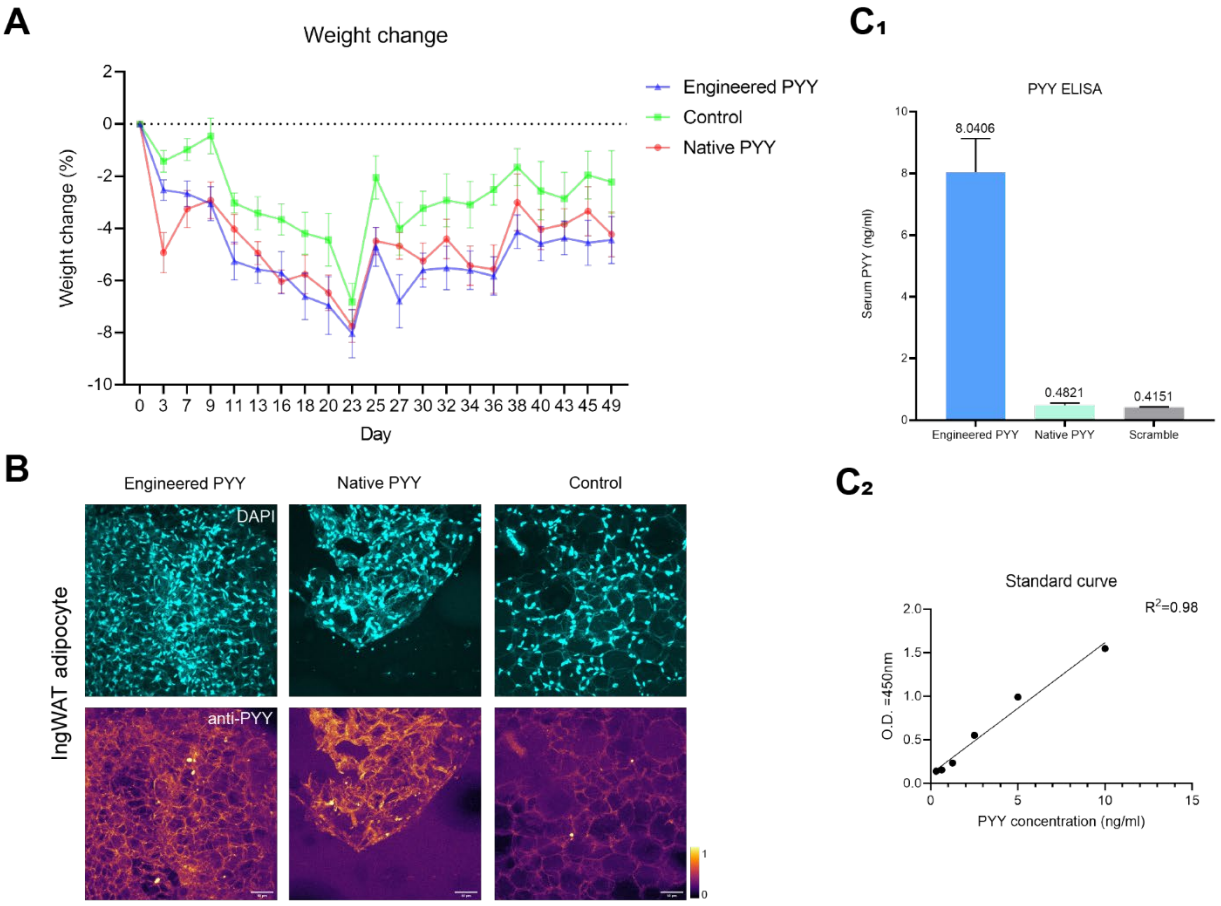

Figure 5: Engineered PYY shows improved tissue distribution and serum concentration.

(A) Weight change plot of experimental mice injected with viruses carry control gene, native PYY transgene and engineered PYY transgene, respectively (N=8 for each group). Day 0 was set as a day after the viral injection. All groups experienced severe weight loss between Day 0 and Day 23, yet the two PYY groups showed less rebound between Day 23 and Day 49. No statistically significant differences were found between native and engineered PYY in terms of their weight loss effects in this experiment. **(B)** PYY IHC of Inguinal white adipose tissue (IngWAT) of each group showed better tissue distribution of PYY staining signals of engineered PYY. Native PYY group exhibited unknown tangled patterns. Images were pseudo-colored to highlight contrast. Scale bar, 50 μm. **(C)** PYY ELISA of blood serum from experimental groups showed that engineered PYY outperforms native PYY as the serum PYY concentration is nearly 20-fold higher **(C1)**, standard curve of the ELISA experiment conveyed strong regressive power of the experiment **(C2)**.

	RNAi KD	CRISPR/Cas9	iD-Ab
NPY	-	+	+
NkB	+	?	-

Table 1: Summary of research progress in NkB and NPY regulation in this study.

Materials and Methods

Molecular cloning

pCAG-PYY and other engineered forms are constructed by replacing CMV promoters in pCMV with CAG promoter through Gibson assembly. Native and engineered PYY DNA molecules were synthesized (Integrated DNA Technologies). All other practices were described in Chapter 3.

CRIPSR experiments

All sgRNA candidates were designed using CHOPCHOP (https://chopchop.cbu.uib.no) (Labun et al., 2019) and top candidates were synthesized and cloned into pSpCas9(BB)-2A-Puro (PX459) V2.0 (Addgene #62988). 24 hours after transfection, medium was replaced and puromycin was added to the new medium to reach final concentration of 1.5μg/ml (PC12 cells) or 3μg/ml (N46 cells). Fresh puromycin-free medium was used to terminate the selection process. All other cell culture practices were identical as in Chapter 3. The best candidate sgNPY #1 targets the sequence GAGGGGTACCCCTCCAAGCCGG. Please note that this sequence is present in both rat and mouse NPY genes, rendering it theoretically effective in both species.

Animal experiments

All experimental procedures involving the use of live mice or their tissues were carried out in accordance with NIH guidelines and approved by the Institute Animal Care and Use Committee (IACUC) and the Institute Biosafety Committee (IBC) at the California Institute of Technology (Caltech). All experimental animals were single-housed 6-month old C57BL/6N male mice (The Jackson Laboratory, #000664). Weight of each mouse was measured with a food scale 3 times a week, 9 weeks in total.

Virus

All AAVs used in this study were customized in this paper with AAV-PHP.S serotype that facilitates peripheral expression (Chan et al., 2017b). They were packaged at the HHMI Janelia Research Campus virus facility, and a high original titer were diluted with clean PBS on the day of use. Viruses were delivered via unilateral retro-orbital injection of 10^{11} genome copies per animal.

Immunocytochemistry (ICC)

For Immunocytochemistry, all reagents and protocols were described in Chapter 3 except the usage of Rabbit anti-PYY (1:500, Bioss Antibodies BS-2265R).

Immunohistochemistry (IHC) and ELISA

Inguinal white adipose *tissues* (*ingWAT) were mined from freshly sacrificed animals and prepared according to (de Jong et al., 2015). The tissues were embedded in OCT compound (Fisher Scientific,* #23-730-571) and *frozen at -80*℃ *overnight* prior to sectioning. To prepare mouse blood serum for ELISA experiments, whole blood was collected right after animal sacrificed, immediately mixed with heparin, and centrifuged for 15 minutes at 1500 rpm at 4℃, clear supernatant was aspirated and stored at -80℃. Assays using the ELISA kits for PYY (Invitrogen EH387RB) was performed according to the user manuals.

Statistical analysis

All data analysis was performed with Graphpad Prism 9, Microsoft Excel and custom Matlab codes. Data underwent normality tests before analysis (Kolmogorov-Smirnov test, Shapiro-Wilk test, D'Agostino & Pearson test), those passed all tests are presented as mean ± s.e.m and used for

parametric comparisons. Otherwise, data are shown as median ± 95% CI and Mann-Whitney U test was used for comparison. Weight data were normalized to day 0 and presented as percentage of change in Figure 5A.

References

Acosta, A., Hurtado, M. D., Gorbatyuk, O., Sala, L. La, & Duncan, M. (2011). Salivary PYY: A Putative Bypass to Satiety. *PLoS ONE*, *6*(10), 26137. https://doi.org/10.1371/journal.pone.0026137

Acuna-Goycolea, C., & Van Den Pol, A. N. (2005). Peptide YY3-36 inhibits both anorexigenic proopiomelanocortin and orexigenic neuropeptide Y neurons: Implications for hypothalamic regulation of energy homeostasis. *Journal of Neuroscience*, *25*(45), 10510–10519. https://doi.org/10.1523/JNEUROSCI.2552-05.2005

Adrian, T. E., Sagor, G. R., Savage, A. P., Bacarese-Hamilton, A. J., Hall, G. M., & Bloom, S. R. (1986). Peptide yy kinetics and effects on blood pressure and circulating pancreatic and gastrointestinal hormones and metabolites in man. *Journal of Clinical Endocrinology and Metabolism*, *63*(4), 803–807. https://doi.org/10.1210/jcem-63-4-803

Arora, S., & Anubhuti. (2006). Role of neuropeptides in appetite regulation and obesity - A review. *Neuropeptides*. https://doi.org/10.1016/j.npep.2006.07.001

Batterham, R. L., Cohen, M. A., Ellis, S. M., Le Roux, C. W., Withers, D. J., Frost, G. S., Ghatei, M. A., & Bloom, S. R. (2003). Inhibition of Food Intake in Obese Subjects by Peptide YY $_{3-36}$. *New England Journal of Medicine*, *349*(10), 941–948. https://doi.org/10.1056/NEJMoa030204

Batterham, R. L., Cowley, M. A., Small, C. J., Herzog, H., Cohen, M. A., Dakin, C. L., Wren, A. M., Brynes, A. E., Low, M. J., Ghatei, M. A., Cone, R. D., & Bloom, S. R. (2002). Gut hormone PYY3-36 physiologically inhibits food intake. *Nature*, *418*(6898), 650–654. https://doi.org/10.1038/nature00887

Beutler, L. R., Chen, Y., Ahn, J. S., Lin, Y. C., Essner, R. A., & Knight, Z. A. (2017). Dynamics of Gut-Brain Communication Underlying Hunger. *Neuron*, *96*(2), 461-475.e5. https://doi.org/10.1016/j.neuron.2017.09.043

Boey, D., Lin, S., Enriquez, R. F., Lee, N. J., Slack, K., Couzens, M., Baldock, P. A., Herzog, H., & Sainsbury, A. (2008). PYY transgenic mice are protected against diet-induced and genetic obesity. *Neuropeptides*, *42*(1), 19–30. https://doi.org/10.1016/j.npep.2007.11.003

Boss, M. A., Kenten, J. H., Wood, C. R., & Emtage, J. S. (1984). Assembly of functional antibodies from immunoglobulin heavy and light chains synthesised in E. coli. *Nucleic Acids Research*, *12*(9), 3791–3806. https://doi.org/10.1093/nar/12.9.3791

Bowers, M. E., Choi, D. C., & Ressler, K. J. (2012). Neuropeptide regulation of fear and anxiety: Implications of cholecystokinin, endogenous opioids, and neuropeptide Y. *Physiology and Behavior*. https://doi.org/10.1016/j.physbeh.2012.03.004

Chan, K. Y., Jang, M. J., Yoo, B. B., Greenbaum, A., Ravi, N., Wu, W. L., Sánchez-Guardado, L., Lois, C., Mazmanian, S. K., Deverman, B. E., & Gradinaru, V. (2017a). Engineered AAVs for efficient noninvasive gene delivery to the central and peripheral nervous systems. *Nature Neuroscience*, *20*(8), 1172–1179. https://doi.org/10.1038/NN.4593

Chan, K. Y., Jang, M. J., Yoo, B. B., Greenbaum, A., Ravi, N., Wu, W. L., Sánchez-Guardado, L., Lois, C., Mazmanian, S. K., Deverman, B. E., & Gradinaru, V. (2017b). Engineered AAVs for efficient noninvasive gene delivery to the central and peripheral nervous systems. *Nature Neuroscience*, *20*(8), 1172–1179. https://doi.org/10.1038/nn.4593

Chelikani, P. K., Haver, A. C., & Heidelberger, R. D. (2005). Intravenous infusion of peptide YY(3-36) potently inhibits food intake in rats. *Endocrinology*, *146*(2), 879–888. https://doi.org/10.1210/en.2004-1138

Chelikani, P. K., Haver, A. C., & Reidelberger, R. D. (2007). Intermittent intraperitoneal infusion of peptide YY(3-36) reduces daily food intake and adiposity in obese rats. *American Journal of Physiology-Regulatory, Integrative and Comparative Physiology*, *293*(1), R39–R46. https://doi.org/10.1152/ajpregu.00164.2007

de Jong, J. M. A., Larsson, O., Cannon, B., & Nedergaard, J. (2015). A stringent validation of mouse adipose tissue identity markers. *American Journal of Physiology - Endocrinology and Metabolism*, *308*(12), E1085–E1105. https://doi.org/10.1152/AJPENDO.00023.2015

Dhillo, W. S., & Bloom, S. R. (2001). Hypothalamic peptides as drug targets for obesity. In *Current Opinion in Pharmacology*. https://doi.org/10.1016/S1471-4892(01)00110-2

Ding, K., Han, Y., Seid, T. W., Buser, C., Karigo, T., Zhang, S., Dickman, D. K., & Anderson, D. J. (2019). Imaging neuropeptide release at synapses with a genetically engineered reporter. *ELife*, *8*. https://doi.org/10.7554/elife.46421

Doudna, J. A., & Charpentier, E. (2014). The new frontier of genome engineering with CRISPR-Cas9. *Science*. https://doi.org/10.1126/science.1258096

Eiger, D. S., Pham, U., Gardner, J., Hicks, C., & Rajagopal, S. (2022). GPCR systems pharmacology: a different perspective on the development of biased therapeutics. *American Journal of Physiology-Cell Physiology*, *322*(5), C887–C895. https://doi.org/10.1152/ajpcell.00449.2021

Elgundi, Z., Reslan, M., Cruz, E., Sifniotis, V., & Kayser, V. (2017). The state-of-play and future of antibody therapeutics. *Advanced Drug Delivery Reviews*, *122*, 2–19. https://doi.org/10.1016/J.ADDR.2016.11.004

Gantz, I., Erondu, N., Mallick, M., Musser, B., Krishna, R., Tanaka, W. K., Snyder, K., Stevens, C., Stroh, M. A., Zhu, H., Wagner, J. A., MacNeil, D. J., Heymsfield, S. B., & Amatruda, J. M. (2007). Efficacy and Safety of Intranasal Peptide YY3–36 for Weight Reduction in Obese Adults. *The Journal of Clinical Endocrinology & Metabolism*, *92*(5), 1754–1757. https://doi.org/10.1210/jc.2006-1806

Griebel, G., & Holsboer, F. (2012). Neuropeptide receptor ligands as drugs for psychiatric diseases: The end of the beginning? *Nature Reviews Drug Discovery*. https://doi.org/10.1038/nrd3702

Guo, Y., Ma, L., Enriori, P. J., Koska, J., Franks, P. W., Brookshire, T., Cowley, M. A., Salbe, A. D., DelParigi, A., & Tataranni, P. A. (2006). Physiological Evidence for the Involvement of Peptide YY in the Regulation of Energy Homeostasis in Humans*. *Obesity*, *14*(9), 1562–1570. https://doi.org/10.1038/oby.2006.180

Halatchev, I. G., & Cone, R. D. (2005). Peripheral administration of PYY3-36 produces conditioned taste aversion in mice. *Cell Metabolism*, *1*(3), 159–168. https://doi.org/10.1016/j.cmet.2005.02.003

Hökfelt, T., Bartfai, T., & Bloom, F. (2003). Neuropeptides: Opportunities for drug discovery. *Lancet Neurology*. https://doi.org/10.1016/S1474-4422(03)00482-4

Hökfelt, T., Pernow, B., & Wahren, J. (2001). Substance P: A pioneer amongst neuropeptides. *Journal of Internal Medicine*. https://doi.org/10.1046/j.0954-6820.2000.00773.x

Holzer, P., Reichmann, F., & Farzi, A. (2012). Neuropeptide Y, peptide YY and pancreatic polypeptide in the gut-brain axis. *Neuropeptides*. https://doi.org/10.1016/j.npep.2012.08.005

Hsu, P. D., Lander, E. S., & Zhang, F. (2014). Development and applications of CRISPR-Cas9 for genome engineering. *Cell*. https://doi.org/10.1016/j.cell.2014.05.010

Jacobson, K. A. (2015). New paradigms in GPCR drug discovery. *Biochemical Pharmacology*. https://doi.org/10.1016/j.bcp.2015.08.085

Jiang, F., & Doudna, J. A. (2017). CRISPR–Cas9 Structures and Mechanisms. *Annual Review of Biophysics*, *46*(1), 505–529. https://doi.org/10.1146/annurev-biophys-062215-010822

Kontermann, R. E., & Müller, R. (1999). Intracellular and cell surface displayed single-chain diabodies. *Journal of Immunological Methods*, *226*(1–2), 179–188. https://doi.org/10.1016/S0022-1759(99)00062-9

Labun, K., Montague, T. G., Krause, M., Torres Cleuren, Y. N., Tjeldnes, H., & Valen, E. (2019). CHOPCHOP v3: expanding the CRISPR web toolbox beyond genome editing. *Nucleic Acids Research*, *47*(W1), W171–W174. https://doi.org/10.1093/NAR/GKZ365

Pedragosa-Badia, X., Stichel, J., & Beck-Sickinger, A. G. (2013). Neuropeptide y receptors: How to get subtype selectivity. *Frontiers in Endocrinology*, *4*(FEB), 1–14. https://doi.org/10.3389/fendo.2013.00005

Pittner, R. A., Moore, C. X., Bhavsar, S. P., Gedulin, B. R., Smith, P. A., Jodka, C. M., Parkes, D. G., Paterniti, J. R., Srivastava, V. P., & Young, A. A. (2004). Effects of PYY[3-36] in rodent models of diabetes and obesity. *International Journal of Obesity*, *28*(8), 963–971. https://doi.org/10.1038/sj.ijo.0802696

Rangwala, S. M., D'Aquino, K., Zhang, Y. M., Bader, L., Edwards, W., Zheng, S., Eckardt, A., Lacombe, A., Pick, R., Moreno, V., Kang, L., Jian, W., Arnoult, E., Case, M., Jenkinson, C., Chi, E., Swanson, R. V., Kievit, P., Grove, K., … Leonard, J. N. (2019). A Long-Acting PYY 3–36 Analog Mediates Robust Anorectic Efficacy with Minimal Emesis in Nonhuman Primates. *Cell Metabolism*, *29*(4), 837-843.e5. https://doi.org/10.1016/j.cmet.2019.01.017

Russell, F. A., King, R., Smillie, S. J., Kodji, X., & Brain, S. D. (2014). Calcitonin gene-related peptide: physiology and pathophysiology. *Physiological reviews*. https://doi.org/10.1152/physrev.00034.2013

Schank, J. R., Ryabinin, A. E., Giardino, W. J., Ciccocioppo, R., & Heilig, M. (2012). Stress-Related Neuropeptides and Addictive Behaviors: Beyond the Usual Suspects. *Neuron*. https://doi.org/10.1016/j.neuron.2012.09.026

Sloth, B., Holst, J. J., Flint, A., Gregersen, N. T., & Astrup, A. (2007). Effects of PYY1-36 and PYY3-36 on appetite, energy intake, energy expenditure, glucose and fat metabolism in obese and lean subjects. *American Journal of Physiology - Endocrinology and Metabolism*, *292*(4), 1062–1069. https://doi.org/10.1152/ajpendo.00450.2006

Toräng, S., Veedfald, S., Rosenkilde, M. M., Hartmann, B., & Holst, J. J. (2015). The anorexic hormone peptide yy3-36 is rapidly metabolized to inactive peptide yy3-34 in vivo. *Physiological Reports*, *3*(7), e12455. https://doi.org/10.14814/phy2.12455

Tyndall, J., & Sandilya, R. (2005). GPCR Agonists and Antagonists in the Clinic. *Medicinal Chemistry*, *1*(4), 405–421. https://doi.org/10.2174/1573406054368675

van den Pol, A. N. (2012). Neuropeptide Transmission in Brain Circuits. *Neuron*. https://doi.org/10.1016/j.neuron.2012.09.014

Wang, P., Mariman, E., Renes, J., & Keijer, J. (2008). The secretory function of adipocytes in the physiology of white adipose tissue. *Journal of Cellular Physiology*, *216*(1), 3–13. https://doi.org/10.1002/jcp.21386

Chapter 5

CONCLUSIONS AND FUTURE DIRECTIONS

Conclusions

The major conclusions and findings are summarized as the following:

Part A. *Drosophila*

- Invention of Neuropeptide Release Reporter (NPRR), a novel method to detect the release of different neuropeptides in intact neural tissue in *Drosophila*.
- NPRR has subcellular spatial and sub-second temporal resolution.
- NPRR responses exhibit triphasic kinetics, including rising, falling, and recovering phases, possibly reflect the slow kinetics of DCV replenishment relative to release.
- NPRR responses exhibit cell type-specific characteristics.
- NPRR exhibit peptide-specific expression pattern. Each NP deserves its own NPRR.

Part B. Mammalian cell lines

- Pilot establishment of an NPLER/NPRR imaging platform which consists of choice of neuropeptide of interest, proper cell lines, and imaging reporters.
- Pioneering evidence of different neuropeptides in the same cell undergo different subcellular trafficking process.
- Harnessing Next-gen pHluorin based Neuropeptide Release Reporters (NPRRs) for cell line imaging
- An NPLER-based RNAi screening platform.
- Engineered PYY outperforms native PYY in tissue distribution and serum concentration.

Future directions

Neuropeptide Imaging Zootopia: Generalization of NPLER/NPRR to other model organisms

Neuropeptides are evolutionarily conserved (Hoyle, 1998) and widely believed to be closely associated with the emergence of nervous systems (Grimmelikhuijzen & Hauser, 2012). Major progress in understanding neuropeptides were done in many well-characterized model organisms, such as *Mus musculus* (mice) (Arora & Anubhuti, 2006; Hökfelt et al., 2000; Kormos & Gaszner, 2013; Nusbaum et al., 2017; Russo, 2017), *Drosophila Melanogaster* (fruit flies) (Nässel & Winther, 2010), *Caenorhabditis elegans* (nematodes) (Bargmann & Marder, 2013), *Danio Rerio* (zebrafish) (Löhr & Hammerschmidt, 2011; Volkoff, 2006) and others. NPRRs were successfully developed and applied in fruit flies (Chapter 2) and mice (Chapter 3). An important future direction is to generalize NPRR and NPLER to the other model organisms.

In the course of NPRR engineering for fruit flies and mice, parallel efforts were made in other species. Nevertheless, generating and validation of NPRRs in *C.elegans* did not yield convincing results due to the complications of previously unknown source of fluorescence. Details are included in this thesis as an appendix chapter. Several NPRR/NPLER constructs were redesigned for zebrafish and jellyfish, yet still in the preliminary screening phase as of the drafting of this thesis.

How to migrate the design of NPRR from one model organism to another? Here are some thoughts and aspects to consider:

(1) Tuning of reporter expression. An ideal NPRR should follow the route of synthesis, sorting, transportation, and release as an endogenous neuropeptide. On the one hand, overly strong expression may lead to the accumulation of transgene products in ER and/or Golgi apparatus, which

in turn can potentially activate the protein degradation signaling pathways. Cells are likely to suffer toxicity by the protein overload or to experience changes of expression/release profiles. Neither are unfavorable for the application of NPRRs. On the other hand, weakly expressed reporters are less identifiable and trackable. To overcome or to alleviate this issue, either highly sensitive imaging technique, or DCV-enriched cells or subcellular regions are required. All these conditions entail heavy investment in extra labors and costs. Therefore, the choice of codon optimization, gene loci, expression vectors and regulatory elements needs prudent design and investigations.

(2) Deep understanding of neuropeptide of interest. The latest discoveries regarding neuropeptides often involve identifying new neuropeptides, uncovering previously unknown functions of a neuropeptide, and a mix of both in new animal models. However, NPRRs were not conceptualized for the research of such kinds. Alternatively, NPRRs take advantage of the understanding of neuropeptides and assist the exploration of means to regulate neuropeptide expression, sorting, trafficking, and release (Chapter 4, Figure 1). Understanding of neuropeptide structures and domains is helpful to optimize the sorting domain designs; whilst the information of cellular organelle markers provides a reference framework to characterize the expression and sorting semi-quantitatively.

(3) The research advance of fluorescent proteins (FPs). NPRRs and NPLERs rely heavily on the development of fluorescent proteins, which are iterated and optimized amazingly fast. Thanks to the generosity of these protein engineers, DNA sequences encoding the new FPs are made public almost immediately. One should pay close attention to the advance of the FP engineering.

Outside the box: Alternative strategies to image neuropeptide localization and release

All the imaging reporters made and discussed in this thesis are genetically encoded. Other genetically encoded strategies are mostly GPCR-based that mimic the expression of neuropeptide receptors to detect binding, notably the GRAB sensors for oxytocin, vasopressin and CCK (Dong et al., 2022; Qian et al., 2022; Wang et al., 2022) . These recently developed sensors are complementary to our reporters. An ideal yet very difficult experiment is to simultaneously image the release of neuropeptide from the upstream cells, and the detection of neuropeptide from the downstream cells. Unfortunately, the excitation and emission spectra of efficient GRAB sensors and NPRR sensors cannot be separated optically. A more red-shifted GRAB or NPRR will be particularly useful for the proposed imaging experiment.

The rapid advance in nucleotide deliveries, as well as the availability of NPY-specific short nucleotide aptamers, lead to the possibility of transferring DCV-targeting aptamers to directly bind intravesicular NPY (Mendonsa & Bowser, 2005; Proske et al., 2002). This idea is similar to the recombinant antibody techniques described in Chapter 4. Neuropeptide-binding, pH-sensitive organic dyes also deserve further investigations, though many technical difficulties are foreseeable.

The holy grail: *In vivo* imaging of neuropeptide release in behaving animals

Calcium imaging experiments in behaving animals are enabled by an optimized genetically engineered calcium indicator, a sensitive detection technique, and several cutting-edge algorithms to process and perfect the collected images. The holy grail is to make *in vivo* imaging of neuropeptide release in behaving animals possible. With prudent genetic manipulation and image registration, we will be able to identify both correlations and causalities between neuropeptide release and behaviors.

More specific sub-questions include (1) what cell/neuron releases neuropeptide; (2) when and how many neuropeptides are released; (3) the characterization of release dynamics and its relation to behavioral phenotypes and intensities; (4) genes/proteins involved in the regulation of neuropeptides. The list goes on. I hope that the prototypical reporters described in this thesis get us a little bit closer to the holy grail.

References

Arora, S., & Anubhuti. (2006). Role of neuropeptides in appetite regulation and obesity - A review. *Neuropeptides*. https://doi.org/10.1016/j.npep.2006.07.001

Bargmann, C. I., & Marder, E. (2013). From the connectome to brain function. *Nature Methods*. https://doi.org/10.1038/nmeth.2451

Dong, C., Zheng, Y., Long-Iyer, K., Wright, E. C., Li, Y., & Tian, L. (2022). Fluorescence Imaging of Neural Activity, Neurochemical Dynamics, and Drug-Specific Receptor Conformation with Genetically Encoded Sensors. *Annual Review of Neuroscience*, *45*(1). https://doi.org/10.1146/annurev-neuro-110520-031137

Grimmelikhuijzen, C. J. P., & Hauser, F. (2012). Mini-review: The evolution of neuropeptide signaling. *Regulatory Peptides*. https://doi.org/10.1016/j.regpep.2012.05.001

Hökfelt, T., Broberger, C., Xu, Z. Q. D., Sergeyev, V., Ubink, R., & Diez, M. (2000). Neuropeptides - An overview. *Neuropharmacology*. https://doi.org/10.1016/S0028-3908(00)00010-1

Hoyle, C. H. V. (1998). Neuropeptide families: Evolutionary perspectives. In *Regulatory Peptides* (Vol. 73, Issue 1, pp. 1–33). Elsevier. https://doi.org/10.1016/S0167-0115(97)01073-2

Kormos, V., & Gaszner, B. (2013). Role of neuropeptides in anxiety, stress, and depression: From animals to humans. *Neuropeptides*. https://doi.org/10.1016/j.npep.2013.10.014

Löhr, H., & Hammerschmidt, M. (2011). Zebrafish in Endocrine Systems: Recent Advances and Implications for Human Disease. *Annual Review of Physiology*, *73*(1), 183–211. https://doi.org/10.1146/annurev-physiol-012110-142320

Mendonsa, S. D., & Bowser, M. T. (2005). In vitro selection of aptamers with affinity for neuropeptide Y using capillary electrophoresis. *Journal of the American Chemical Society*, *127*(26), 9382–9383. https://doi.org/10.1021/ja052406n

Nässel, D. R., & Winther, Å. M. E. (2010). Drosophila neuropeptides in regulation of physiology and behavior. *Progress in Neurobiology*. https://doi.org/10.1016/j.pneurobio.2010.04.010

Nusbaum, M. P., Blitz, D. M., & Marder, E. (2017). Functional consequences of neuropeptide and small-molecule co-transmission. *Nature Reviews Neuroscience*. https://doi.org/10.1038/nrn.2017.56

Proske, D., Fliger, M. H., Sö Ll, R. M., Beck-Sickinger, A. G., & Famulok, M. (2002). A Y2 receptor mimetic aptamer directed against neuropeptide Y. *Journal of Biological Chemistry*, *277*(13), 11416–11422. https://doi.org/10.1074/jbc.M109752200

Qian, T., Wang, H., Wang, P., Geng, L., Mei, L., Osakada, T., Tang, Y., Kania, A., Grinevich, V., Stoop, R., Lin, D., Luo, M., & Li, Y. (2022). Compartmental Neuropeptide Release Measured Using a New Oxytocin Sensor. *BioRxiv*, 2022.02.10.480016. https://doi.org/10.1101/2022.02.10.480016

Russo, A. F. (2017). Overview of Neuropeptides: Awakening the Senses? *Headache*, *57*(Suppl 2), 37–46. https://doi.org/10.1111/head.13084

Volkoff, H. (2006). The role of neuropeptide Y, orexins, cocaine and amphetamine-related transcript, cholecystokinin, amylin and leptin in the regulation of feeding in fish. *Comparative Biochemistry and Physiology - A Molecular and Integrative Physiology*. https://doi.org/10.1016/j.cbpa.2005.10.026

Wang, H., Qian, T., Zhao, Y., Zhuo, Y., Wu, C., Osakada, T., Chen, P., Ren, H., Yan, Y., Geng, L., Fu, S., Mei, L., Li, G., Wu, L., Jiang, Y., Qian, W., Peng, W., Xu, M., Hu, J., … Li, Y. (2022). A toolkit of highly selective and sensitive genetically encoded neuropeptide sensors.

BioRxiv, 2022.03.26.485911. https://doi.org/10.1101/2022.03.26.485911

A P P E N D I X

FLUORESCENCE DYNAMICS OF LYSOSOMAL-RELATED ORGANELLE FLASHING IN THE INTESTINAL CELLS OF *CAENORHABDITIS ELEGANS*

C. Tan., Ding, K., Anderson, D. J., Sternberg, P.W. Fluorescence dynamics of lysosomal-related organelle dissipation in the intestinal cells of *Caenorhabditis elegans* (In preparation)

Summary

Autofluorescent lysosome-related organelles (or gut granules) in the intestinal cells of *Caenorhabditis elegans* have been shown to play an important role in metabolic and signaling processes, but they have not been fully characterized. Using a preparation comprising live worms with intestinal tissue exposed, we report here a previously undescribed phenomenon in which gut granule autofluorescence is quenched in a rapid and dynamic manner. We show that at least two types of fluorophores are present in the gut granules. One displayed a "flashing" phenomenon, in which quenching is preceded by a sharp increase in fluorescence intensity that expands into the surrounding area. The flashing phenomenon is strongly correlated with food availability, suggesting that the underlying activities are likely to be physiological and may be part of a metabolic process.

Introduction

The intestinal cells of *Caenorhabditis elegans* and related nematodes are known to contain a type of organelle known as gut granules or rhabditin granules (Chitwood & Chitwood, 1950; Laufer, Bazzicalupo, & Wood, 1980). These birefringent and autofluorescent granules are robustly present in intestinal and intestinal precursor cells and thus serve as a useful marker for the intestinal linage

(Hermann et al., 2005; Laufer et al., 1980). Based on morphological, biochemical, and genetic evidence, these granules are considered to be lysosome-related organelles (Clokey & Jacobson, 1986; Hermann et al., 2005; Kostich, Fire, & Fambrough, 2000). As with lysosome-related organelles in other organisms, the biological roles of gut granules are not fully understood. There is evidence, however, that these organelles are likely to be involved in metabolic and homeostatic processes such as the storage of fat and cholesterol (Lee et al., 2015; Schroeder et al., 2007) and trace metal storage and detoxification (Chun et al., 2017; Roh, Collier, Guthrie, Robertson, & Kornfeld, 2012). In addition, gut granules are also known to play a signaling role through the biogenesis of ascarosides (Le et al., 2020).

In this study, we show that in partially exposed *C. elegans* intestinal tissue, some autofluorescent granules underwent a rapid and dynamic change in fluorescence intensity. Since the spatio-temporal pattern of the dynamic changes in green and red fluorescence channels are different, we concluded that at least two different fluorophores are present in the gut granule and were involved in this process. Prior to fluorescence dissipation, there was a sharp and significant increase in green fluorescence intensities that extended to the surrounding areas, a phenomenon that we describe as "flashing." Gut granule flashing was strongly dependent on food availability at the time of the experiments, being almost entirely absent in preparations without added food. Finally, we show that the worm ortholog of human Rab32/38, *glo-1* (Gut granule LOss) (Hermann et al., 2005; Morris et al., 2018), which has been shown to be required for gut granules biogenesis, was necessary for the flashing phenotype, suggesting that the source of the autofluorescent flashing signals was indeed gut granules. We have yet to identify the fluorophores responsible for the phenomenon, the underlying

biochemical processes or its biological significance. However, we found this to be an intriguing phenomenon providing insights into the functions and mechanisms of lysosome-related organelles.

Results

Some autofluorescent granules in intestinal cells displayed dynamic changes in fluorescent intensities

During our observational analysis of exposed *Caenorhabditis elegans* intestine with fluorescence confocal microscopy, in which the worm is cut open near the anus to expose the intestine (Fig 1B), we observed that some of the fluorescent granules in the intestinal cells displayed dynamic changes in fluorescence intensity (Fig 1A, C, S1 Movie). In these granules, the green fluorescence, illuminated with the 473nm laser of the confocal microscope, rises sharply and significantly (Fig 1A, C, D, S1 Movie). The intensity increase is not only limited to the original "core" area (the granule proper), as identified by the high level of fluorescence at a steady-state prior to the rapid intensity changes, but also to the surrounding areas (which we refer to as the "cloud." Details of how the area is identified are in the Methods; Fig 1E). The fluorescence intensity in both the "core" and the surrounding areas subsequently dropped off, with the intensity at the "core" dropping to a level that is lower than the previous steady-state, and the intensity in the surrounding areas ("clouds") decreasing to a level that is similar to the previous steady-state (Fig 1E). We estimated that the rapid changes in fluorescence intensity occur in less than 10 seconds, in a way that resembles the bursting of fireworks or the flashing of a light (Fig 1E). In contrast, the red fluorescent signal, illuminated with the 561nm laser of the confocal microscope, lacked the initial sharp increase observed within the green fluorescence channel, but fell concurrently (Fig 1F). The dynamic differences observed in the green and red fluorescent channels suggest that they may represent at least two distinct types of

fluorophores presented in the autofluorescent granules. This phenomenon is rare but is consistently observed in a portion of the animals in this preparation through over two years of study. The fluorophore is not exogenous, as the phenomena can be observed in wild-type animals, which were used exclusively in this study.

The autofluorescent granules flashing phenomena are strongly correlated with food availability

Since the primary function of the intestine is food digestion, we reasoned that the autofluorescent granules flashing phenomena could be associated with nutrient uptake. In *C. elegans*, food availability significantly influences the rhythmic defecation cycle (Thomas, 1990), which is controlled by calcium oscillations in the intestinal cells (Dal Santo, Logan, Chisholm, & Jorgensen, 1999). To test whether granule flashing phenomena are associated with food availability, we provided food (*Escherichia coli* OP50) to the experimental animal on the microscopic slides. We found that in worms with a significant amount of food near the head region, the occurrence of the granule flashing phenomena increased dramatically (Fig. 2A-D, S1 Movie). All seven worms provided with food displayed the phenomena (Fig. 2C, D, H), while only 1 of 7 without food did at a low frequency (Fig. 2A, B, H). It is worth noting that a small amount of food is still present in the "no food" group, which may explain the occasional occurrence of the phenomena.

The flashing autofluorescent granules are lysosome-related organelles

The worm intestinal cells are known to contain numerous autofluorescent granules known as "gut granules" (Hermann et al., 2005; Laufer et al., 1980). Gut granules are lysosome-related organelles that have been shown to play an important physiological role in both nutrient homeostasis and signal

transduction (Chun et al., 2017; Le et al., 2020; Roh et al., 2012; Schroeder et al., 2007). To characterize the nature of the observed autofluorescent granules flashing phenomena, we analyzed *glo-1(lf)* mutant animals that are defective in gut granules biogenesis. *glo-1* (Gut granule LOss) encodes an ortholog of Rab32/38 that localize to gut granules (Hermann et al., 2005; Morris et al., 2018). *glo-1(lf)* animals displayed a large reduction in the number of autofluorescent granules in the intestine, similar to what was described in Hermann et al. (2005), and also completely eliminated the granules flashing phenomena (Fig. 2E, F, H). Even with food provided, none of the seven *glo-1(lf)* animals observed displayed the phenomena, as compared with seven of seven in wild-type animals as previously described (Fig. 2H), suggesting that the flashing autofluorescent granules are lysosome-related organelles.

Discussion

Some lysosome-related organelles in the worm intestine exhibit dynamic flashing autofluorescence

In the process of establishing a baseline for fluorescence dynamics in ex vivo intestines, we characterize an intriguing dynamic of lysosome-related organelles. When provided with food, some of the lysosome-related organelles in intestinal cells underwent a rapid change in fluorescence intensities. We observed two distinctive fluorescence dynamics in green and red fluorescence. The dynamic of the green fluorescence is characterized by a sharp and rapid increase in intensity that diffuses into the surrounding area, followed by a rapid decrease and dissipation of the autofluorescence. On the other hand, the dynamic of the red fluorescence is only that of decreases in intensity (Fig. 1). The green and red fluorescence dynamic combination coincidentally resemble the predicted outcome of our original experiment, in which a green pH-sensitive encoded vesicle release

reporter is paired with a red non-pH-sensitive control. The very rare occurrence of the event under conditions without food being present initially misled us as to the source of the fluorescence. Only after the discovery of the effect of food presence did we realize what we were studying was likely a pair of naturally occurring worm fluorophores with an intriguing dynamic.

The gut granule flashing phenomena may be part of a metabolic or signaling process

In the worm intestine, gut granules coexist with more conventional lysosomes (Campbell & Fares, 2010; Kostich et al., 2000; Morris et al., 2018), and although prevailing and distinctive (Chitwood & Chitwood, 1950; Clokey & Jacobson, 1986; Hermann et al., 2005) are not thought to be the major site of intracellular digestion as with lysosome-related organelles in many other spices (Delevoye, Marks, & Raposo, 2019). In *C. elegans*, gut granules have been shown to have both metabolic and signaling functions. The lysosome-related organelles are a site for fat and cholesterol storage (Lee et al., 2015; Schroeder et al., 2007) as well as functioning both as a storage and a sequestering site for micronutrient metals (Chun et al., 2017; Roh et al., 2012). Lysosome-related organelles are also the site of biosynthesis for signaling molecules such as ascarosides (Le et al., 2020). Other than being static sites of storage and metabolic processes, gut granules have been shown to undergo structural and morphological changes responding to changes in dietary conditions. For example, in response to high dietary zinc, gut granules are remodeled from the typical round sphere to bilobed granules with asymmetrical distribution of both internal content and membrane proteins (Roh et al., 2012). The mechanism of such a structural rearrangement remains largely uncharacterized.

The gut granule flashing phenomena were highly associated with the immediate presence of food (Fig. 2). This observation implies that the phenomena could be a part of or a consequence of a

metabolic or signaling process in food intake. One possibility is that this phenomenon is associated with a vesicle content release of the gut granules, and the fluorophores or the content that it is released with plays metabolic or signaling roles in food uptake. Another possibility is that the phenomenon is associated with the breakdown of gut granules, either as part of a physiological process or as a result of our *ex-vivo* experimental conditions. Two reasons argue that the second possibility is less likely than the first. First of all, we have, on rare instances, observed similar events in intact worms, albeit we have not been able to record such events. We have also observed multiple flashing events in some of the granules. Secondly, the phenomenon is visually different from that of the visualized fluorescently labeled gut granules disruption in osmotic sensitive mutants under hypotonic shock (Luke et al., 2007), although there is some similarity in the diffusion of the fluorescence. Whatever the case, it would be interesting to know the identity of the at least two fluorophores involved.

C. elegans are long known to be autofluorescent (Babu, 1974), with most of the autofluorescence from the gut granules (Clokey & Jacobson, 1986). Particular interest has been paid to the increasing level of autofluorescence as the worms age (Clokey & Jacobson, 1986; Davis, Anderson, & Dusenbery, 1982; Forge & Macguidwin, 1989; Klass, 1977; Pincus, Mazer, & Slack, 2016). However, the fluorophores responsible for gut granule autofluorescence remain largely undefined. One of the fluorophores emitting blue fluorescence has been identified as anthranilic acid (Babu, 1974; Coburn et al., 2013), and changes in the blue fluorescence near the death of the animals (death fluorescence, or DF) has been described (Coburn et al., 2013; Pincus et al., 2016). Although both green and red fluorescence also increase with age and green fluorescence intensifies near the death of the animals (Coburn et al., 2013; Pincus et al., 2016), the patterns of the fluorescence changes are different, and they are also likely emitted by different fluorophores. It is also important to note that

the fluorescence dynamic of DF is also distinct from the phenomenon that we are describing in this research, both spatially and temporally.

A major caveat of this study is its *ex-vivo* nature. One could argue that the fluorescence dynamic we observed may not be physiological. It is important to stress, however, that besides the fact that we have been able to observe the phenomenon in live worms on a few occasions, the phenomenon is dependent upon a potential environmental cue- the presence of food; and is genetically dependent on the gene *glo-1*. It is also worth noting that conditions such as oxidative stress does not appear to increase autofluorescence in *C. elegans* (Pincus et al., 2016). Regardless, even if the phenomenon is not itself naturally occurring, it is a beautiful experimental phenotype that could also be informative.

Further understanding of the phenomenon would likely require the characterization of the green and red fluorophores. It is unclear how to best identify these fluorophores, although we would predict that the green fluorophores emit stronger fluorescence under low pH conditions, while the red fluorophores are likely pH neutral. Nonetheless, we described a visually spectacular fluorescence dynamic phenomenon that involves a type of lysosome-related organelles known as gut granules in nematode intestines. It is possible that what we observed is part of a common cellular process but only visualized through the strong autofluorescence of the fluorophores. If that is the case, the gut granules of *C. elegans*, with its naturally occurring fluorophores, may be a potential platform for the understanding of lysosome-related organelles as well as cellular vesicle membrane dynamics.

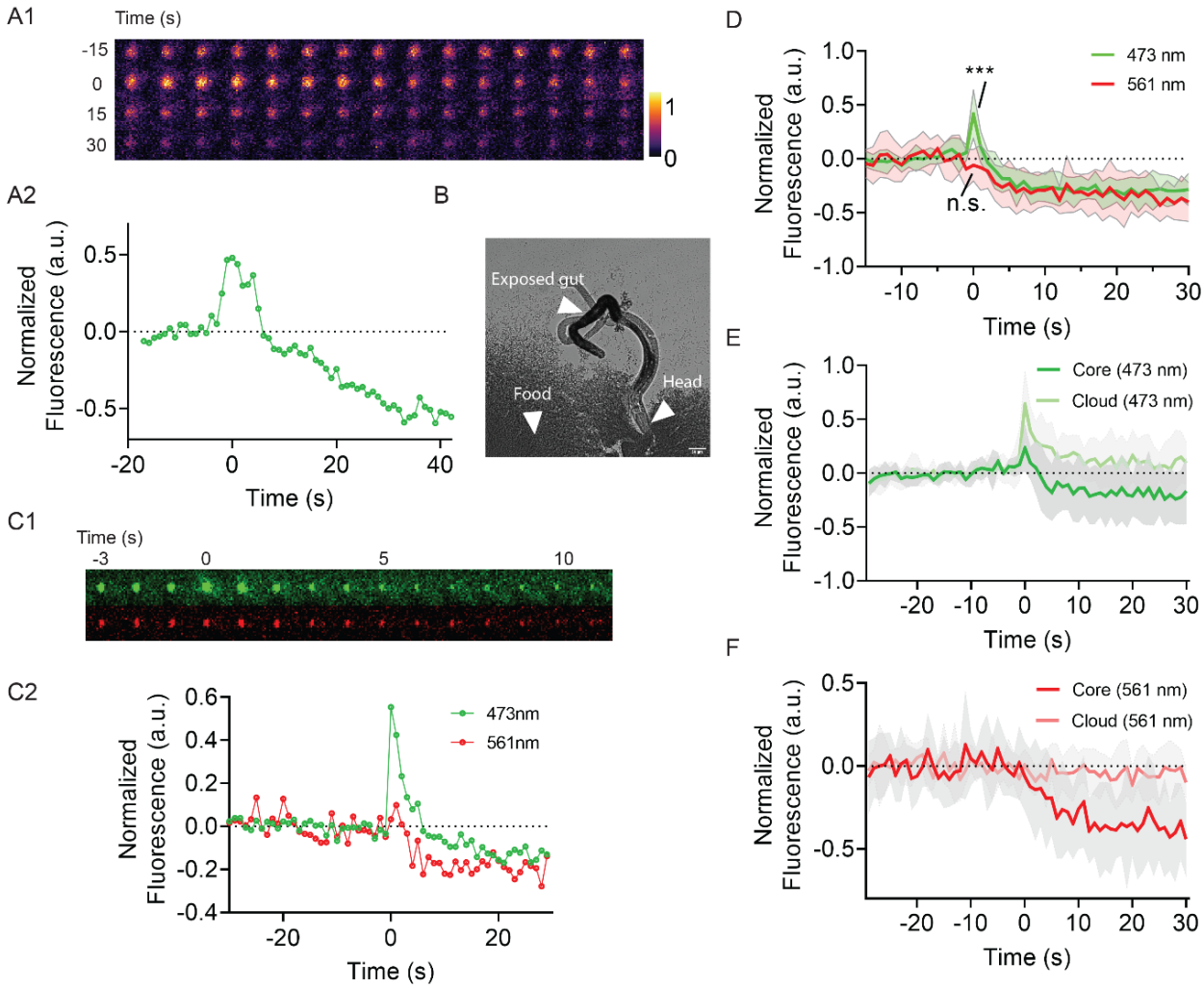

Figure 1: The dynamics of gut granule dissipation.

(A) The green fluorescence in the granule increases and falls sharply. Representative example of changes in green fluorescence intensity during gut granule dissipation. (A1) A 1-minute pseudo-color time series of a gut granule dissipation event. Imaging rate: 1Hz. The time axis is zeroed at the dissipation onset (see Methods). (A2) Normalized green fluorescent intensity plot of (A1). (B) An example of the ex-vivo experimental setting. L4 stage nematodes were carefully incised near the anus to expose the gut. In the "with food" conditions, nematodes were positioned to embed their heads in food. (C-D) The green fluorescence in the granule increases and falls sharply, while the red lack the initial sharp increase. (C) A representative example of two-color time-lapse imaging (C1) and normalized quantifications (C2). The fluorescence intensity is normalized by the baseline fluorescence calculated as the mean of fluorescence in the ROIs prior to the dissipation onset. (D) The average fluorescence intensity of all recorded dissipations in one sample. (E-F) Gut granule flashes during dissipation. Two-color imaging of all recorded gut granule dissipation events in a representative sample. (E-F) The granular area ("core"), as well as the surrounding ring area that presents diffusion of fluorescence ("cloud"), were measured separately in both 473nm (E) and 561nm (F) illumination. (E). The intensity increase in green fluorescence is not only limited to the original "core" area but also to the surrounding areas "cloud ."(F) No intensity increase was observed with the red fluorescence, neither in the "core" nor the "cloud ." Raw images for analysis were

identical to (D), except a longer pre-onset timeframe was selected for normalization. In (D-F), pooled values are presented as mean ± s.d (N=11 in D, N=8 in E and F). The time axis is zeroed at the dissipation onset. Scale bar, 50 μm.

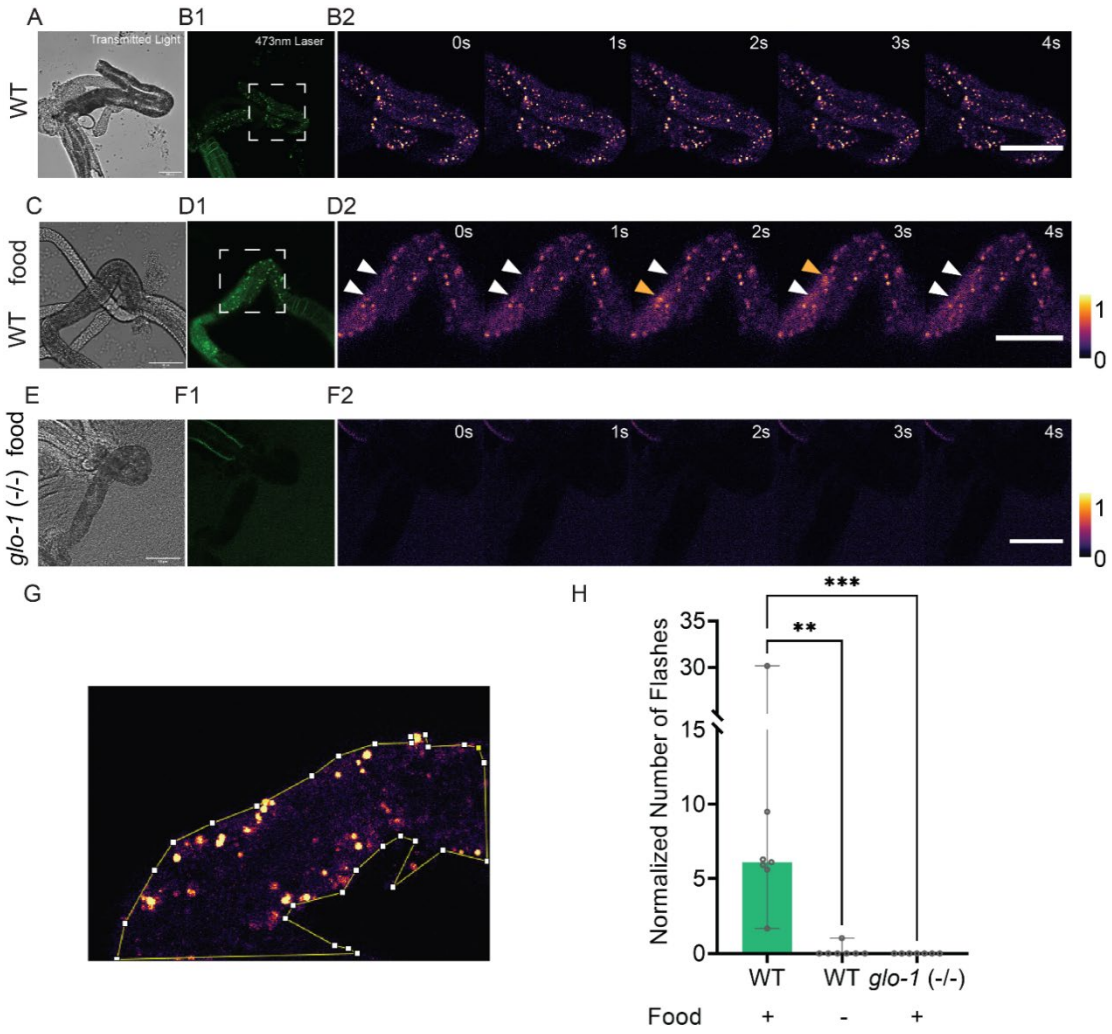

Figure 2: The gut granule dissipation phenomena are dependent on the presence of food.

The field of view was illuminated and recorded with transmitted light (A, C, E), epifluorescence (B1, D1, F1), and 473nm laser illumination (B2, D2, F2). In (B2, D2, F2) 5-second clips of time-series with 473nm laser illumination were pseudo-colored and shown. (A-B) In wild-type worms not provided with food on slide, the phenomena were rarely observed. (C-D) In wild-type worms provided with food on slide, the occurrences of phenomena were increased dramatically. Orange arrows in (D2) indicate the onset of gut granule dissipation events. White arrows point to the same region of interest before and after onset. (E-F) There is no detection of events in *glo-1(lf)* worm even with the presence of food on slide. (G-H) Gut granule dissipation events were manually identified and scored. To normalize the number of events for comparison, the counts for each sample were divided by (1) the area of exposed intestine within the field of view as shown in (G) and (2) by the length of time series (details in Materials and Methods). (H) Normalized data from all conditions were plotted (N=6-7), and each group was compared with the WT + food group (**P<0.01, ***P<0.001, Mann-Whitney *U* test). Scale bar, 50 μm.

Methods

Nematode strains maintenance and general methods.

The culture and maintenance of *C. elegans* w were done similarly to the standard procedure as described in Brenner (1974). Briefly, worms were cultured on Nematode Growth Medium (NGM) dishes with a lawn of *Escherichia coli* strain OP50 at 20°C. The Bristol N2 strain (Brenner, 1974) was used as the wild-type reference strain, and from which the mutant strain was derived. The five times out-crossed *glo-1(zu391 lf)* X (Hermann et al., 2005) mutant strain OJ1347 (Wang et al., 2013) was a gift from Dr. Derek Sieburth of the University of Southern California.

Sample preparation for *ex-vivo* imaging.

L4 stage hermaphrodite worms were transferred to a drop of Iwasaki–Teramoto (I–T) solution (Teramoto & Iwasaki, 2006) [136mMNaCl, 9mMKCl, 1mM $CaCl_2$, 3mM $MgCl_2$, 77mM glucose, and 5mM HEPES (pH 7.4)] and immobilized with 1mM levamisole on a microscopic slide. To expose the intestine for imaging, worms were incised with a pair of 30G 5/8" needles (PrecisionGlide, BD, Franklin Lakes, NJ) near the anus. For experiments with food added on the slide, a glob of OP50 collected by scrapping the lawn off an NGM plate using a cell scraper was transferred into the droplet via the platinum wire worm pick. An insulation spacer was drawn using a PAP pen (RPI, #195506) around the solution droplet, and a piece of cover-glass was mounted atop subsequently.

Microscopy

Confocal time series were acquired using a Fluoview FV3000 Confocal laser scanning biological microscope (Olympus) with a 60×, 1.30 N.A. silicone oil objective (Olympus). Frame rate was

calibrated to 1Hz by adjusting the size of the imaging window and the line averaging multiplier. 5-min time lapse imaging was acquired for each sample. All image processing and analyses were done using ImageJ (National Institute of Health). The transmitted light channel was illuminated simultaneously with the imaging laser (473nm) for positional imaging. Panel A1 in Figures 1, as well as Panels B2, D2, F2 and G in Figure 2, were pseudo-colored with mpl-inferno LUT in FIJI.

Imaging data processing

ROIs of granules were manually selected in FIJI for all data. For Figure 2(G-H), ROIs of peri-granule "cloud" were defined based on the identification of fluorescent pattern of dissipation events. The time series data were zeroed at the flashing onsets of each granule and pooled into metadata.

ROI selection: ROIs were defined based on visual identification of granules in the intestine region, fluorescence normalization baseline was set accordingly as the average of pre-dissipation period. Standard deviation envelopes were visualized in the time series. For Figure 2(H), the number of gut granule dissipation events was normalized as per minute *10-4 μm^2 of the intestinal surface area from single optical sections, which are manually delineated (Figure 2(G)). Nonparametric Mann-Whitney U test was used for comparison between WT food vs. no-food, and WT food vs. *glo-1(lf)*.

Data and Statistical analysis

Data were plotted as mean± s.d, except in Figure 2(H), as raw data failed to passed all normality tests (Kolmogorov-Smirnov test, Shapiro-Wilk test, D'Agostino & Pearson test). Data in Figure 2(H) were plotted as median ± 95% CI instead. All data analysis was performed with Graphpad Prism 9 and Microsoft Excel.

References

Babu, P. (1974). Biochemical Genetics of Coenorhabditis-Elegans. *Molecular and General Genetics*, *135*(1), 39-44. https://doi.org/10.1007/Bf00433899

Brenner, S. (1974). The genetics of Caenorhabditis elegans. *Genetics*, *77*(1), 71-94.

Campbell, E. M., & Fares, H. (2010). Roles of CUP-5, the Caenorhabditis elegans orthologue of human TRPML1, in lysosome and gut granule biogenesis. *BMC Cell Biol*, *11*, 40. https://doi.org/10.1186/1471-2121-11-40

Chitwood, B., & Chitwood, M. (1950). Introduction to nematology (reprinted 1974). In: Baltimore: University Park Press.

Chun, H., Sharma, A. K., Lee, J., Chan, J., Jia, S., & Kim, B. E. (2017). The Intestinal Copper Exporter CUA-1 Is Required for Systemic Copper Homeostasis in Caenorhabditis elegans. *Journal of Biological Chemistry*, *292*(1), 1-14. https://doi.org/10.1074/jbc.M116.760876

Clokey, G. V., & Jacobson, L. A. (1986). The autofluorescent "lipofuscin granules" in the intestinal cells of Caenorhabditis elegans are secondary lysosomes. *Mech Ageing Dev*, *35*(1), 79-94. https://doi.org/10.1016/0047-6374(86)90068-0

Coburn, C., Allman, E., Mahanti, P., Benedetto, A., Cabreiro, F., Pincus, Z., Matthijssens, F., Araiz, C., Mandel, A., Vlachos, M., Edwards, S. A., Fischer, G., Davidson, A., Pryor, R. E., Stevens, A., Slack, F. J., Tavernarakis, N., Braeckman, B. P., Schroeder, F. C., . . . Gems, D. (2013). Anthranilate fluorescence marks a calcium-propagated necrotic wave that promotes organismal death in C. elegans. *PLoS Biol*, *11*(7), e1001613. https://doi.org/10.1371/journal.pbio.1001613

Dal Santo, P., Logan, M. A., Chisholm, A. D., & Jorgensen, E. M. (1999). The inositol trisphosphate receptor regulates a 50-second behavioral rhythm in C. elegans. *Cell*, *98*(6), 757-767. https://doi.org/10.1016/s0092-8674(00)81510-x

Davis, B. O., Jr., Anderson, G. L., & Dusenbery, D. B. (1982). Total luminescence spectroscopy of fluorescence changes during aging in Caenorhabditis elegans. *Biochemistry*, *21*(17), 4089-4095. https://doi.org/10.1021/bi00260a027

Davis, P., Zarowiecki, M., Arnaboldi, V., Becerra, A., Cain, S., Chan, J., Chen, W. J., Cho, J., da Veiga Beltrame, E., Diamantakis, S., Gao, S., Grigoriadis, D., Grove, C. A., Harris, T. W., Kishore, R., Le, T., Lee, R. Y. N., Luypaert, M., Muller, H. M., . . . Sternberg, P. W. (2022). WormBase in 2022-data, processes, and tools for analyzing Caenorhabditis elegans. *Genetics*. https://doi.org/10.1093/genetics/iyac003

Delevoye, C., Marks, M. S., & Raposo, G. (2019). Lysosome-related organelles as functional adaptations of the endolysosomal system. *Curr Opin Cell Biol*, *59*, 147-158. https://doi.org/10.1016/j.ceb.2019.05.003

Forge, T. A., & Macguidwin, A. E. (1989). Nematode autofluorescence and its use as an indicator of viability. *J Nematol*, *21*(3), 399-403.

Hermann, G. J., Schroeder, L. K., Hieb, C. A., Kershner, A. M., Rabbitts, B. M., Fonarev, P., Grant, B. D., & Priess, J. R. (2005). Genetic analysis of lysosomal trafficking in Caenorhabditis elegans. *Mol Biol Cell*, *16*(7), 3273-3288. https://doi.org/10.1091/mbc.e05-01-0060

Klass, M. R. (1977). Aging in the nematode Caenorhabditis elegans: major biological and environmental factors influencing life span. *Mech Ageing Dev*, *6*(6), 413-429. https://doi.org/10.1016/0047-6374(77)90043-4

Kostich, M., Fire, A., & Fambrough, D. M. (2000). Identification and molecular-genetic characterization of a LAMP/CD68-like protein from Caenorhabditis elegans. *J Cell Sci*, *113 (Pt 14)*, 2595-2606. https://doi.org/10.1242/jcs.113.14.2595

Laufer, J. S., Bazzicalupo, P., & Wood, W. B. (1980). Segregation of developmental potential in early embryos of Caenorhabditis elegans. *Cell*, *19*(3), 569-577. https://doi.org/10.1016/s0092-8674(80)80033-x

Le, H. H., Wrobel, C. J., Cohen, S. M., Yu, J., Park, H., Helf, M. J., Curtis, B. J., Kruempel, J. C., Rodrigues, P. R., Hu, P. J., Sternberg, P. W., & Schroeder, F. C. (2020). Modular metabolite assembly in Caenorhabditis elegans depends on carboxylesterases and formation of lysosome-related organelles. *Elife*, *9*. https://doi.org/10.7554/eLife.61886

Lee, H. J., Zhang, W., Zhang, D., Yang, Y., Liu, B., Barker, E. L., Buhman, K. K., Slipchenko, L. V., Dai, M., & Cheng, J. X. (2015). Assessing cholesterol storage in live cells and C. elegans by stimulated Raman scattering imaging of phenyl-Diyne cholesterol. *Sci Rep*, *5*, 7930. https://doi.org/10.1038/srep07930

Luke, C. J., Pak, S. C., Askew, Y. S., Naviglia, T. L., Askew, D. J., Nobar, S. M., Vetica, A. C., Long, O. S., Watkins, S. C., Stolz, D. B., Barstead, R. J., Moulder, G. L., Bromme, D., & Silverman, G. A. (2007). An intracellular serpin regulates necrosis by inhibiting the induction and sequelae of lysosomal injury. *Cell*, *130*(6), 1108-1119. https://doi.org/10.1016/j.cell.2007.07.013

Morris, C., Foster, O. K., Handa, S., Peloza, K., Voss, L., Somhegyi, H., Jian, Y., Vo, M. V., Harp, M., Rambo, F. M., Yang, C., & Hermann, G. J. (2018). Function and regulation of the Caenorhabditis elegans Rab32 family member GLO-1 in lysosome-related organelle biogenesis. *PLoS Genet*, *14*(11), e1007772. https://doi.org/10.1371/journal.pgen.1007772

Pincus, Z., Mazer, T. C., & Slack, F. J. (2016). Autofluorescence as a measure of senescence in C. elegans: look to red, not blue or green. *Aging (Albany NY)*, *8*(5), 889-898. https://doi.org/10.18632/aging.100936

Roh, H. C., Collier, S., Guthrie, J., Robertson, J. D., & Kornfeld, K. (2012). Lysosome-related organelles in intestinal cells are a zinc storage site in C. elegans. *Cell Metab*, *15*(1), 88-99. https://doi.org/10.1016/j.cmet.2011.12.003

Schroeder, L. K., Kremer, S., Kramer, M. J., Currie, E., Kwan, E., Watts, J. L., Lawrenson, A. L., & Hermann, G. J. (2007). Function of the Caenorhabditis elegans ABC transporter PGP-2 in the biogenesis of a lysosome-related fat storage organelle. *Mol Biol Cell*, *18*(3), 995-1008. https://doi.org/10.1091/mbc.e06-08-0685

Teramoto, T., & Iwasaki, K. (2006). Intestinal calcium waves coordinate a behavioral motor program in C. elegans. *Cell Calcium*, *40*(3), 319-327. https://doi.org/10.1016/j.ceca.2006.04.009

Thomas, J. H. (1990). Genetic analysis of defecation in Caenorhabditis elegans. *Genetics*, *124*(4), 855-872.

Wang, H., Girskis, K., Janssen, T., Chan, J. P., Dasgupta, K., Knowles, J. A., Schoofs, L., & Sieburth, D. (2013). Neuropeptide secreted from a pacemaker activates neurons to control a rhythmic behavior. *Curr Biol*, *23*(9), 746-754. https://doi.org/10.1016/j.cub.2013.03.049